NAVAL POSTGRADUATE SCHOOL

MONTEREY, CALIFORNIA

THESIS

EVALUATION AND TESTING OF THE NAVAL POSTGRADUATE SCHOOL SATELLITE (NPSAT1) SOLAR CELL MEASUREMENT SYSTEM

by

Benson W. Lo

September 2004

Thesis Advisor:	Sherif Michael
Second Reader:	Herschel H. Loomis

Approved for public release; distribution is unlimited.

THIS PAGE INTENTIONALLY LEFT BLANK

REPORT DOCUMENTATION PAGE			Form Approved OMB No. 0704-0188
Public reporting burden for this collection of information is estimated to average 1 hour per response, including the time for reviewing instruction, searching existing data sources, gathering and maintaining the data needed, and completing and reviewing the collection of information. Send comments regarding this burden estimate or any other aspect of this collection of information, including suggestions for reducing this burden, to Washington headquarters Services, Directorate for Information Operations and Reports, 1215 Jefferson Davis Highway, Suite 1204, Arlington, VA 22202-4302, and to the Office of Management and Budget, Paperwork Reduction Project (0704-0188) Washington DC 20503.			
1. AGENCY USE ONLY ***(Leave blank)***	**2. REPORT DATE** September 2004	**3. REPORT TYPE AND DATES COVERED** Master's Thesis	
4. TITLE AND SUBTITLE: Evaluation and Testing of the Naval Postgraduate School Satellite (NPSAT1) Solar Cell Measurement System			**5. FUNDING NUMBERS**
6. AUTHOR(S) Lo, Benson W.			
7. PERFORMING ORGANIZATION NAME(S) AND ADDRESS(ES) Naval Postgraduate School Monterey, CA 93943-5000			**8. PERFORMING ORGANIZATION REPORT NUMBER**
9. SPONSORING /MONITORING AGENCY NAME(S) AND ADDRESS(ES) N/A			**10. SPONSORING/MONITORING AGENCY REPORT NUMBER**
11. SUPPLEMENTARY NOTES The views expressed in this thesis are those of the author and do not reflect the official policy or position of the Department of Defense or the U.S. Government.			
12a. DISTRIBUTION / AVAILABILITY STATEMENT Approved for public release; distribution is unlimited.			**12b. DISTRIBUTION CODE**

13. ABSTRACT (maximum 200 words)

The Naval Postgraduate School Spacecraft Architecture and Technology Demonstration Satellite, NPSAT1, launching in the fall of 2006, will include a system to measure the performance of new experimental triple-junction solar cells. The measuring circuit in the Solar Cell Measurement System (SMS) is based on a circuit developed at the Naval Postgraduate School many years ago. It will trace the cells' current-voltage (*I-V*) curves while in orbit. The SMS consists of a radiation-hardened microcontroller that uses a radiation-hardened FPGA to monitor a collection of sensors. A current-sink circuit is used to measure the current and voltage on the test cells. Prior to launch, extensive testing is being performed on the system to ensure proper operation. The tests consist of subjecting solar cells and the measuring circuit electronics under conditions modeling the space environment while taking cell measurements. This thesis presents the mission information, system design, test setup, and test results of the SMS measuring circuit.

14. SUBJECT TERMS NPSAT1, solar cell, solar cell measurement, triple junction, SMS, I-V curve, solar simulator			**15. NUMBER OF PAGES** 123
			16. PRICE CODE
17. SECURITY CLASSIFICATION OF REPORT Unclassified	**18. SECURITY CLASSIFICATION OF THIS PAGE** Unclassified	**19. SECURITY CLASSIFICATION OF ABSTRACT** Unclassified	**20. LIMITATION OF ABSTRACT** UL

NSN 7540-01-280-5500 Standard Form 298 (Rev. 2-89)
Prescribed by ANSI Std. 239-18

THIS PAGE INTENTIONALLY LEFT BLANK

Approved for public release; distribution is unlimited.

EVALUATION AND TESTING OF THE NAVAL POSTGRADUATE SCHOOL SATELLITE (NPSAT1) SOLAR CELL MEASUREMENT SYSTEM

Benson W. Lo
Ensign, United States Naval Reserve
B.S., University of California, Los Angeles, 2003

Submitted in partial fulfillment of the
requirements for the degree of

MASTER OF SCIENCE IN ELECTRICAL ENGINEERING

from the

NAVAL POSTGRADUATE SCHOOL
September 2004

Author: Benson W. Lo

Approved by: Sherif Michael
Thesis Advisor

Herschel H. Loomis
Second Reader

John P. Powers
Chairman, Department of Electrical and Computer Engineering

THIS PAGE INTENTIONALLY LEFT BLANK

ABSTRACT

The Naval Postgraduate School Spacecraft Architecture and Technology Demonstration Satellite, NPSAT1, launching in the fall of 2006, will include a system to measure the performance of new experimental triple-junction solar cells. The measuring circuit in the Solar-Cell Measurement System (SMS) is based on a circuit developed at the Naval Postgraduate School many years ago. It will trace the cells' current-voltage (*I-V*) curves while in orbit. The SMS consists of a radiation-hardened microcontroller that uses a radiation-hardened FPGA to monitor a collection of sensors. A current-sink circuit is used to measure the current and voltage on the test cells. Prior to launch, extensive testing is being performed on the system to ensure proper operation. The tests consist of subjecting solar cells and the measuring circuit electronics under conditions modeling the space environment while taking cell measurements. This thesis presents the mission information, system design, test setup, and test results of the SMS measuring circuit.

THIS PAGE INTENTIONALLY LEFT BLANK

TABLE OF CONTENTS

LIST OF SYMBOLS, ACRONYMS, AND ABBREVIATIONS

T	temperature
k	Boltzmann's constant
E_F	Fermi energy
E	energy
h	Planck's constant
f	frequency
E_p	photon energy
c	speed of light
λ	wavelength
E_g	bandgap energy
I	current
V	voltage
I_{sc}	short-circuit current
V_{oc}	open-circuit voltage
P_{max}	maximum output power
η	efficiency
ff	fill factor
V_T	thermal voltage
I_0	diode saturation current
I_{mp}	current at max power
V_{mp}	voltage at max power
q	electronic charge
β	BJT common-emitter current gain
V_{BE}	base-emitter voltage
R	resistance
P	power

eV	electron-Volts
NPS	Naval Postgraduate School
SSAG	Space Systems Academic Group
DoD	Department of Defense
STP	Space Test Program
SMC	Space and Missile Systems Center
PV	Photovoltaic
TPV	Thermophotovoltaic
AM	Air mass
EM	Electromagnetic
SMS	Solar-Cell Measurement System
MOSFET	metal-oxide semiconductor field-effect transistor
MOS	same as MOSFET
NMOS	n-channel MOSFET
PMOS	p-channel MOSFET
BJT	bipolar junction transistor

MUX	multiplexer
PCB	printed circuit board
CDB	Coupon Driver Board
VI	Virtual Instrument
USN	United States Navy
USNR	United States Naval Reserve
USMC	United States Marine Corps

EXECUTIVE SUMMARY

The Naval Postgraduate School Spacecraft Architecture and Technology Demonstration Satellite, NPSAT1, launching in the fall of 2006, will include a system to measure the performance of new experimental triple-junction solar cells. The measuring circuit used in the system is based on a circuit developed at the Naval Postgraduate School many years ago. The Solar-Cell Measurement System (SMS) will trace the cells' current-voltage (*I-V*) curves while in orbit. The System consists of a radiation-hardened microcontroller that uses a radiation-hardened FPGA to monitor a collection of sensors. A current-sink circuit is used to measure the current and voltage on the test cells. A total of 24 cells on the satellite will be tested, 22 of which are the experimental cells, and two are dual-junction cells serving as reference cells. Prior to launch, extensive testing is being performed on the system to ensure proper operation. This thesis presents the mission information, system design, test setup, and test results of the SMS measuring circuit.

The tests performed include temperature variation on the solar cells and the circuit electronics, and variation of the light incidence angles on the solar cells. The SMS measuring circuit will take *I-V* curves of the solar cells under these various conditions, and the curves will be compared to control curves to describe accuracy. The test conditions are meant to simulate some of the conditions expected in space, or at least to observe if there are any conditions that might not be specific to space that would affect the circuit's performance.

For the temperature-variation tests, the cells were kept at three temperatures while curves were traced. In the incidence-angle tests, the cells were illuminated at four angles, arbitrarily chosen for convenience of the setup. In both tests, the curves traced by the SMS measuring circuit were compared to curves taken by a control device. In a third test, the measuring circuit was heated to observe any effects by temperature. The curve taken was compared to the curve taken while the circuit was at room temperature.

The results are not entirely conclusive. Test equipment affected the output of the circuit. Noise appears at the A/D and D/A converter card, and the curves are affected. To obtain results that are more conclusive, the digital portion of the SMS will need to be completed to connect to the analog measuring circuit for a more compatible test. The

digital controller is expected to generate an output signal much cleaner than the converter card. The output of the analog circuit would then be unaffected by outside factors.

ACKNOWLEDGMENTS

There are many who have helped me reach this accomplishment. I wish to express my gratitude to the faculty and staff of the Space Systems Academic Group, where without you, there would be no satellite. The work that you do is important to every student that passes through here, and important to our Country in more ways than we will ever realize. Dan Sakoda, Jim Horning, and Dave Rigmaiden: thank you for sharing your insights and for always being there to answer my questions. I must thank Ron Phelps for his patience in assisting me in the project and answering my endless questions. I don't know if I could have gotten anything done on time, or simply *done* for that matter, if not for Ron's help.

I would also like to express my deepest appreciation to the professors here, who chose a profession to pass on what they have learned and educate the young minds of the future. I would like to especially thank:

- Professor Rudy Panholzer, for your leadership. Thank you for your support and words of wisdom.
- Professor Hersch Loomis, for your insights in improving this work.
- And of course, Professor Sherif Michael, thank you for the opportunity to be a part of this project, answering my question, and your contribution to my education.

Lastly, I thank my loving parents. They left our native country to come to a strange land so I can live free and get a good education. Their love, support, encouragement, and sacrifice will never be forgotten.

Being a part of the NPSAT1 project was exciting, and I look forward to seeing the rocket launch in 2006!

THIS PAGE INTENTIONALLY LEFT BLANK

I. INTRODUCTION

A. BACKGROUND

The Naval Postgraduate School (NPS) is in the process of building its second satellite. Its first satellite, the Petite Amateur Navy Satellite (PANSAT) launched in 1998, was a success. Managed by the NPS Space Systems Academic Group (SSAG), the satellite project allowed NPS students to gain hands-on experience in the design and testing of the systems onboard the satellite. The current satellite, NPSAT1, again offers the same opportunity, and when it is launched in the fall of 2006, students will have an opportunity to participate in satellite flight operations.

The Naval Postgraduate School Spacecraft Architecture and Technology Demonstration Satellite, NPSAT1, is a low-cost technology demonstration satellite with several integrated experiments. The NPSAT1 mission, conceived and developed by NPS SSAG, is sponsored and executed by the Department of Defense Space Test Program (SMC Det 12).

One of the systems onboard the satellite is the Solar-Cell Measurement System (SMS). It is considered an experiment on the satellite, as it is the first time being used by NPS and it will measure current-voltage characteristics of experimental solar cells. The data gathered will be beneficial for the satellite sponsors for future projects.

The SMS contains an analog subsystem and a digital subsystem. The digital subsystem is the system controller. It will control the analog subsystem in setting the appropriate voltages, and process and store the output from the analog portion. The analog subsystem is the focus of this thesis. The main part of the analog subsystem is made up of analog current-sink circuits to measure the voltage across the solar cell while a current is drawn from the cell. The analog current-sink circuit is based on the work of LT Robert Callaway, USN, and Professor Sherif Michael at NPS in 1986 [1]. Their work will be introduced in Chapter V.

B. PURPOSE AND OBJECTIVE

To ensure the design of the SMS analog circuit is valid, it is essential that the design be tested thoroughly prior to flight. The preflight testing will reveal any potential

problems in the circuit, and will allow engineers to make revisions. This will help ensure the proper operation of the system while in orbit.

This thesis examines the analog circuit design and operation. It describes the testing procedure, the tests performed, and their results. The tests consisted of the following:

- Observed the accuracy of the SMS analog circuit output while measuring solar cells at various cell temperatures.
- Observed the output of the circuit while the temperature was varied on the circuit itself.
- Observed the accuracy of the circuit output while the solar cells were illuminated at various incidence angles.

The tests were meant to simulate some of the conditions that will be met in space, although they will not be an exact replication. The temperature of the satellite will vary over a wide range, and the temperature will affect both the electronics of the circuit and the solar cells. The cells will also be receiving sunlight at various angles. The tests on the circuit will determine if it can measure the cells accurately under those conditions.

To qualitatively describe the SMS analog circuit's performance, its outputs will be compared to a trusted measuring device acting as the experiment control. The goal is to have the SMS analog circuit to achieve accuracy to within 2% of the control measurements.

C. ORGANIZATION

The thesis is organized in *chapters*, with *sections* within the chapters, and *subsections* within the sections. These terms will be used throughout the text to refer to various portions of the document. The next chapter introduces the physics of a solar cell and its operation. Chapter III discusses the NPSAT1 satellite and its mission in more detail. Chapter IV describes the NPS Solar Simulation Laboratory and the equipment used to test solar cells and the SMS. Chapter V returns to the SMS and its analog subsystem to discuss in detail its mission, origins, and operation. The chapter then describes in detailed the testing procedures and results. Chapter VI provides the conclusion and recommendation for future research. Several appendices are at the back of this thesis, and they

contain useful information for future students. Appendix A lists the numerical constants used in the text. Appendices B and C contain procedures to replicate the tasks performed in the experiment. Appendix D shows the circuit schematic and board layout of the prototype printed circuit board used in testing, while Appendix E provides readers with the source code for the program used in the experiment. Finally, Appendix F includes all results from the tests performed.

THIS PAGE INTENTIONALLY LEFT BLANK

II. THE PHYSICS OF PHOTOVOLTAICS

A photovoltaic (PV) device, or simply photovoltaic, is a general term for devices that convert radiant energy into electrical energy. This conversion of photons to voltage is often called the *photovoltaic effect*. Solar cells are a type of photovoltaic devices that convert solar radiation (the sun's energy) into useful electrical energy. There are other PV cell technologies, such as the thermophotovoltaic (TPV) cells, that convert, for example, infrared rays into electrical energy.

The fundamental of solar cells is presented early because the remainder of this thesis requires an understanding of the material in this chapter. The sun's energy, the basic operation of the solar cell, and characteristics of solar cell performance are explained here. Relevant topics are discussed in some detail, but no attempt has been made to derive or present every property of photovoltaic devices. There are many good textbooks on semiconductor and photovoltaic physics, and interested readers can refer to the references cited, such as [2], for more details.

The organization of this chapter assumes the reader is familiar with semiconductor physics (*p-n* junctions). After discussing the sun's energy, the chapter continues with an introduction to the operation and properties of solar cells. Understanding the operation of the solar cell requires knowledge of diodes, since solar cells are essentially *p-n* junction diodes.

A. SOLAR CONSTANT, IRRADIANCE, AND AIR MASS NUMBER

Before discussing the operation of solar cells, it is important to discuss the sun and its energy. After all, it is what solar cells use to produce electrical energy.

The sun delivers light and energy to us constantly. It is a radiator whose spectrum can be approximated by a 6050K blackbody [2]. This spectrum can vary due to differing temperature across the sun. Energy delivered by the sun, or any radiant power source, can be described by its irradiance. Irradiance is defined to be the radiant power incident per unit area on a surface, usually measured in Watts per square meter. The irradiance of the sun in space just outside of the atmosphere is about 1.353 kW/m^2 [2,3]. Because this number is so commonly used, it is also called the *solar constant*. The solar constant will

change due to seasons, where the earth-sun distance varies. However, the variation is only about 3% [2].

Another item important in understanding solar cell performance is the *air mass number*. One should not confuse "air mass" in meteorology to the "air mass number" when discussing the solar spectrum. The air mass discussed here is the *optical air mass*. The air mass number is defined to be the path length through the atmosphere relative to the shortest path [2]. For example, for a path through the atmosphere that is normal to the earth's surface, which is the shortest path from space to the earth surface, the air mass number is defined to be one, written and read "air mass one," or abbreviated as AM1. For a path length at a zenith angle z, the air mass number AM is defined in [2] to be

$$\mathrm{AM} = \sec z \, . \tag{2.1}$$

Alternatively, the air mass number can be estimated by measuring the length of the shadow s cast by a vertical structure of height l and calculating (given in [4])

$$\mathrm{AM} \approx \sqrt{1+\left(\frac{s}{l}\right)^2} \, . \tag{2.2}$$

Figure II-1 illustrates the relationship between the sun zenith angle and air mass number [5]. As the angle is increased, the path for sunlight increases, the air mass number increases, and the intensity of the solar spectrum decreases. Air mass numbers are often used to describe the entire solar spectrum at a particular location. Because in space the path length through the atmosphere is zero, AM0 is often used to describe the solar spectrum in outer space. Other AM numbers are used in terrestrial solar cell applications.

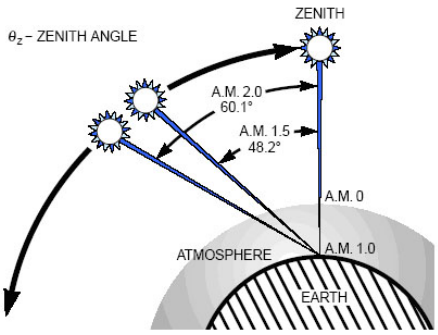

Figure II-1. Illustration of the air mass number, path lengths, and zenith angles (From [5]).

Figure II-2 shows the AM0 spectrum for wavelengths up to 3000nm. The *x*-axis is wavelength of the radiation in nanometers (nm). The *y*-axis is irradiance in micro-Watts per square centimeter per nanometer. Integrating the AM0 curve, which is the area under the curve, would give the solar constant: 1.353 kW/m^2.

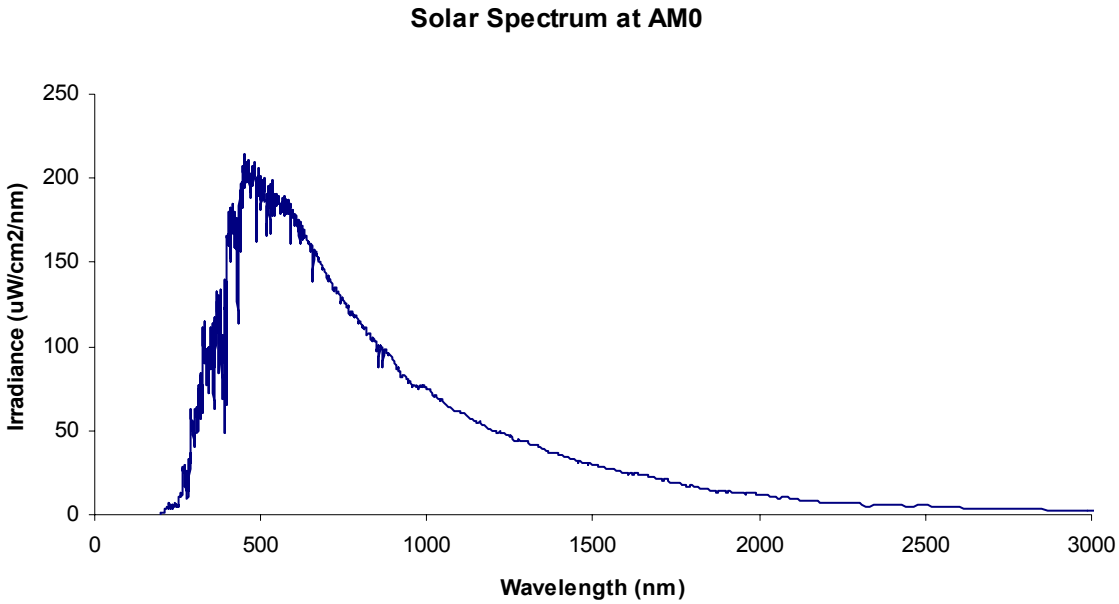

Figure II-2. The AM0 solar spectrum (Data from DoE/NREL).

The sun radiates electromagnetic (EM) waves of wavelengths from about 200 nm to over 5000 nm (very small in energy at that point). The visible spectrum is from about 400 nm (violet) to 700 nm (red). One can see that the visible spectrum is a very small part of the wavelengths the solar spectrum occupies. It is in the visible spectrum, however, where the solar radiation is the strongest. The neighboring region of wavelengths less than 400 nm is the ultraviolet spectrum, and the neighboring region of wavelengths higher than 700 nm is the infrared spectrum (heat).

B. SOLAR CELLS

1. Light Absorption and Material Selection

Any electromagnetic (EM) radiation consists of photons, and all photons contain a particular amount of energy. The difference between the different photons of different

portions of the EM spectrum is the energy contained in the photon. The photon's energy E_p is related to its frequency by

$$E_p = hf \tag{2.3}$$

where h is Planck's constant and f is the frequency of an EM field in Hertz (Hz) [6]. Thus, each frequency in the EM spectrum has an energy associated with it. Since frequency is related to wavelength and speed of propagation, the photon energy can also be rewritten in terms of wavelength by

$$E_p = \frac{hc}{\lambda} \tag{2.4}$$

where c is the speed of light and λ is the electromagnetic wavelength [6]. At any specific wavelength or frequency, all photons have the same amount of energy, regardless of the strength of the field or the brightness of the light. The intensity depends on the amount of photons striking a surface area per unit time.

Semiconductors are characterized by their energy bandgap E_g. To excite an electron in the valence band to move to the conduction band, energy greater than the bandgap is necessary. This can be provided by photons with sufficient energy. The semiconductor will be able to absorb photons containing energy $E_p > E_g$. When a photon is absorbed, its energy is taken to excite an electron to the conduction band. Each photon will generate only one electron-hole pair; any excess energy is dissipated as heat [6]. For photons containing less energy than the bandgap, they simply pass through the semiconductor and do not generate any electron-hole pair. Therefore, to absorb the sun's light, where most of the stronger irradiance is in the visible spectrum, a semiconductor material with the appropriate energy bandgap is chosen. This is crucial to taking advantage of the solar spectrum. Using Equation (2.4), for silicon with a bandgap of about 1.11 eV ($1\text{ eV} = 1.6\times10^{-19}$ J) and assuming the speed of light in a vacuum, the maximum wavelength it can absorb is 1.1 μm. This places most of the absorbable photons in the visible spectrum. This is the reason why silicon was a choice in designing the first solar cells. The energy bandgaps for typical semiconductors are listed in Table II-1 [7].

Solar cells made of other materials also satisfy the above condition. As explained in a later section, advanced cells made of multiple layers of material use this property to

absorb as many photons as possible in a wide range of wavelengths. Recent research has led to using photovoltaic cells that convert source energy from other spectra into electrical energy, such as thermophotovoltaic cells (absorbing heat, or infrared rays) [8]. The idea is the same; the material used will be selected specifically to absorb the desired wavelengths.

Material	Symbol	Bandgap (eV)
Diamond	C	5.5
Silicon	Si	1.11
Germanium	Ge	0.67
Gallium Phosphide	GaP	2.26
Gallium Arsenide	GaAs	1.43
Indium Phosphide	InP	1.34
Indium Antimonide	InSb	0.18

Table II-1. Energy bandgap for typical semiconductors. The unit "eV" is electron-Volts, a common unit for describing electron energy (after [7]).

2. Current Generation

A diode alone does not generate external current. Internally, there are drift and diffusion currents, but that is invisible outside of the diode. However, if there is excitation of electrons by some energy source, the excess free electrons will want to flow and create current. The excitation generates electron-hole pairs. Electrons freed in the *n* side will be repelled by the electric field, forcing them away from the depletion region. They will gather at cathode (the *n* terminal). The holes will be swept by the electric field to the *p* side, resulting in excess holes in the *p* side, gathered at the anode (the *p* terminal). If the anode and the cathode of the *p*-*n* junction are connected together through a conductor (short circuit), the excess electrons at the cathode will want to follow the wire toward the anode. The holes will go in the opposite direction from the anode to the cathode, consequently resulting in an external current flow. Because of current direction convention, the direction of current for the solar cell is out of the anode and into the cathode. This current is called the *short-circuit current*, I_{sc} [6]. Note that the solar cell current direction is opposite of that for a regular diode.

The electron excitation source in a solar cell is the photon. Photons with sufficient energy bombarding the cell will generate electron-hole pairs, allowing the above phenomenon to occur. Therefore, when a cell is illuminated, a current I_{sc} is generated.

High temperature will also cause thermal excitation, but the amount is small compared to photon excitation [6].

3. Characterization of Solar Cells

A solar cell is characterized by its current-voltage curve, or *I-V* curve, and the following properties that describe the cell's performance [2]:

I_{sc}	Short-circuit current
V_{oc}	Open-circuit voltage
P_{max}	Maximum output power
η	Conversion efficiency
ff	Fill factor – "squareness" of the curve

The solar cell *I-V* curve is a plot of the output current versus its output voltage under illumination. The plot is very much like that for a diode. For a regular diode, the current-voltage relationship is given by

$$I = I_0\left(e^{V/nV_T} - 1\right) \tag{2.5}$$

where I_0 is the saturation current that is a property of the diode, n is a constant dependent on the diode material, and V_T is the thermal voltage [10]. For a solar cell in the dark, its current-voltage relationship is the same as that given by Equation (2.5). If the solar cell is illuminated, it will generate its own current. At zero voltage (short-circuit), the current generated is simply I_{sc} [4]. Then for an illuminated solar cell, the ideal *I-V* relationship is

$$I = I_0\left(e^{V/nV_T} - 1\right) - I_{sc}. \tag{2.6}$$

The result is the *I-V* curve of the diode translated downward by I_{sc} [4]. The sign in front of I_{sc} is negative because the short circuit current is flowing opposite of the direction of a regular diode. Figure II-3 shows a generic plot of the dark and illuminated *I-V* curves obtained by Equations (2.5) and (2.6) [4]. The illuminated *I-V* curve is in the fourth quadrant of the *I-V* plane indicating that power is being supplied to the load [8].

Generally when speaking of solar cells, the *I-V* plot is reflected about the voltage axis (x-axis) so that the current is considered positive [4]. Then we obtain a typical *I-V* curve looking similar to that of Figure II-4, where the I_{sc} is positive. This is the configuration shown in manufacturer's specification sheets.

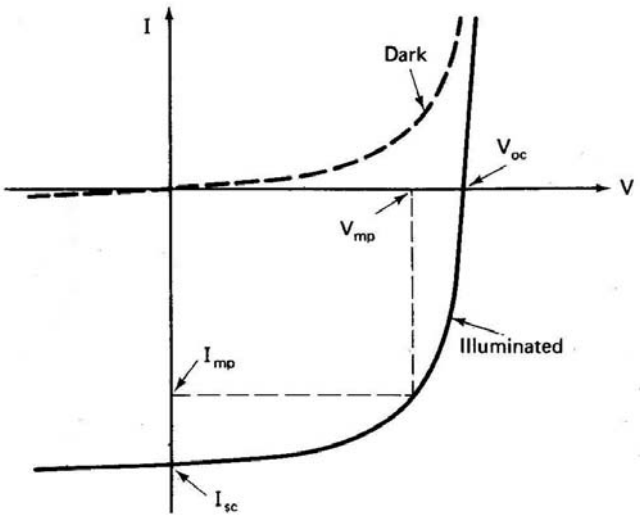

Figure II-3. Output current-voltage relationship for a *p-n* junction when dark and illuminated (After [4]).

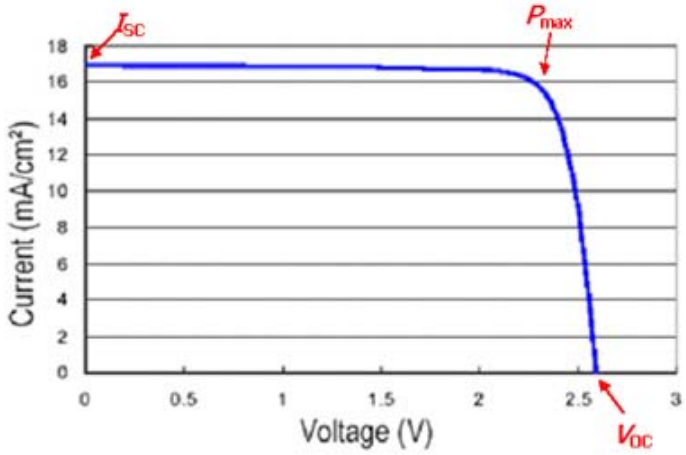

Figure II-4. A sample *I-V* curve for a solar cell with properties marked. In this example, the curve is for a triple-junction solar cell (After [11]).

The *open-circuit voltage* is the voltage across the cell when the output current is zero [4]. Hence, to find the open-circuit voltage V_{oc}, set I to zero in Equation (2.6) to obtain

$$V_{oc} = nV_T \ln\left(\frac{I_{sc}}{I_0} + 1\right). \tag{2.7}$$

Therefore, the open-circuit voltage is dependent on the short-circuit current of the solar cell.

The cell output power is found by $P = IV$, and there is a point (V_{mp}, I_{mp}) that will maximize the output power [4], resulting in

$$P_{max} = I_{mp} V_{mp} . \tag{2.8}$$

This is the maximum power delivered by the solar cell. In typical situations, the load is adjusted so that the cell operates near this maximum power point.

The energy-conversion efficiency depends on the input power. For AM0, the input power would be the solar constant (1.353 kW/m^2). Letting C be the solar constant and A be the area of the receiving surface in square meters, the efficiency η, given in [4], is

$$\eta = \frac{P_{max}}{P_{in}} = \frac{P_{max}}{AC} . \tag{2.9}$$

The final property, the fill factor, ff, is found by

$$\text{ff} = \frac{P_{max}}{V_{oc} I_{sc}} . \tag{2.10}$$

The fill factor is a measure of how "square" the curve is [4]. Typically, the fill factor will be between 0.7 and 0.85 [4].

Finally, a common circuit symbol for the solar cell is a diode symbol with a circle around it, and with arrows pointing toward the diode/circle to indicate light shining on the cell, as shown in Figure II-5. Although there may be other conventions, this symbol will be used for this thesis. Whereas for a diode the current goes into the "fat" end of the arrow (the anode) and comes out of the arrowhead (the cathode), the solar cell's current direction is the opposite [12].

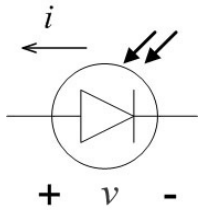

Figure II-5. Circuit symbol for the solar cell. Note the current direction.

4. Factors Affecting the Solar Cell Output

Many factors could affect the performance of the solar cell, including radiation, temperature, light incidence angle, series and parallel resistance, to name a few [4]. For the purpose of this thesis and the tests done on the NPSAT1 SMS, the discussion only includes the effects of temperature and light incidence angle.

If the incident light is perpendicular to the surface of the solar cell, the cell's output will be at its maximum. As the incidence angle deviates from the normal, the output current will decrease. The new value of the short-circuit current, with a light incidence angle θ from the normal (i.e., the angle between the incident light ray and the normal to the cell surface), is $I_{sc}\cos\theta$ [12]. The open-circuit voltage is not strongly dependent on the amount of light received, but does decrease slightly for large angles from the normal. The prediction of current follows well with experimental data for minor θ. As the angle from the normal approaches 60° and above, the current becomes less than the predicted value of $0.5I_{sc}$. This is due to optical refraction and reflection at the surface of the cell, whose effects become important at large angles. This will be demonstrated in the test results.

Studying the effect of temperature is important for solar cells operating in space. The temperature in space swings very widely. The short-circuit current is not strongly dependent on temperature, but it does increase slightly with increasing temperature [4]. The open-circuit voltage, however, is more temperature-dependent.

Green [4] gives an expression for the variation of voltage with respect to temperature. The expression given in [4], stated here without proof, is

$$\frac{dV_{oc}}{dT} = -\frac{\left(E_{g0}/q\right) - V_{oc} + \gamma V_T}{T} \tag{2.11}$$

where E_{g0} is the "linearly extrapolated zero temperature bandgap of the semiconductor" making up the cell, V_T is the thermal voltage, and γ includes the temperature dependencies of the parameters determining I_0 of the cell. Equation (2.11) states that the voltage decreases linearly with temperature. Substituting values for silicon (given in [4] as $E_{g0}/q \sim 1.2$ V, $V_{oc} \sim 0.6$ V, $\gamma \sim 3$, $T = 300$K) gives

$$\frac{dV_{oc}}{dT} = -\frac{1.2 - 0.6 + 0.078}{300} = -2.3 \text{ mV/°C}. \quad (2.12)$$

Hence, one can expect a decrease in open-circuit voltage of 2.3 mV for every degree Celsius (or Kelvin) increase (Figure II-6). The calculation agrees with experimental results and will be shown in the test results.

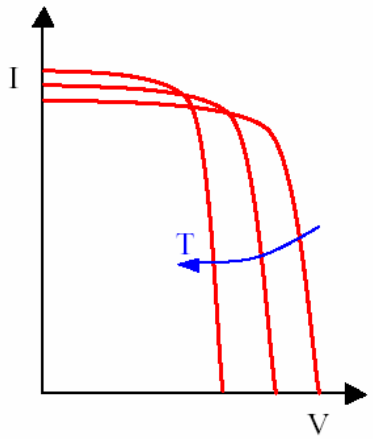

Figure II-6. The effect of temperature on the solar cell's output. Increasing temperature will decrease the open-circuit voltage, while slightly raising the short-circuit current (From [9]).

For a multi-junction solar cell, the effect of temperature is greater. A good estimate is to predict a –2 mV/°C change for each *p*-*n* junction [12]. For a triple-junction solar cell, discussed in the next section, there are three *p*-*n* junctions. Therefore, the triple-junction cell's open-circuit voltage is dependent on temperature by about –6 mV/°C.

5. Silicon and Single-Junction Solar Cells

In a typical silicon solar cell, an *n*-type material sits atop a *p*-type material. The top layer is thin while the bottom layer is thick. Generally, in silicon cells, the *n*-type material is doped with phosphorus and the *p*-type material is doped with boron. To carry current out of the cell, a metal back surface is attached under the bottom layer, and metal contact grids are placed on top of the top layer. At one edge on the top of the cell, a "conductor bus" is mounted where loads may attach to the cell. The bus can be seen in the silicon cells in Figure II-7 (the silver-colored strip on the cell) [11]. The open-circuit voltage on the silicon cell is typically around 0.6 V [1]. The short-circuit current, usually

expressed by milliampere per unit area, will depend on the doping properties of the solar cell.

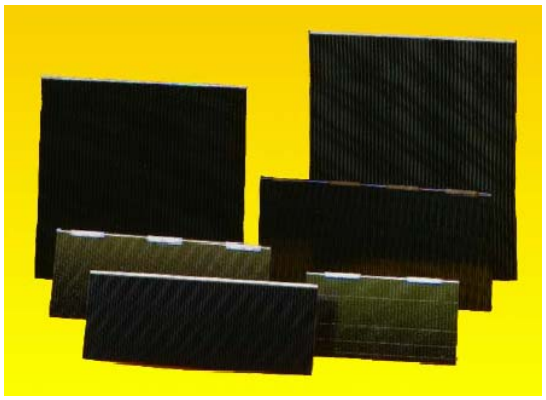

Figure II-7. Examples of silicon cells by Boeing Spectrolab (From [11]).

There are other popular single junction cells such as germanium and gallium arsenide cells. These work similarly to the silicon solar cells, but they have different bandgaps, short-circuit currents, and open-circuit voltages. Germanium has a higher I_{sc} per unit area than other materials, but its V_{oc} is much lower. From Figure II-8, one can see it is a trade-off between I_{sc} and V_{oc} [9].

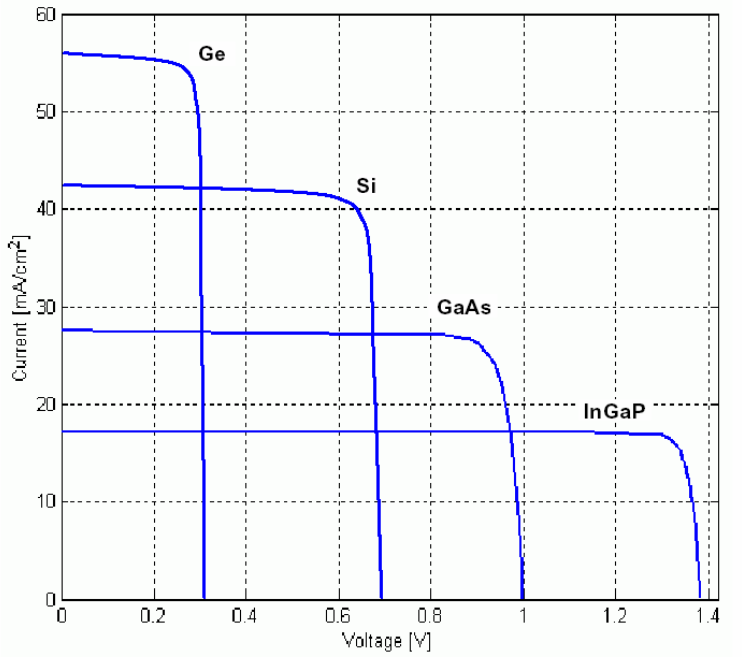

Figure II-8. Typical *I-V* curves for the various single-junction cell technologies (From [9]).

6. Multi-junction Solar Cells

To improve the efficiency of photon absorption, multiple layers of different material can be stacked. Recent advancements have produced multi-junction cells by this method. Present commercially-available multi-junction cells contain two and three junctions. In dual junction (DJ) cells, two *p-n* junctions are stacked on top of one another. For triple-junction (TJ) cells, three *p-n* junctions are stacked. Each of the layers is made of a different material, selected carefully to try to absorb photons in a wide range of wavelengths. The common TJ cells are made of $GaInP_2$/GaAs/Ge layers, with the $GaInP_2$ (higher bandgap) placed on top and Germanium placed on the bottom, depicted in Figure II-9 [11]. The higher bandgap material is placed on top to absorb the higher energy photons while letting the lower energy photos pass into the lower layers. The $GaInP_2$ layer will absorb photons of less than approximately 0.7 μm, the GaAs will absorb less than 0.87 μm, and the Ge will absorb less than 1.85 μm [9]. From this, one can see that the cell will be able to absorb more photons and provide a better efficiency than single junction cells. The tunnel junctions depicted in the figure are inserted to allow the flow of current through the layers, and more information can be found in [9].

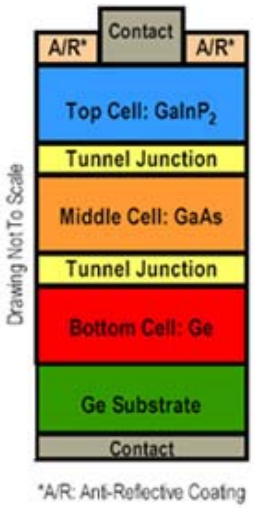

Figure II-9. A simplified cross-sectional view of a triple-junction solar cell (From [11]).

These advanced triple-junction cells can have efficiencies above 25%. Spectrolab's Improved Triple Junction cells, which we use in this thesis for our tests, have stated efficiencies up to 26.8%, while their best space cells, the Ultra Triple Junction cells, have

efficiencies up to 28.3%. The V_{oc} for TJ cells can be between 2.5 V to 2.7 V [11]. For interested readers, Michalopoulos [9] provides an excellent detailed explanation of the structure and operation of a multi-junction solar cell.

This chapter presented a brief introduction to photovoltaic physics. The material included is useful to understand the goal of the NPSAT1 SMS project and will be referred to later in this thesis. The topics discussed here are only an introduction and in no means constitute a rigorous study of solar cell operation or factors that may affect it. Readers interested in a detailed look at solar cell design and physics should refer to [2], [4], [6], or [8]. The following chapter provides a background on the NPSAT1 satellite and the onboard systems to familiarize the reader with the numerous other mission objectives included in the NPSAT1 project.

THIS PAGE INTENTIONALLY LEFT BLANK

III. THE NPS SPACECRAFT ARCHITECTURE AND TECHNOLOGY DEMONSTRATION SATELLITE, NPSAT1

The solar cell and circuit tests in this thesis are part of the design and preflight testing for the Solar-Cell Measurement System (SMS) experiment onboard the NPSAT1. To better understand the experiment and the reason for testing, it is best to have knowledge of the satellite and its mission. This chapter provides a brief background of the satellite and discusses the various experiments onboard. The SMS experiment is presented in detail at the end of this chapter. Further details of the NPSAT1 project can be found in [13], [14], and [24].

A. ORIGINS AND OBJECTIVES

The United States Naval Postgraduate School (NPS) established the Space Systems Academic Group (SSAG) in 1982 in response to the increased focus in space systems by the Department of Defense (DoD). The SSAG is an interdisciplinary group, comprised of faculty members from eight academic departments. It provides guidance for the Space Systems Engineering and the Space Systems Operations curricula at NPS, and oversees various space-related research projects. Its major goal is to pair ongoing research with the graduate education of military officer students.

In 1998, the first satellite of NPS and SSAG, the Petite Amateur Navy Satellite (PANSAT), was launched from the Shuttle Orbiter *Discovery* on Shuttle mission STS-95 into a low-Earth orbit. The PANSAT project was for the academic benefit of NPS students and, as a result, over 50 Master's theses are part of PANSAT's legacy. The value of such hands-on experience for the students was tremendous; it allowed them to be exposed to the development and design phases of a working satellite.

The Naval Postgraduate School Spacecraft Architecture and Technology Demonstration Satellite (NPSAT1) will build on lessons learned from PANSAT. As with PANSAT, this satellite's main objective is to enhance the academic experience for officer students at NPS. NPSAT1 is a low-cost technology demonstration satellite holding several experiments, and the results can give insight for future designs for space applications. The mission is sponsored by the DoD Space Test Program (STP), and NPSAT1

will be one of five satellites on mission STP-1 scheduled to launch on an Atlas V Evolved Expendable Launch Vehicle (EELV) in the fall of 2006.

B. SPACECRAFT ARCHITECTURE

NPSAT1 is an 81.6-kg, twelve-sided, semi-cylindrical satellite, covered with solar panels on each of the 12 faces [13]. Figure III-1 shows a computer model of the satellite. The solar cell array is divided into three rings (each with 12 sides or panels) of equal size: top, middle, and bottom ring. Body-mounted solar arrays were chosen instead of deployable arrays to reduce risk of any malfunction during deployment. Antennas are mounted on both ends of the spacecraft to allow communication in the event that the satellite is not pointing correctly toward Earth. The satellite is three-axis stabilized, controlled by the NPSAT1 Attitude Control System (ACS). It will orbit at 560 km and 35.4° inclination, providing about 16 orbits per day [13,15].

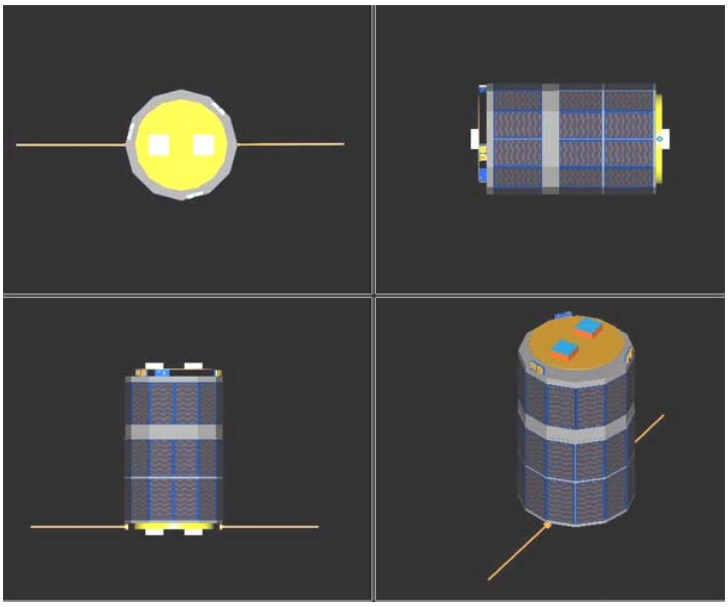

Figure III-1. Computer-generated model of NPSAT1. Note the three "rings" of solar arrays. The middle ring will contain the experimental solar cells (From [16]).

The spacecraft is attached to the launch vehicle using the EELV Secondary Payload Adapter (ESPA). NPSAT1 will be powered off while attached to the launch vehicle, and is powered on upon separation. Communication with NPS ground station will commence shortly after, allowing NPS to determine the spacecraft's status.

C. ONBOARD SUBSYSTEMS

NPSAT1 is expected to operate with a great deal of autonomy. To do so, it contains four major systems onboard: the Command and Data Handler (C&DH), the Electrical Power Subsystem (EPS), the Attitude Control Subsystem (ACS), and the Radio Frequency Subsystem (RFS), along with some mechanical subsystems. Figure III-2 shows an expanded view of NPSAT1 and Figure III-3 shows the block diagram of the subsystems onboard NPSAT1 described in this section. Because the spacecraft is still under development, the system components could still change.

1. Command and Data Handler Subsystem

The C&DH contains various circuit boards connected via the PC/104 bus. It is the brain of the spacecraft, controlling the other subsystems. It contains a motherboard, analog-to-digital conversion circuits, the Configurable Fault-Tolerant Processor experiment (CFTP), RFS components, and data storage. The C&DH uses an Advanced Reduced Instruction Set Computer (RISC) Machine (ARM) processor by Sharp Electronics Corporation (model KEV79520). The processor runs at very low power, which became the logical choice for the limited power available on the satellite. It will use the Linux operating system, chosen for its configurability. Mass data storage will be on a commercial off-the-shelf (COTS) integrated drive electronics (IDE) solid-state drive, similar to a flash memory, with about 256 megabytes of memory for storing all experiment's data and telemetry information [13].

2. Electrical Power Subsystem

The EPS is comprised of triple-junction (TJ) solar cells, lithium-ion (Li-ion) batteries, and control electronics. The solar cells are Boeing Spectrolab Improved Triple Junction[1] (ITJ) cells, commercially-available and space-qualified. The ITJ cells are mounted only on the top and bottom rings of the solar cell array and will provide the spacecraft with power and charge the batteries while NPSAT1 is not in eclipse. Some of the solar cell panels for the top and bottom rings can be seen in Figure III-4. The middle

[1] More information on Spectrolab space-qualified solar cells, including specifications, are at http://www.spectrolab.com/prd/space/cell-main.asp

ring will be covered with new experimental TJ (abbreviated XTJ for the purpose of this document) cells. They too will serve as a power source. Also on the middle ring, on each of the 12 panels, there will be two additional cells mounted separately from the electrical system and used only for the SMS experiment on the satellite. More on the SMS is given in the next section.

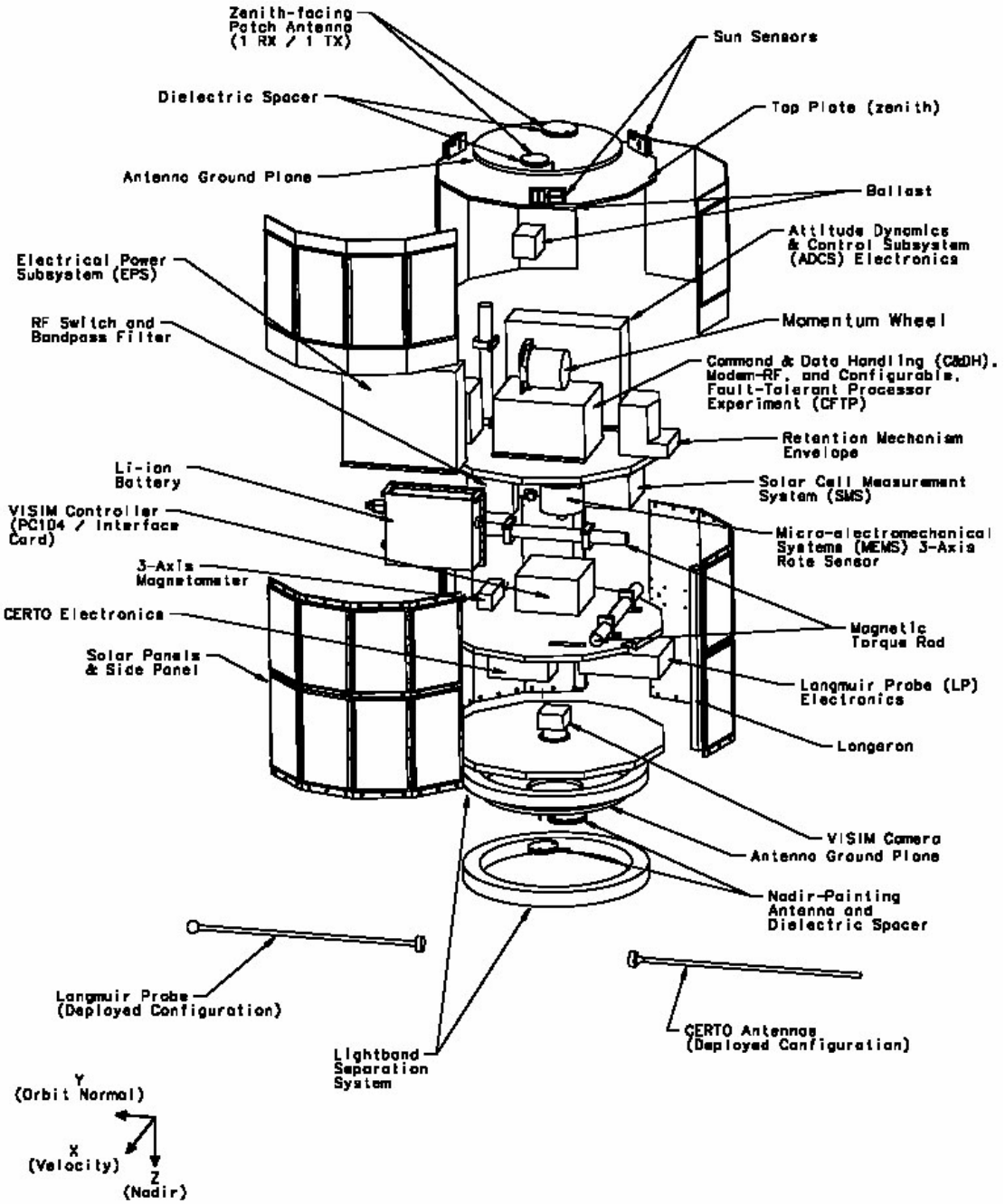

Figure III-2. NPSAT1 expanded view (From [16]).

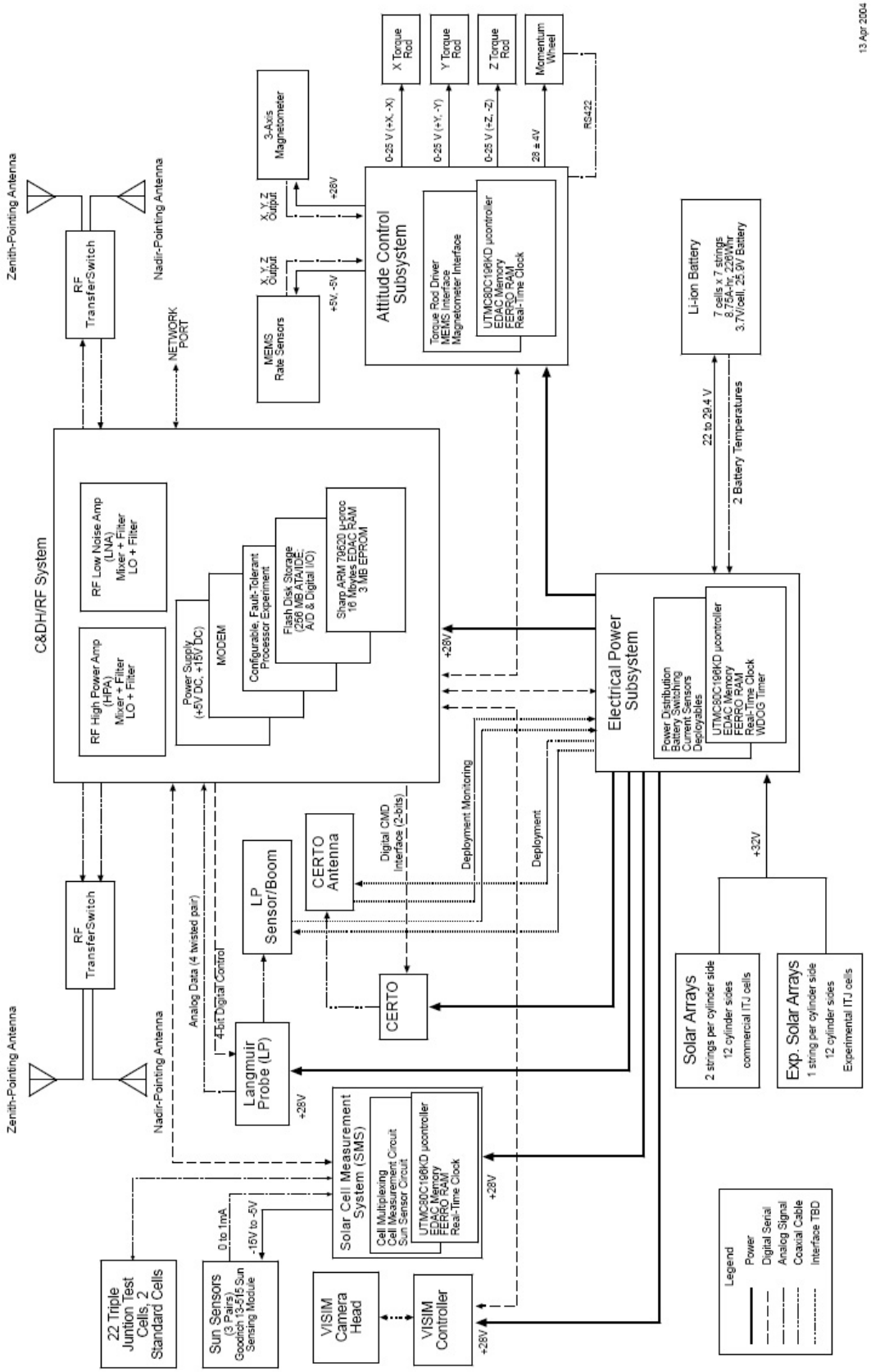

Figure III-3. NPSAT1 block diagram (From [16]).

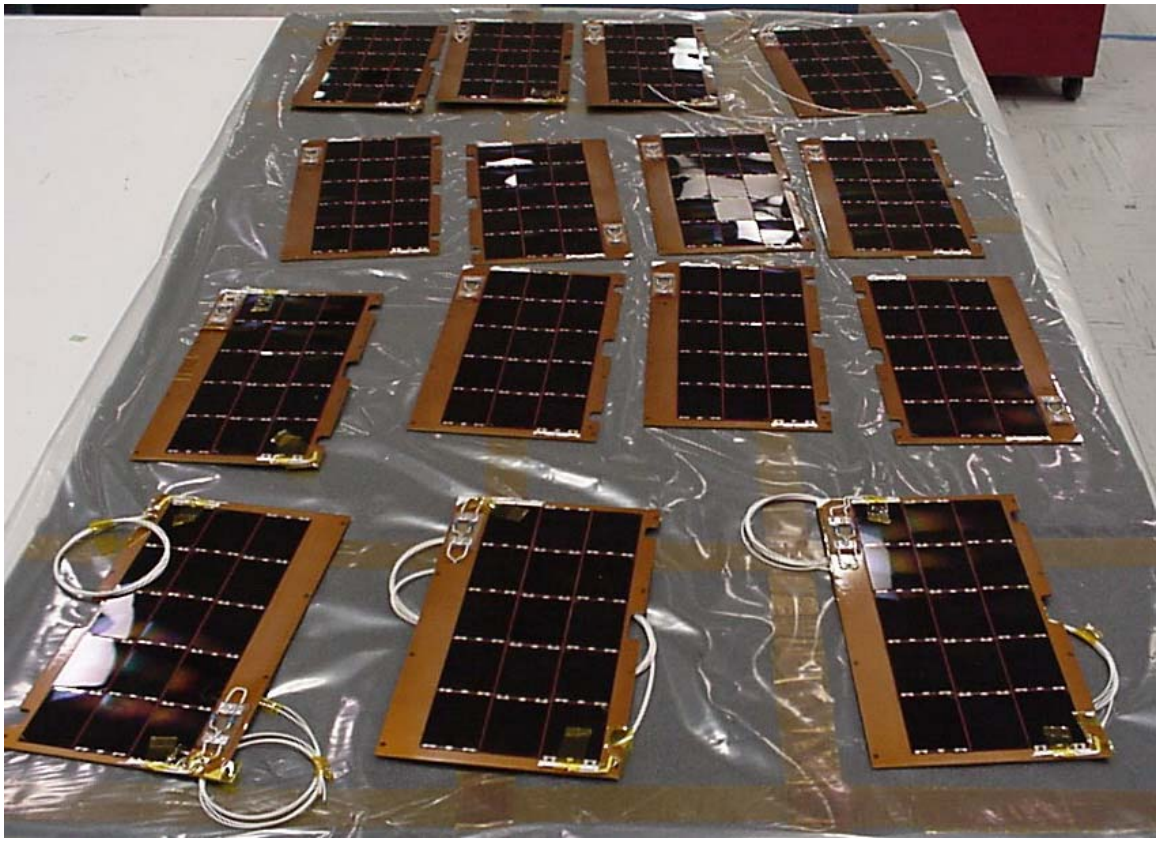

Figure III-4. Some of the solar cell panels for NPSAT1, populated with Spectrolab ITJ cells (photo courtesy of Spectrolab).

3. Attitude Control Subsystem

The ACS provides the three-axis stabilization control for the spacecraft. It consists of magnetic torque rods as actuators, a three-axis magnetometer as the sensor, and the controller. The ACS uses the control algorithm designed by Dr. Barry Leonard [17]. The hardware design of the ACS implements the Leonard algorithm. A momentum wheel is used as a backup for stability. The ACS uses orbit information to obtain the satellite's location. It performs a table look-up for the magnetic field vector at the location, and the control system compares it to the magnetometer measurement. The control algorithm, using torque rods, tries to correct for any difference.

4. Radio Frequency Subsystem

The RFS is a full-duplex system capable of 100-kbps transmission on both uplink and downlink. The system uses the Gaussian Minimum Shift Keying (GMSK) for modulation. The modem is a COTS device and the conversion electronics for the intermediate frequency (IF) will be designed and built at NPS. NPSAT1 will operate at 1767.565 MHz for uplink and at 2207.3 MHz for downlink, using a 70-MHz IF.

D. MISSION EXPERIMENTS

NPSAT1 is a technology demonstration satellite and carries several experiments onboard. These experiments will provide insight for future research.

1. CERTO and Langmuir Probes

CERTO stands for coherent electromagnetic radio tomography, and Langmuir probes are used on rockets and satellites to measure electron and ion densities and electron temperatures in the ionosphere. The CERTO and Langmuir experiments are provided by the Naval Research Laboratory (NRL). The experiment will be used to develop tomographic algorithms for reconstruction of ionospheric irregularities.

2. Configurable Fault-Tolerant Processor (CFTP)

The CFTP is a NPS project, with the goal of designing a triple-modular redundant (TMR) configurable processor able to mitigate single event upsets (SEU). This mitigation is necessary when the processor is used in space, where it resides in a harsh radiation

environment and bits can be flipped unintentionally. It is centered on a field-programmable gate array (FPGA), which has the capability of being reconfigured. For the experiment, the FPGA will be programmed to act as a TMR processor. Currently, the hardware design is complete, and testing is underway. More information can be found in [18] and [19].

3. Visible Wavelength Imager (VISIM)

The VISIM is a COTS digital camera operated by a single-board computer. The camera will be used to take pictures when commanded, but will be powered off for the majority of the time. The camera provides a resolution of 652 x 494 pixels, and, when at NPSAT1's orbit of 560 km, will have a field of view of about 200 x 150 km. The VISIM can create a lossy representation of the image using JPEG at very high compression and transmit these thumbnails to ground station. The ground controller can then decide to download the original, raw (large) data on the next pass.

4. Solar-Cell Measurement System (SMS)

The SMS experiment is the focus of this thesis project. The goal for the system is to gather data from new, experimental solar cells in space. The system will collect *I-V* curves with a timestamp, along with temperature and sunlight angle information.

On NPSAT1, the experimental cells are mounted on the 12 panels of the middle ring. Recall from the EPS description that the solar cells on the middle ring are all experimental triple-junction (XTJ) cells and will be used to provide power. Two additional cells are mounted separately near the top of each panel on the middle ring, wired only to the SMS experiment. Data will be gathered from only those separate cells on the panel, and not from the power-providing cells. Two space-qualified dual-junction (DJ) cells, placed separately from each other on different panels, will act as reference cells. Therefore, for the 12 sides of the satellite, there will be 24 total cells used for the SMS, of which 22 are the experimental TJ cells and two are the DJ cells. Figure III-5 shows a layout drawing of one panel on the middle ring.

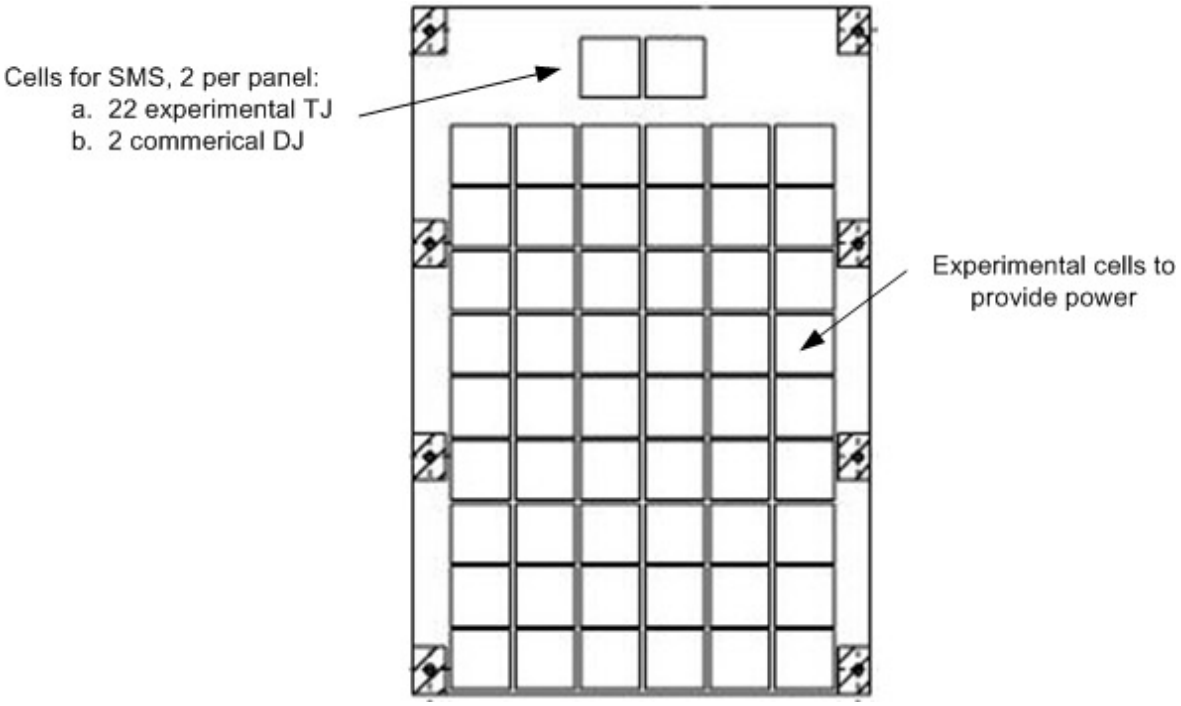

Figure III-5. Layout of one panel of the middle ring of the solar array on NPSAT1 (After [20]).

The SMS consists of an analog subsystem and a digital subsystem. The analog circuit acts as the data gatherer, sensing the voltages, temperature, and sunlight angle. The digital subsystem acts as the controller, and interprets the data given by the analog circuit. Analog-to-digital and digital-to-analog converters (abbreviated A/D and D/A, respectively) are used to interface between the two circuits. A general system block diagram is shown in Figure III-6.

The thesis work ([21]) of Captain John Salmon, USMC, included both the analog and digital portions of the SMS. This thesis and the experiments within will concentrate only on the analog circuit of the SMS, and readers interested in the design of the digital portion should consult Salmon's thesis ([21]) or his technical paper ([15]).

As previously mentioned, this thesis's objective was to perform a preflight performance testing and evaluation of the SMS analog circuit design. Detailed discussion of the actual circuit design and its operation is presented in Chapter V. First, the next chapter describes the testing facility at NPS.

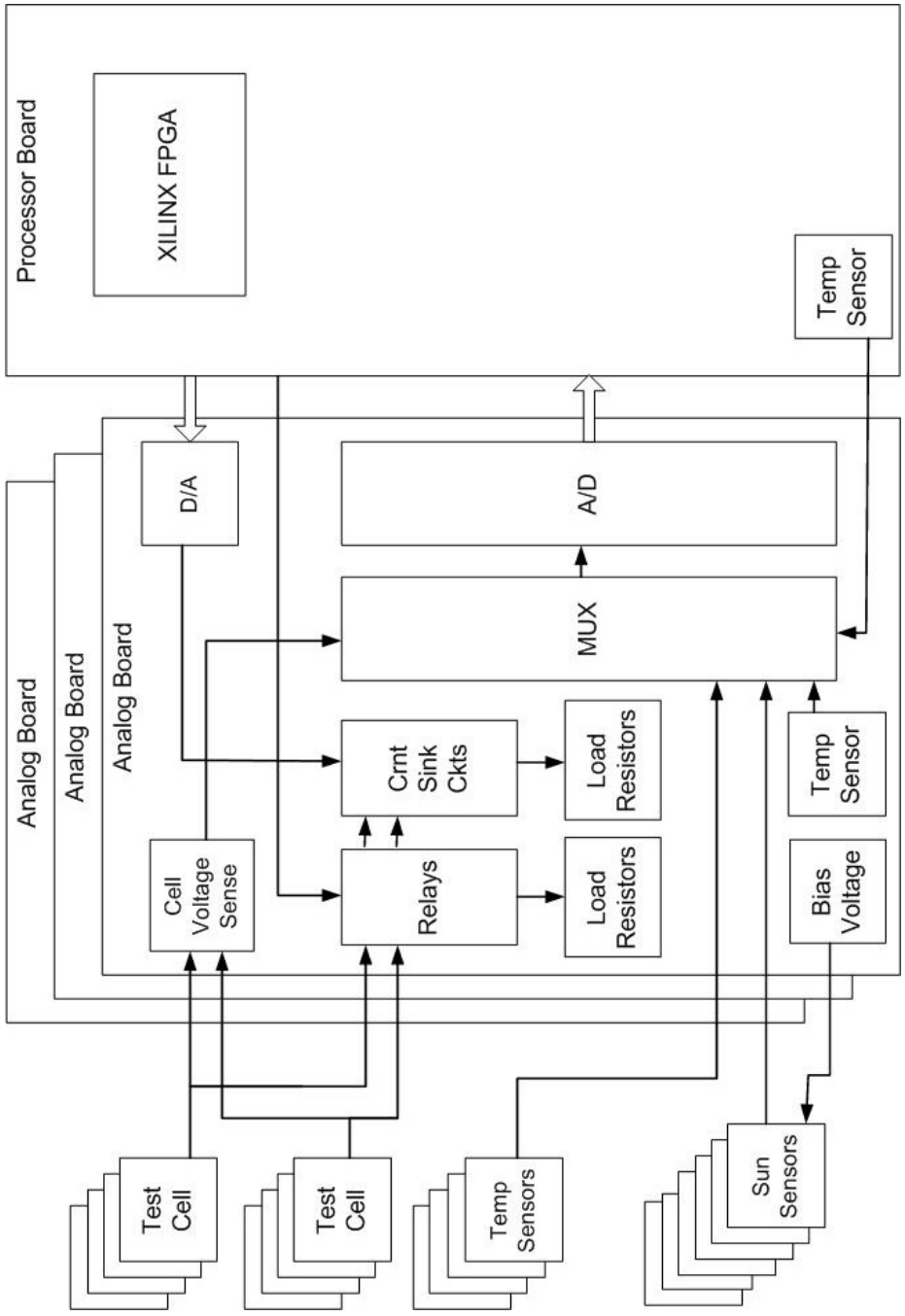

Figure III-6. SMS block diagram (From [21]).

IV. NPS SOLAR SIMULATION AND CELL TESTING FACILITY

The Space Systems Academic Group's Solar Simulation Laboratory at NPS contains equipment for preflight performance testing of solar cells and the cell-measurement circuit. The major component of the Laboratory is the solar simulator and is discussed first. Brief descriptions of other lab equipment follow, but readers are encouraged to consult [21] and [22] for further descriptions of the experimental setup. This chapter introduces the solar simulation facility and the equipment used in taking the experiment control curves, and the following chapter focuses on the operation and testing of the measurement circuit that will be used on NPSAT1.

A. SOLAR SIMULATOR

The Solar Simulation Laboratory has an Optical Radiation Corporation Solar Simulator 1000 (Figure IV-1) that uses a xenon arc lamp to provide light close to AM0 condition. (Recall that AM0 condition is the sunlight outside of the Earth's atmosphere, where the spacecraft will orbit.) The simulator outputs collimated light beams onto an area of about 8 inches by 8 inches, and it has adjustments to simulate light in AM1, AM1.5, and AM2 conditions. It is driven by a regulated power supply with adjustable current control, which controls the lamp's intensity. Light output is controlled by a shutter switch; when it is off, internal mechanisms block the light from shining onto the test surface area.

In the past, one could only hope the solar simulator is performing as expected and as specified in its data sheet. It was expected to output a spectrum close to AM0. However, without a spectrometer, there was no way to measure its actual output spectrum. Past students calibrated the simulator by adjusting the intensity of the light so that the I_{sc} of a *reference cell* matched the known AM0 I_{sc} for that cell. The intensity of the simulator can be adjusted by changing the current supplied to the simulator, but matching I_{sc} is not a complete solution for calibration. Because different materials absorbs only a certain region of the light spectrum, matching the I_{sc} for, say, a gallium arsenide cell, does not indicate if the spectrum outside of the GaAs effective wavelengths is close to AM0.

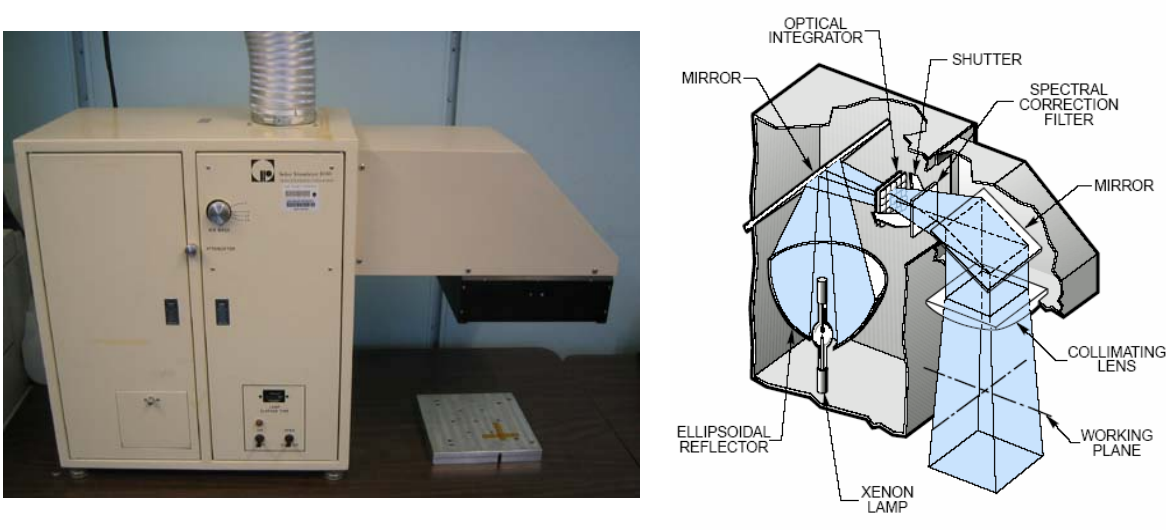

(a) **(b)**

Figure IV-1. (a) Optical Radiation Corporation Solar Simulator 1000 at NPS; (b) Light path inside the solar simulator (From [4]).

1. Solar Simulator Calibration

A spectrometer was procured to verify the operation of our solar simulator. The spectrometer, sometimes called a spectroradiometer, is a radiometric device that detects and measures the intensity of a radiant energy. The Ocean Optics HR2000CG-UV-NIR High-resolution Miniature Fiber Optic Spectrometer (Figure IV-2a) provides detection in the range of 200 nm to 1100 nm. The spectrometer connects to a computer via a Universal Serial Bus (USB) cable, and software interprets the data from the spectrometer and presents it to the user. A fiber optic cable attaches to the spectrometer and is placed under the light source, using a custom-made stand to hold the fiber parallel to the light beam (see Figure IV-2b). For our purpose, to handle the intensity of our solar simulator, a 200 μm fiber was used (a wider fiber is used for lower intensity sources, and vice versa). A cosine-corrected fiber optic irradiance probe (Ocean Optics model CC-3-UV) was also attached at the receiving end of the fiber. The probe, commonly called a cosine corrector, is designed to collect light in a near-180° field of view. It is used so that placing the fiber exactly parallel to the light beam is not necessary. It has a Teflon® diffusing material at its tip, optimized for wavelengths of 200 nm to 1100 nm. Figure IV-3 shows the cosine corrector attached to a fiber optic cable.

(a) **(b)**

Figure IV-2. (a) Ocean Optics HR2000CG spectrometer; (b) fiber optic cable holder[2].

Figure IV-3. Fiber optic cable with cosine corrector attached at its tip (the black/white item at the end of the cable). The white element is the Teflon diffusing material (From [23]).

Before the spectrometer's first use, it must be calibrated using a calibration light source. This is required before being able to measure the absolute irradiance of a source using the spectrometer. Recalibration should be performed after about 50 hours of use to ensure accuracy.

[2] Fiber holder designed by Andrew Miller at the Naval Postgraduate School

The Ocean Optics/Micropack DH-2000-CAL Deuterium Tungsten Halogen Calibration Standard (Figure IV-4) is an ultraviolet (UV), visible (VIS), and near-infrared (NIR) light source used to calibrate the absolute spectral response of a spectrometer. It has two calibration lamps to provide calibration from 200 nm to 1050 nm, which spans the UV, visible, and the lower part of the IR spectra. The deuterium lamp is used for calibration of wavelengths of 200 nm to 400 nm, while the tungsten halogen lamp is for 400 nm to 1050 nm. To calibrate the spectrometer, the fiber optic cable is inserted into the covered hole on the front of the lamp unit. The DH-2000-CAL is shipped with factory calibration data to be used in the calibration and measurement software, and the lamp itself requires calibration after every 50 hours of use.

Figure IV-4. Ocean Optics DH-2000-CAL calibration lamp. The metal cover toward the lower right is covering the fiber cable insertion hole.

The software used to calibrate and analyze data from the spectrometer is Ocean Optics OOIIrrad-C. The application uses the spectrometer's calibration setting to interpret the raw data and displays the absolute irradiance of a light source. It also allows the user to export the data to a file, permitting the user to open it in a spreadsheet application such as Microsoft Excel and create a plot. The OOIIrrad-C displays data in real-time. Excerpts from the OOIIrrad-C user's manual, including instruction on the calibration procedure using OOIIrrad-C, are given in Appendix B. The calibration results and the solar simulator spectrum are presented in the following sections.

2. Spectrometer Calibration

Without a calibration, the user will only be able to see raw data from the spectrometer in *Scope Mode*. In this mode, the y-axis is labeled in *intensity counts*, but it is not very meaningful. This count is relative for each spectrometer, and is different between one spectrometer and another. Each time a detector pixel in the spectrometer gets enough photons, it generates a *count*. The number of counts is related to the number of photons falling on the pixel, as well as the response of the detector material to that given wavelength. (The silicon detector response varies by a factor of 100 times over the entire range.) Before the photons reach the detector, however, they hit a grating, which disperses the light. This grating reflectivity also varies with wavelength. When acquiring data in scope mode, the spectrum plot shown has been modified in shape by both the grating and detector, so it might not look anything like the actual irradiance plot. In order to correct these effects, it is necessary to measure a reference source of known spectrum. This is where the DH-2000-CAL is used.

A *calibration curve* is produced after calibration (see Appendix B for calibration procedures). This is a graph of the conversion factor, used by the program to convert "counts" to a meaningful unit (Watt or Joule). After several attempts in calibrating the spectrometer, it soon became apparent that the entire system was susceptible to noise. Tall spikes appeared in the calibration curve around the 1000 nm region during calibration and caused errant irradiance readings. A few attempts at recalibration had lowered the noisy spikes, and the best calibration result was used. Figure IV-5 shows the result of a satisfactory combined calibration for both the UV and VIS spectra.

The top graph in the figure shows the factory data for the calibration lamp, which in this case is the halogen calibration lamp. The middle graph shows the result (in "counts") from the spectrometer after a scan of the calibration lamp. Using those two plots, the calibration curve is produced to show a conversion factor for each wavelength. Ocean Optics technical support explained that noise is inevitable at the limiting wavelength regions of the spectrometer, near the 1000 nm range. The detector at that point has a weak response, and is susceptible to noise. Therefore, data at the limits of the spectrometer should not be taken too literally.

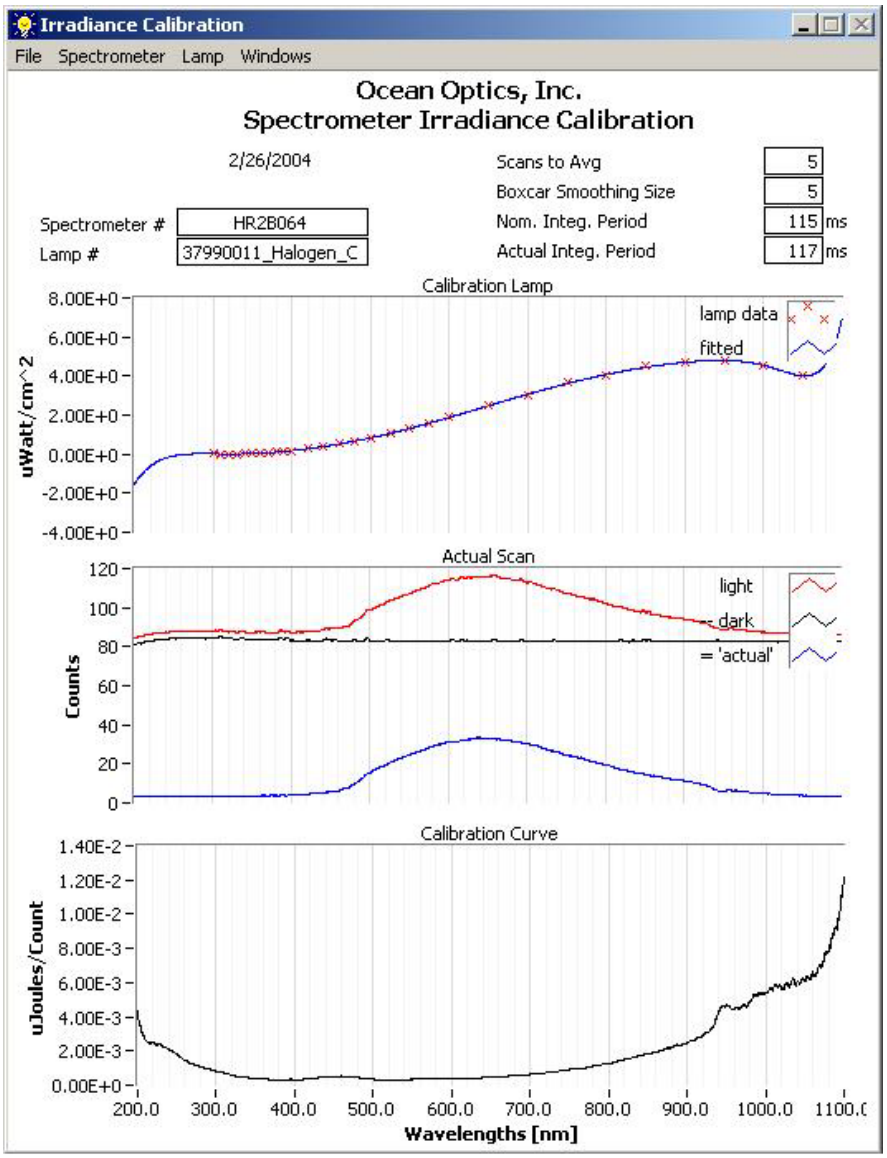

Figure IV-5. The calibration setting used for finding the spectrum of the solar simulator. The calibration curve (bottom graph) converts *Counts* to micro-Joules. The curve shown here is a result of combining the UV and Visible spectrum calibration data of the deuterium and halogen lamps.

What also seemed to have caused problems was the dark scan. The dark scan is taken by blocking all light to the spectrometer and taking a scan. This establishes a base-line reference for the calibration. However, the baseline for the spectrometer seems to drift over time. Dark scans taken over two days showed differences. Ocean Optics also explained that the spectrometer tends to drift since it is a charge-coupled device (CCD).

3. Obtaining the Spectrum of the Simulator

With the spectrometer correctly calibrated (or to the best ability) for the spectrum region in which we are interested, it was ready to take irradiance measurements. The simulator should be allowed to warm up (about 15 minutes) to reach stability before taking any measurements.

The fiber cable, with the cosine corrector attached on the receiving end, was placed under the solar simulator with its tip pointing at the light source using the fiber stand. The fiber was placed as closely in the center of the lit area as possible because there are slight intensity variations at the outskirts of the illuminated area. A snapshot of the spectrum was taken and exported to Microsoft Excel for analysis. A graph of the simulator's measured spectrum plotted with the AM0 spectrum is shown in Figure IV-6. As mentioned before, the intensity of the simulator can be adjusted by changing the current supplied to the simulator. For the simulator spectrum shown in Figure IV-6, the current was adjusted to match as closely as possible the irradiance of the simulator to AM0 in the visible spectrum. The spikes at the higher wavelengths were expected from the manufacturer's data, but the spikes here are higher than expected due to the noise in calibration.

There is a noticeable drop in the simulator irradiance below the AM0 standard between 700 nm and 800 nm. It is understood that no solar simulator can replicate AM0 conditions exactly in the entire spectrum, and the spectrometer calibration can drift over time. Comparing to the simulator specification data and spectrum, the gap around 700 nm seems to be normal. This drop is also present in the expected output spectrum given by the simulator manufacturer, although not as wide as is shown in this spectrum. With what equipment was at hand, the simulator has been adjusted by the current supplied to the simulator to the best duplication of AM0 as possible.

Thus with the arrival of the spectrometer, it is now possible to see a close approximation of the spectrum given by the solar simulator. Whereas in previous research the calibration procedure involved using a reference cell's known I_{sc} at AM0 and adjusting the power supply to the simulator to obtain the same I_{sc} on that cell, the ability to take the spectrum of the simulator provides a much more accurate and meaningful way to adjust and calibrate the simulator to better simulate AM0.

One important thought to note is that obtaining a good replica of the AM0 spectrum for the tests performed in this thesis was not necessary. The goal was to compare the performance of the SMS circuit against an experiment control (the control will be discussed in the next section). As long as the solar cell is illuminated by the same spectrum of light when taking *I-V* curves by the SMS and the experiment control, it does not make much difference if the spectrum were a perfect AM0. AM0 replication is important when attempting to gather the expected performance of a solar cell in space, which is not the goal here. If in the future the Laboratory needs to perform that task, the simulator will have to be adjusted to provide a better approximation of AM0. One possibility is to use optical filters on the lamp.

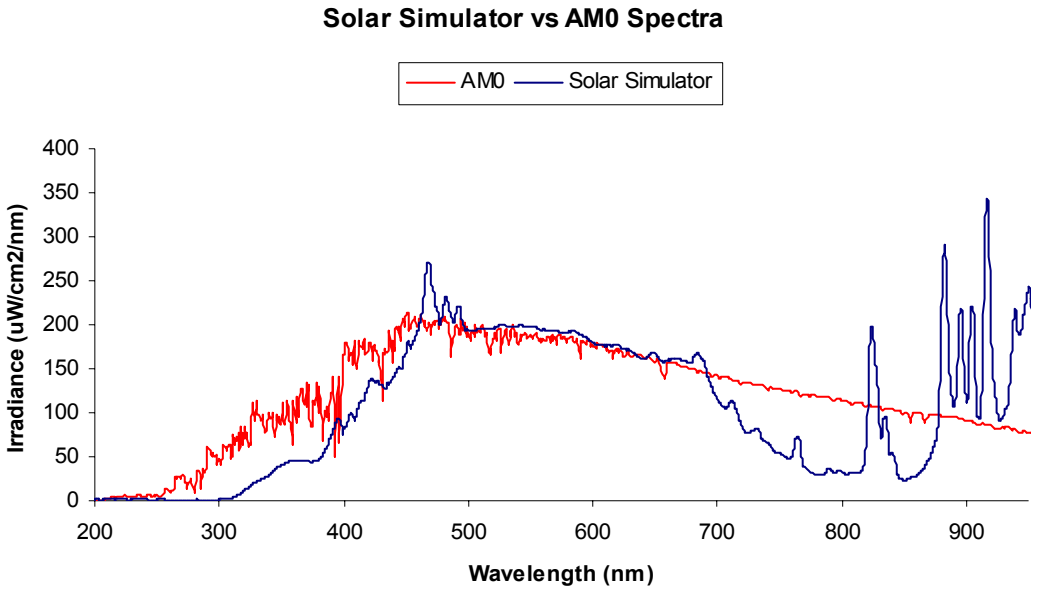

Figure IV-6. The spectra of AM0 and Solar Simulator. Note the drop in irradiance by the simulator around 700 to 800 nm (AM0 data from DoE/NREL).

B. MEASUREMENT EQUIPMENT

Several other hardware and software work together to trace an *I-V* curve for a solar cell. While many items were in this system, it is a relatively simple system. The hardware description is given here, and tracing an *I-V* curve using LabVIEW Virtual Instruments (software) is discussed in the next section.

1. Temperature Control

The temperature of the solar cell under illumination is controlled by a chilled-water loop system. The Forma Scientific CH/P Temperature Control System Bath and Circulator Model 2067 acts as the cool-water reservoir, working with the ThermoHaake DC-10 temperature control unit to maintain a selected water temperature [22]. The two devices are shown in Figure IV-7. The water is routed through the solar cell mounting plate, acting as a coolant. Because of the intense heat from the lamp, the temperature of the coolant needs to be set to several degrees below the desired temperature on the plate. The current setup can give a minimum cell mount temperature (while illuminated) of approximately 18°C to a maximum beyond 40°C, which is sufficient for the our experiment.

Figure IV-7. The Forma Scientific (left) and ThermoHaake (right) water temperature controllers.

2. Variable Angle Cell Mounting Plate

The coolant hoses are connected to a custom-made mounting plate that holds the solar cell being tested. Taken from the concept of a mounting block used by The Aerospace Corporation[3] and implemented by SSAG engineer Ron Phelps and intern Tara Holz, this plate is an improved version of the mounting fixture used in previous experiments at SSAG. The new plate, shown in Figure IV-8, allows for the angle of the cell's surface toward the light to be varied, thereby changing the angle of incidence of the

[3] The mounting block concept was brought to NPS by John Nocerno of The Aerospace Corporation on a visit to the NPS Solar Simulation Laboratory in June 2003.

sunlight on the cell. The plate also has new mechanisms for four simultaneous contact probes on the top side, versus only one probe in the previous version, thereby reducing series wire resistance. The leads from the probes connect to the curve tracer. The holes visible on the plate are vacuum holes. A vacuum pump is connected to the plate via a hose, to hold the test cell down onto the plate for better contact between the back electrode of the cell and the plate, which is acting as a probe. The location of the holes allow for larger size cells to be tested. In Figure IV-9, a 2 cm by 2 cm cell is shown mounted on the plate with measurement probes in place on the solar cell conductor bus. Unused vacuum holes are covered.

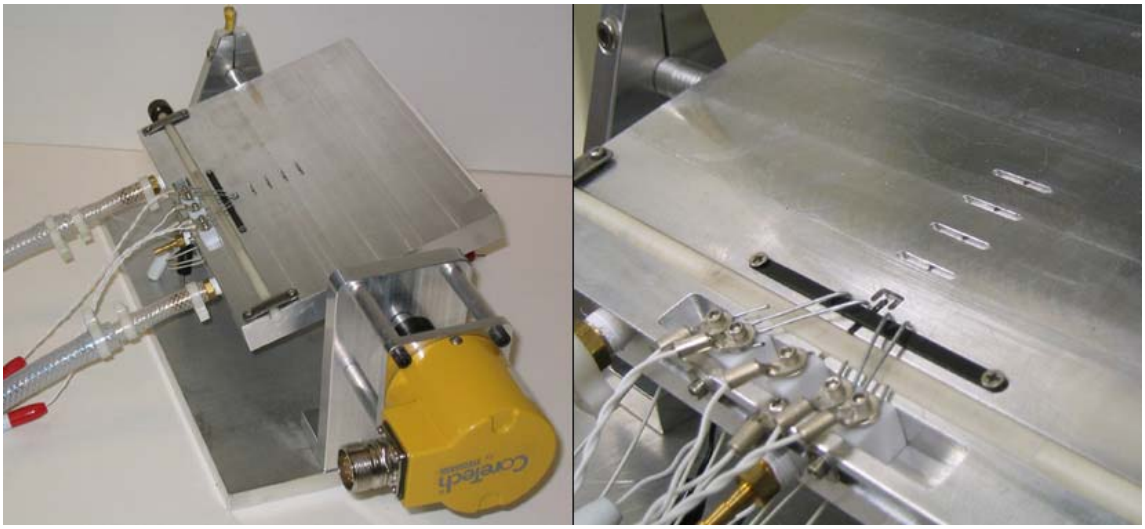

Figure IV-8. Variable angle cell mounting plate, made in-house at NPS (left); Close up of the plate, showing the probes (right)

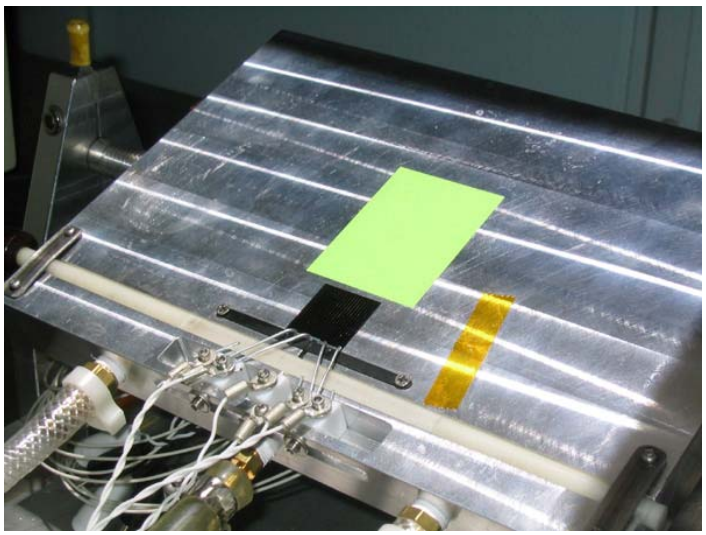

Figure IV-9. A test cell is shown here placed on the mounting plate. The extra vacuum holes have been covered.

3. I-V Curve Tracer – The Experiment Control

Experiment control curves were taken using the Hewlett-Packard 6626A power supply, shown in Figure IV-10. The power supply is capable of supplying power and being a voltage and current sensor. It can be controlled by computer software through its IEEE-488 General Purpose Interface Bus (GPIB). For this experiment, the power supply is controlled by a LabVIEW program.

Figure IV-10. The Hewlett-Packard 6626A power supply.

The power supply has four channels, and two of them were used for solar cell *I-V* curve measurements. Channels 1 and 2 are connected in series, with Channel 1 acting as the sensing probe and Channel 2 set to bias the cell to 4 V. The bias allows the power supply to measure accurately small voltage changes on the solar cell. Choosing 4 V was arbitrary; other reasonable bias voltage values can be used. In tracing a curve, the software directs Channel 1 to set a voltage on the test cell, and then sense the current through the cell. This is repeated for each desired voltage increment from a chosen starting voltage to the ending voltage. (The determination of the ending voltage, which is the cell's V_{oc}, is discussed in the next section.) The power supply reports the voltage and current data back to the computer. Figure IV-11 shows the connections between the power supply and the solar cell under test. Appendix C provides instructions for the necessary settings to trace an *I-V* curve using the HP6626A.

When connecting the solar cell to the power supply, care must be taken with the polarities. Reversing the polarity connection can seriously damage the cell with reverse

bias voltage. While silicon cells can withstand some reverse bias, the same is not true for multi-junction cells.

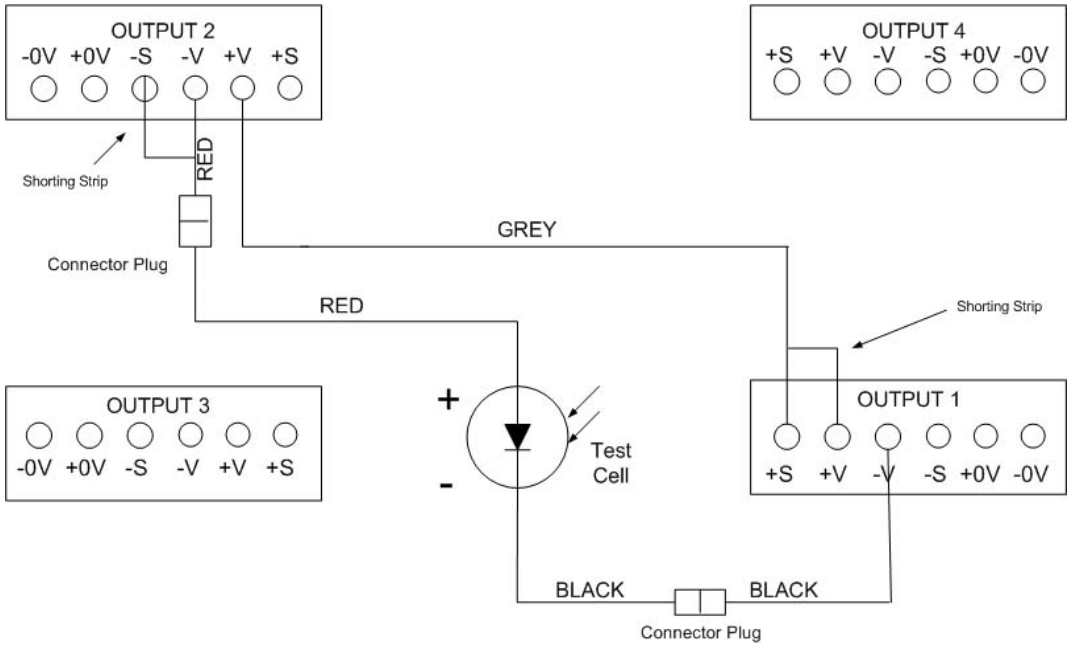

Figure IV-11. A diagram of the back of the HP6626A, showing the connections to the test cell. The "S" terminals are for sensing. Channels 3 and 4 are unused.

Figure IV-12 demonstrates the setup when a test is being conducted, to give the reader a sense of how the equipment is used.

Figure IV-12. The solar simulator setup, with the cell mounting plate illuminated. The measurement equipment sits to the right.

C. TRACING A CONTROL I-V CURVE: USING HP6626A WITH LABVIEW

As discussed previously, the HP6626A power supply can be controlled via the GPIB interface. A LabVIEW program[4] was written to use the HP6626A to trace an *I-V* curve for a solar cell. First, a discussion about LabVIEW is necessary to understand the function of these programs.

1. LabVIEW

National Instrument Laboratory Virtual Instrument Engineering Workbench, or LabVIEW for short, is a graphical programming environment popularly used in engineering. It is analogous to traditional text programming languages, but LabVIEW does not require much text. LabVIEW relies completely on a graphical interface where *nodes* are wired together, and the program compiles and checks the graphical code in real time. These nodes can perform various tasks or calculations (such as arithmetic or Boolean algebra calculations). A piece of LabVIEW code would look similar a complicated block diagram or flow chart. In the end, the programmer constructs a user interface to provide for data input and output, much like instrument panels on typical laboratory equipment. Hence, the written program acts like an instrument and is called a *Virtual Instrument* (or VI).

Often times a VI contains calls to *subVI*s. The subVIs are simply VIs that do tasks for the calling VI, similar to a traditional C++ program calling on a function. In the VI that controls the power supply for tracing an *I-V* curve, a specific subVI is called to communicate with the HP6626A model. What follows is a description of only the top-level VI that performs the task of *I-V* curve tracing; the lower-level details of GPIB communication are omitted.

2. The HP6626A Virtual Instrument for I-V Curve Tracing

Figure IV-13 shows the user interface for the main VI to trace the curve using the HP6626A. The VI allows the user to input the starting and ending voltage to sweep, and a voltage increment. The starting voltage should be the value to which Channel 2 is set

[4] The original author is unknown. The original code was modified to correct an error and improve efficiency.

as the bias voltage. The user will have to input the ending voltage based on the knowledge of the material of the cell under test; it is the cell's nominal open-circuit voltage V_{oc} plus the bias voltage. For example, to trace a silicon cell, the user should enter 4 V as the starting voltage, and 4.63 V for the ending voltage, based on silicon solar cells' nominal V_{oc}. The graph preview area shows the collected data points after a trace.

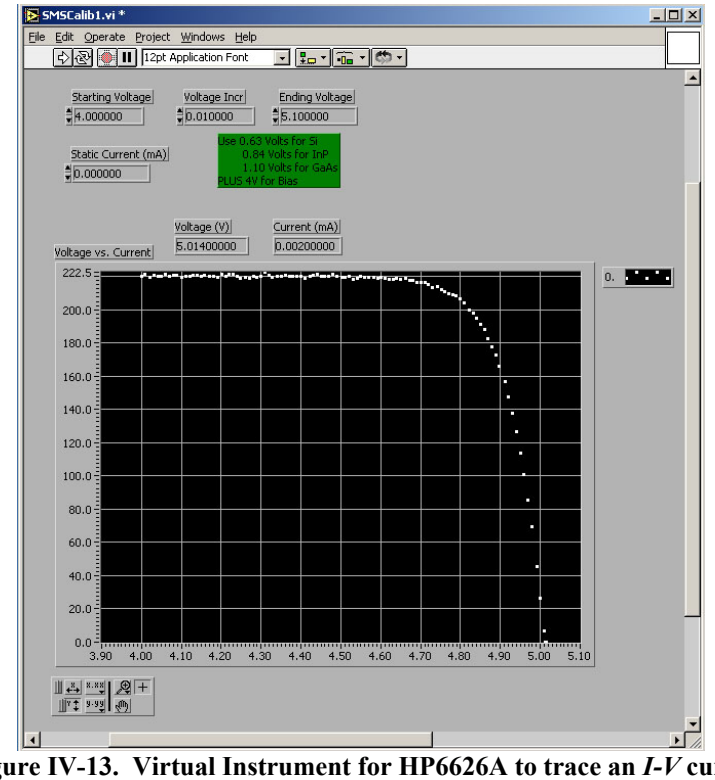

Figure IV-13. Virtual Instrument for HP6626A to trace an *I-V* curve.

As the power supply is told to step through the voltages, internal circuitry of the power supply senses the current through the cell. The voltage-current data pair is recorded in a file specified by the user, allowing it to be used in Microsoft Excel. Figure IV-14 shows the graphical LabVIEW code behind the main VI. The VI directs the power supply to sweep the *I-V* curve from I_{sc} (0 V) to V_{oc}. While the starting voltage entered into the VI is not 0 V – it is the bias voltage – the sweep is starting at 0V with respect to the solar cell. Because the sweep starts at 0 V and the maximum voltage on the cell can only be V_{oc} at 0 A (going lower, or negative, in current would require a higher voltage than V_{oc}, which is impossible), there is no danger of reverse biasing the cell, provided that the connections from the HP6626A to the cell is proper.

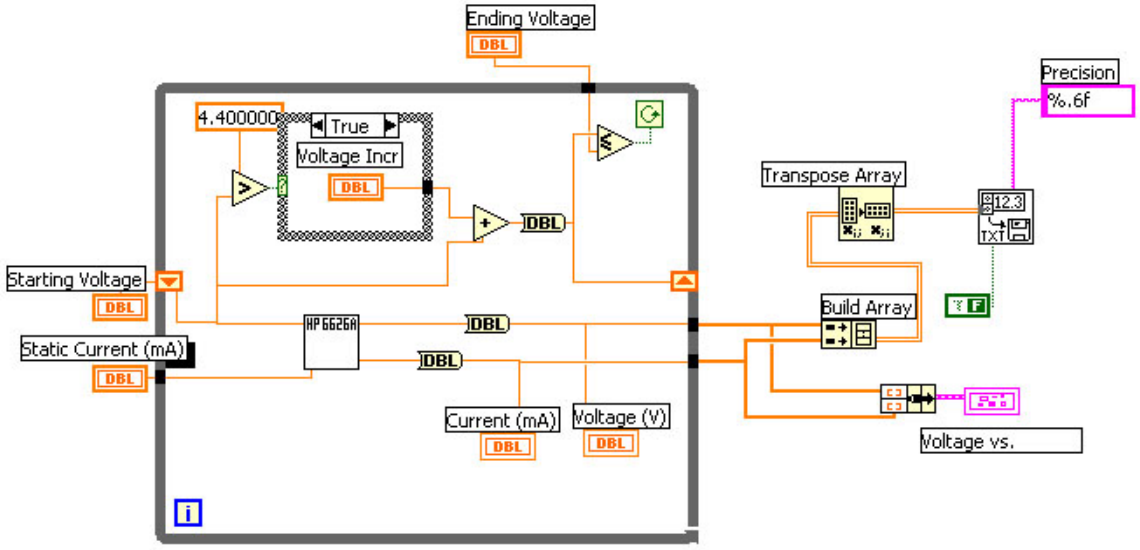

Figure IV-14. The LabVIEW graphical code for the HP6626A main VI to trace an *I-V* curve.

This VI is only used with the HP6626A power supply to trace an *I-V* curve. The HP6626A serves as the control in the experiment. Recall that the goal is for the *I-V* curves taken by the experimental measurement circuit to match closely to the curves obtained by the HP6626A in various environments.

The NPS Solar Simulation Laboratory contains all the necessary equipment to test solar cells. The solar simulator provides a near-AM0 illumination for the cells, and the HP6626A measures the cell output performance. It is, however, impractical to launch the measurement equipment, such as the HP6626A, with the satellite to measure the experimental cells in space. The next chapter introduces the design and testing of the cell measurement circuit to be used on NPSAT1.

THIS PAGE INTENTIONALLY LEFT BLANK

V. THE SMS ANALOG SUBSYSTEM, TESTING, AND RESULTS

We return to the Solar-Cell Measurement System (SMS) in this chapter to examine the analog circuit in the analog subsystem. The system is discussed in detail here, including the operation of the analog circuit. The test platform is then presented, and a more detailed description of the tests and procedures is discussed. The results of the tests are analyzed in the final part of the chapter.

A. THE SOLAR-CELL MEASUREMENT SYSTEM – THE ANALOG SUBSYSTEM

1. Origins

The idea of developing a solar cell measuring circuit came out of the need of a simple and portable method to do so in space. While it is easy to trace a curve on the ground using a device similar to our HP6626A power supply, it is more challenging to do it in space.

The origins of the concept for the SMS date back to the mid-1980s. In 1986 at NPS, LT Robert Callaway, USN, and Professor Sherif Michael developed a novel circuit to trace the *I-V* curve of a solar cell [1]. In his thesis, Callaway controlled the circuit by using a simple digital system where it stepped through the current while measuring the voltage. The Callaway circuit is shown in Figure V-1.

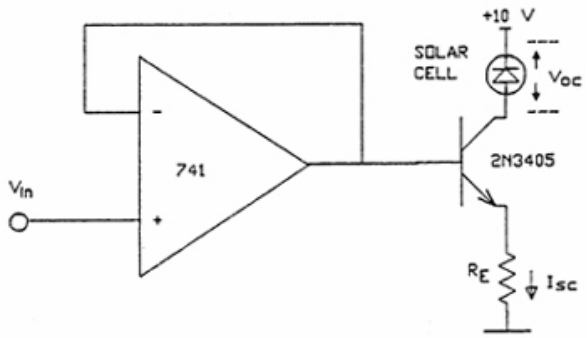

Figure V-1. The Callaway current-sink circuit (From [1]).

The Callaway circuit is set up to be a current sink; the transistor and other components pull a current through the solar cell. The op amp is configured to be a voltage follower or a buffer, placing V_{in} at the base of the transistor. If we assume the common-

emitter current gain β is large, the current through the cell (labeled I_{sc} in the figure) is related to V_{in} by

$$I_{sc} = \frac{V_{in} - V_{BE}}{R_E} \tag{5.1}$$

where V_{BE} is the base-emitter voltage for the transistor [1]. Therefore, the user can set a desired current through the solar cell, and measure the voltage across the cell using, for example, a voltmeter. This is repeated by stepping through the current until getting to I_{sc} and the *I-V* curve is completed.

Michael later improved the circuit by using feedback to control the current. The Michael circuit, with minor updates in device technology, serves as the basis for the SMS.

2. Operation of the SMS Analog Circuit

The SMS analog circuit, an update of the Michael circuit by Phelps and Salmon [15], is shown in Figure V-2. The circuit is only for measuring one solar cell. Recall from earlier descriptions that the mission will have 24 cells set aside for curve tracing. Therefore, the complete analog subsystem will contain 24 of these circuits, one for each solar cell under test.

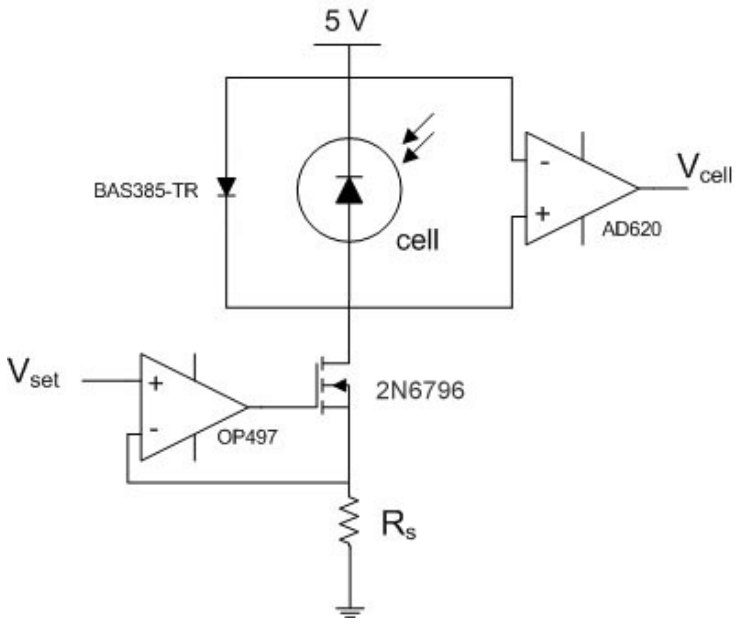

Figure V-2. SMS analog circuit for one solar cell under test.

The circuit uses an *n*-channel MOSFET (also called an NMOS transistor) with a feedback loop. It is also a current sink and works similarly to the Callaway circuit. An input voltage, V_{set}, is set on the non-inverting terminal of the OP497 op amp on the left in Figure V-2. Setting a voltage V_{set} pulls a current of V_{set}/R_S through the solar cell. The initial (small) difference in voltage between the terminals is highly amplified and placed on the gate of the NMOS transistor. The voltage difference between the gate and the source of the NMOS will be greater than the threshold voltage, turning on the transistor. A current starts to flow through the cell, the NMOS, and the resistor until the desired value of V_{set}/R_S. The feedback loop ensures the flow of the desired current. An instrumentation amplifier (AD620B), with very high input impedance (on the order of giga-Ohms), is used to measure the voltage across the solar cell. With its gain set to unity, the output of the AD620B is simply the difference in voltage between the input terminals, which is the voltage across the solar cell.

A diode is placed across the solar cell as a measure of protection against reverse bias. In the unintentional case that more current is driven through the solar cell than the cell's I_{sc}, a negative voltage will appear across the cell, reverse biasing the cell. In such case, because the polarity of the diode is connected opposite of the cell, the protection diode turns on when a large enough negative voltage appears across the solar cell and prevents a build-up of the negative voltage. Reverse bias can cause irreparable damage on multi-junction solar cells.

3. Integration of the Analog and Digital Subsystems

Ron Phelps and Capt John Salmon, USMC, began work on the SMS design to include the Michael circuit and a digital controller. The design process is described in [15] and [21]. In addition to the analog subsystem, the SMS also contains a digital subsystem. The digital subsystem is the system controller. It sets the voltage on the analog-circuit input to drive a desired current through the cell. It also takes the output of the analog circuit, and stores it into memory. Figure V-3 shows a simplified diagram of the analog circuit with the digital controller. The diagram shows the concept for one cell being measured. In comparison to the test setup in the Solar Simulation Lab, the digital system is like that of the computer and LabVIEW VI controlling the HP6626A power supply.

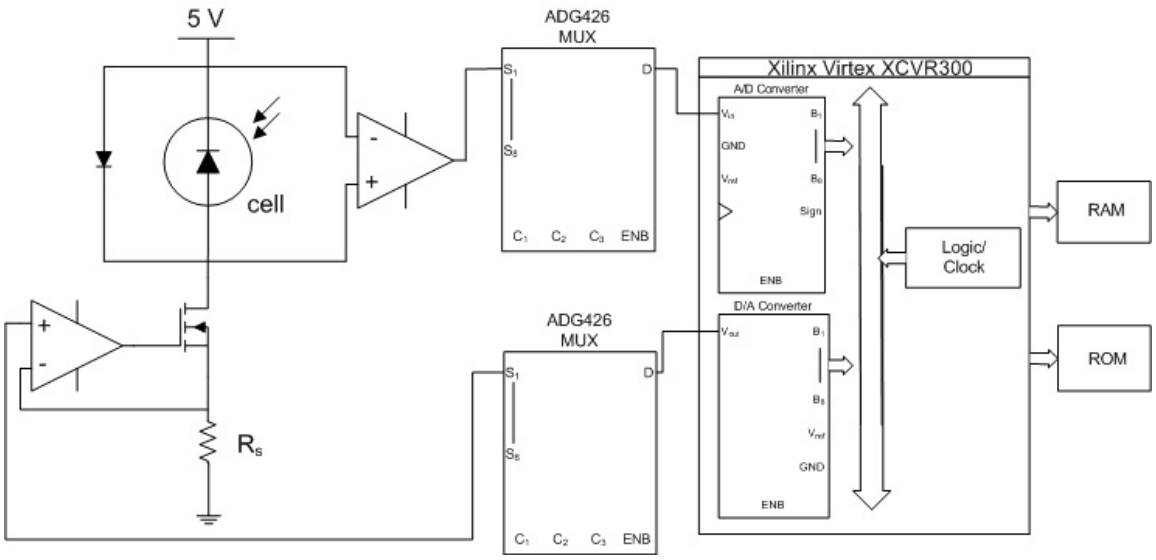

Figure V-3. Simplified block diagram of the analog current-sink circuit with the controller for one solar cell, with the analog subsystem on the left and the digital controller on the right.

As seen in Figure V-3, the input to the analog subsystem (left side of the figure) is fed from the digital controller through a multiplexer (MUX). The output of the analog circuit, which is the voltage across the solar cell, is fed through another MUX to the digital controller for processing and storage. On the actual SMS on the satellite, as shown in a simplified diagram in Figure III-6, 24 analog circuits will be connected to one digital controller via the MUXes. The MUXes will choose from the 24 analog circuits and cells.

The design of the digital controller is also described in detail in [15] and [21]. It is, however, still under development. Once the design and implementation is complete, it will undergo thorough testing with the analog circuit, at which time we will have a complete and independent curve-tracer for one solar cell. From that, completing the entire SMS will only require 23 more analog circuits and MUXes to support all the analog circuits.

B. TEST PLATFORM FOR THE ANALOG CIRCUIT

1. Circuit Prototype – The Coupon Driver Board (CDB)

To test the SMS analog circuit, the circuit was put onto a printed circuit board (PCB), designed by Ron Phelps and John Salmon and shown in Figure V-4. This prototype, often referred to by the SSAG engineers as the Coupon Driver Board (or CDB), ac-

tually contains four analog circuits to use with the four-cell coupon (of experimental triple-junction cells) provided by Boeing Spectrolab, hence the name "Coupon" Driver Board. Each circuit on the board is referred to as a *channel*. It is not required that there be four cells connected to the channels at one time; just one channel can be used to test a single cell. The channels are wired to multiplexers (MUX), allowing the digital controller to select the desired channel for tracing a curve. There is one MUX for the input line and one MUX for the output line from the analog circuit. Draper provides an excellent detailed description of the prototype board components and connections in [22].

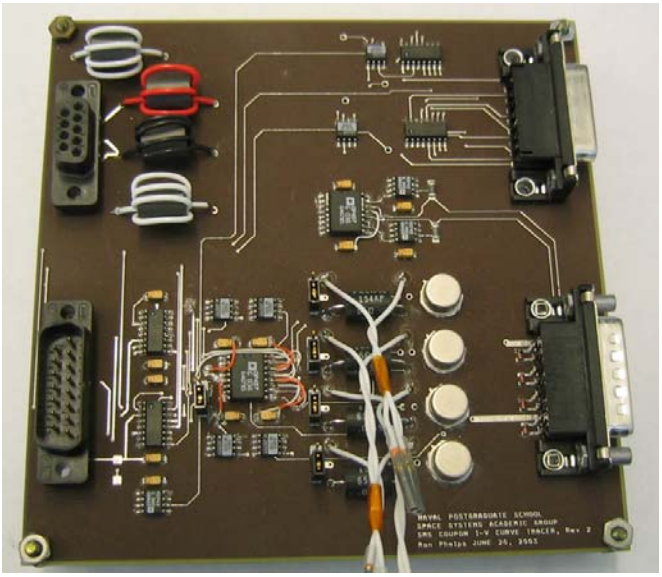

Figure V-4. The Coupon Driver Board (CDB), version 2. The connectors can be seen at the left and right edges of the board.

In addition to the curve-tracing circuit, the CDB contains interface electronics for thermistors, based on the circuit used on PANSAT. They were implemented to be able to sense the temperature of the solar cells under test. However, at the current time, the thermistors are not used and will be tested further later. The board also contains circuitry to read the voltage from the sun-angle sensors and report the angle of the light illuminating the sensor. These will be used on the satellite as a verification of the curves obtained by the SMS in orbit. Testing for those devices will also begin at a later date. Four connectors are mounted on the board to interface the circuit with a power supply, the cells, sun-angle sensors, and the controller. The pin assignments for each connector are described in detail by Draper [22].

The CDB has gone through two revisions. The first version contained non-precision resistors and used differential amplifiers to measure the voltage across the cell. Salmon found that the error of the measurement was too great than the initially allowed margins. Testing found that the errors were due to losses at the input of the differential amplifier and the inaccuracies of the non-precision resistors. The circuit was revised to utilize high-precision resistors and instrumentation amplifiers because of its high input impedance [15]. The schematic of the circuit and the PCB layout for the second version CDB are included in Appendix D.

2. Controlling the CDB Using LabVIEW

Because the digital subsystem of the SMS is still under development, there needed to be a temporary method to control the analog circuit for testing. SSAG intern Tara Holz worked on a LabVIEW VI to perform the duties of the digital controller and was able to complete it in part. Draper describes the partially completed program in detail in [22]. For explanation purposes, the VI associated with the CDB will be called the CDB VI. The program at the time was able to control only one of the channels on the CDB. The CDB is interfaced with a laptop via a data acquisition card, the National Instrument DAQCard-1200, shown in Figure V-5.

Since the SMS analog circuit is current-controlled – where a chosen current is pulled from the cell to measure the cell voltage – the CDB VI allows the user to input a starting and ending current to sweep. The user also enters a current increment and the resistance connected to the source of the NMOS. The resistance is used to set the proper voltage at the input to the circuit. The voltage V set at the input of the circuit with resistance R for a desired current I is simply $V = IR$.

The CDB VI performs nine steps in tracing an I-V curve [22]. The VI is broken into nine *frames* that run sequentially from beginning to end, analogous to a film reel for a motion picture. The actions of the frames are summarized in Table V-1. Draper provides further description of the VI code that performs these actions.

Figure V-5. The data acqusition card (top) inserted into the laptop's PCMCIA port (bottom).

Frame 0	Input the initial voltage to the CDB via the data acquisition card (DAQ card).
Frame 1	Set proper MUX line address to use the thermistor circuit[5].
Frame 2	Enable the input and output MUXes.
Frame 3	Take initial temperature reading, converting the thermistor voltage into temperature
Frame 4	Re-address the MUX to select the desired circuit to trace a curve.
Frame 5	Trace the *I-V* curve by stepping through the current.
Frame 6	Same as Frame 1, selecting the same MUX address in preparation to measure final temperature.
Frame 7	Same as Frame 3, reads the final cell temperature.
Frame 8	Deactivate all channels and circuits, and bleed off any voltages to avoid damage.

Table V-1. Summary of steps taking by the CDB VI to trace an *I-V* curve.

[5] Currently the thermistors are not used, but in the future this step can provide the cell temperature at the start of *I-V* curve tracing.

To trace *I-V* curves using the three other channels of the CDB, the VI needed to be able to select the other channels via the MUX on the board. The VI was modified to add code using the frames above for the other three channels, and the MUX selection addresses were set to select the proper lines. The completed VI code, along with a screenshot of the user interface, is included in Appendix E. The MUX addresses for selecting any of the four circuits are shown in Table V-2. The addresses for selecting the thermistor and sun-angle sensor circuits have been ignored here.

	MUX Select Lines		
Channel	**A2**	**A1**	**A0**
Circuit 1	1	0	0
Circuit 2	1	0	1
Circuit 3	1	1	0
Circuit 4	1	1	1

Table V-2. Logic table for MUX select lines. A0 is the least significant bit.

C. TESTS PERFORMED AND RESULTS

This section describes the testing of the SMS analog circuit, the focus of this thesis. To describe the performance of the circuit, we compare the curves produced by the circuit (using the CDB with the CDB VI) to the curves produced by the HP6626A. The following tests were performed on the circuit:

- Tracing *I-V* curves using all four channels on the same cell to ensure all four channels output the same results.
- Varying the temperature of the CDB electronics and to observe any differences in the output from that taken under room temperature.
- Varying the solar cell temperature and taking *I-V* curves using the CDB and HP6626A to compare the CDB and HP6626A outputs at each temperature.
- Varying the light incidence angle on the cell and taking curves using the CDB and HP6626A to compare the CDB and HP6626A outputs at each angle.

The tests are described in detail in the following subsections. Some of the plots are presented in the subsections to illustrate the analog circuit's performance. The complete set of results is included in Appendix F.

All of the tests traced *I-V* curves on the XTJ cells and on a commercially-available triple-junction cell – the Improved Triple Junction (ITJ) cells[6] – by Spectrolab. This was done to demonstrate that the circuit is able to work with different cell technologies and to show the result was not dependent on the technology. The XTJ cell size was 1.64 cm by 1.64 cm, while the ITJ cells were 2 cm by 2 cm. The *I-V* curves taken here will not match the manufacturer's data sheets because the NPS solar simulator does not replicate AM0 exactly. All of the plots are averaged from five runs.

1. Light Incidence Angle Test and Initial Problems

The first test that was performed and results first obtained was the light incidence angle test, and the results are presented here first. The test aims to observe the characteristics of the solar cells when subjected to light at various angles and to observe whether the test circuit (the CDB) can measure the light incidence angle effect accurately.

In this test, the cells were placed on the cell mounting plate tilted at four different angles. The angles were chosen at arbitrary intervals, mostly done for the convenience of the setup. We are only interested in comparing the CDB output with the HP6626A output. The actual angle used is not important as long as the outputs compared are from the same angle. The cells were kept at 28 ± 1°C, and the CDB was at room temperature.

Figure V-6 shows the "family of curves" for an ITJ cell for four different light incidence angles. The plots are a bit troubling because of the noise seen at the knee. The problem with the noise was apparent when attempting to take the curves using the CDB VI. The CDB VI steps through the current from 0 mA to I_{sc} while recording the cell voltage. Most of the plots obtained had large drops in voltage at currents just below I_{sc}, resulting in wiggly plots. These were caused mostly by the noise in the output of the DAQ card. As the DAQ card outputs a voltage to the analog current-sink circuit to set a desired current, noise is added on top of that voltage, resulting in a higher voltage than desired. For example, when the trace nears about (I_{sc} – 0.3) mA, the desired sink current is (I_{sc} – 0.3) mA. However, the voltage from the DAQ, at the input of the op amp in the circuit, will sink a slightly higher current due to the unintended noise that resulted in a higher set voltage. Because the trace is at the knee, a slight rise in the sink current will

[6] Specifications can be found on Boeing Spectrolab's product page at http://www.spectrolab.com/prd/space/cell-main.asp

cause a large voltage drop. Therefore, the intended current of (I_{sc} – 0.3) mA is actually paired with a voltage for, say, (I_{sc} – 0.1) mA, whose voltage is lower than the voltage for (I_{sc} – 0.3) mA. This results in curves with false data points that cause the wild horizontal zigzags at the knee. The output of the DAQ was probed with an oscilloscope, and the noise was measured to have a peak-to-peak of voltage of about 200 mV.

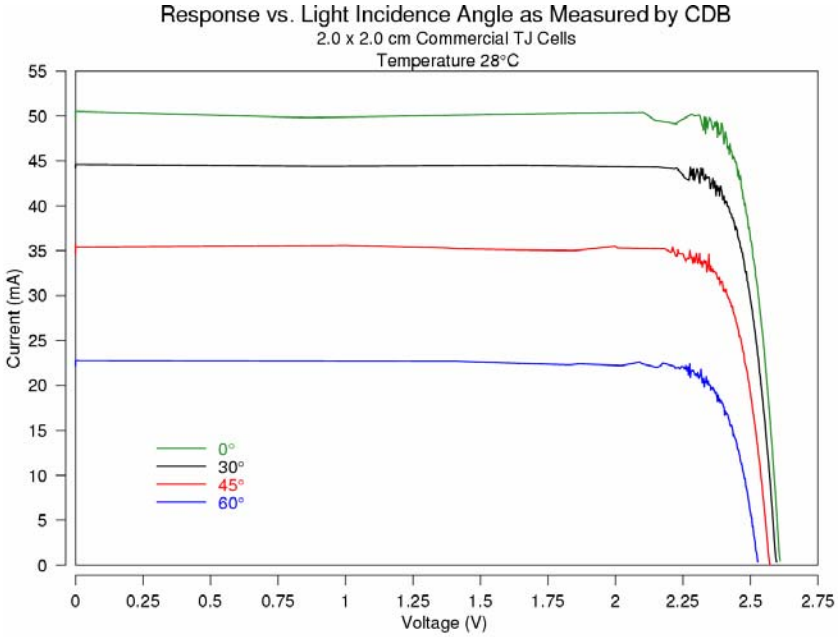

Figure V-6. *I-V* curves of an ITJ cell for various incidence angles, taken by CDB, cell at 28°C.

The plot shown above does not show the horizontal zigzags because they have been averaged by voltage. The raw data from the CDB VI are indexed by the current being pulled. One way of averaging would be to take the current as the index and average all the voltages obtained in the five runs. Here, however, the voltages are used as the index, while averaging the currents with that particular voltage. This is how the HP6626A data is handled, since the HP6626A VI sets a cell voltage and measures the current; the data is indexed by voltage, and the currents are averaged. Thus, the curves in Figure V-6 show slight vertical zigzags after being treated.

Although the zigzags are now small, they are still a concern. The short-circuit currents measured by the CDB are not reliable. Because the curve is so flat at the top, any slight increase of current in that region will cause a large voltage drop. Therefore,

the cell is very sensitive at this area. This is a drawback of a current-controlled *I-V* tracer.

To show a smoother curve more representative of the cell's performance, smoothing was applied on the data, where it considers the averages of neighboring data points. The result of this processing done on the same data of Figure V-6 is shown in Figure V-7. The vertical zigzags have mostly been eliminated. The remainder of the results presented will have gone through smoothing, but it is important to keep in mind the noise from the DAQ still exists.

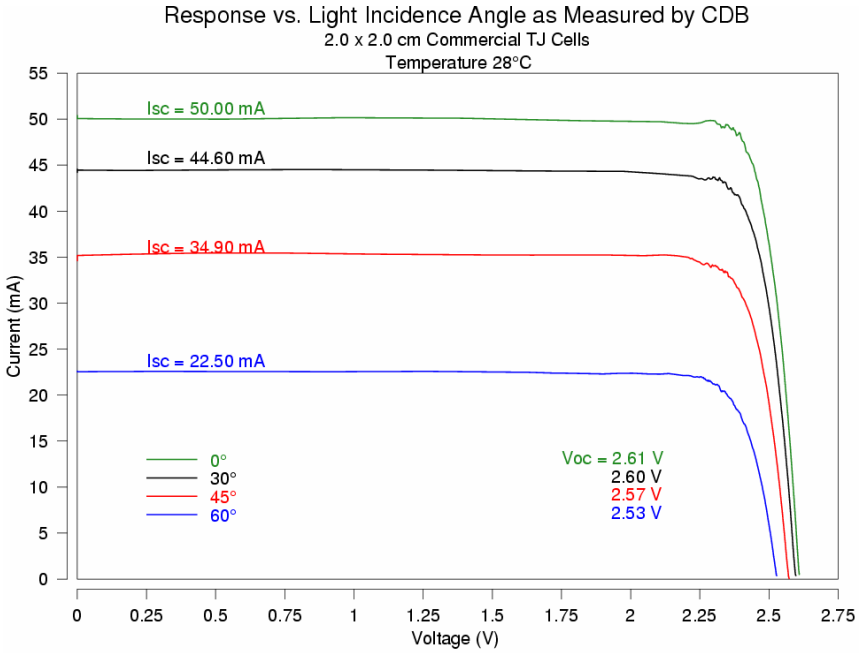

Figure V-7. Family of curves for various light incidence angles taken by the CDB, after being smoothed.

Figure V-8 shows a comparison of the curves taken by the CDB and the HP6626A, the control measurement. The figure shows the curve for a 45° light incidence angle as an example (comparison of other angles are given in Appendix F). The CDB matches the HP6626A very well for voltages to the right of the knee, but the CDB's I_{sc} is lower than expected. Many of the tests resulted in a lower I_{sc} for the curve by the CDB than the expected value taken by the HP6626A. The speculation is that the sensitivity of the cell and circuit, and the noise from the DAQ card, is causing much of the problem.

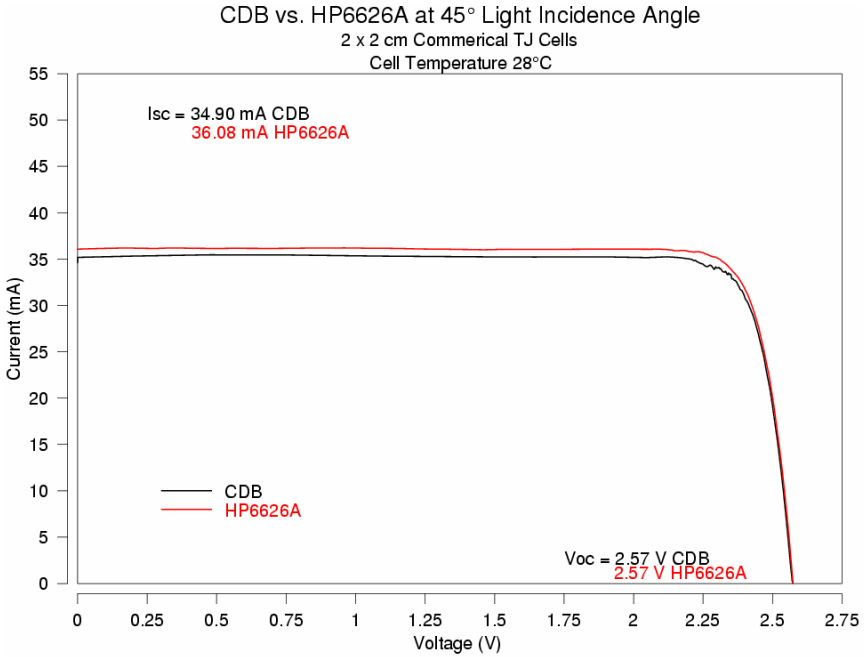

Figure V-8. CDB's output against HP6626A's output for a 45° incidence angle for ITJ cell. Both curves have been smoothed.

To confirm that the DAQ is part of the cause of the problem, the CDB was disconnected from the DAQ, and it was connected to a regular variable power supply. The power supply output was confirmed with an oscilloscope to be sufficiently clean with a peak-to-peak voltage of less than 20 mV. Using the power supply to set the input voltage for a desired sink current, the data points were recorded manually, and the plot is shown in Figure V-9. When the trace neared the top of the knee, the voltage reading became a bit erratic because of the sensitivity. The slope seen at the top of the curve is not an accurate representation of the cell's *I-V* characteristics. While attempting to take data points at that region, the voltage fluctuated, and the best approximation of the current and voltage was recorded. However, the readings on the voltmeter and oscilloscope showed that *I-V* curve tracing by hand using a variable power supply resulted in less noisy data.

Returning to the results and analyzing the incidence angle tests, the short-circuit currents by both the CDB and HP6626A for angles less than 60° do tend to follow the predicted decrease. The anticipated I_{sc} for an angle θ from the normal is $I_{sc}\cos\theta$ for angles less than 60° from the normal. The plots in Figure V-7 do show that trend. At 60°, the effects of refraction and reflection at the surface of the cell become substantial causing the current to decrease further and no longer follow $I_{sc}\cos\theta$.

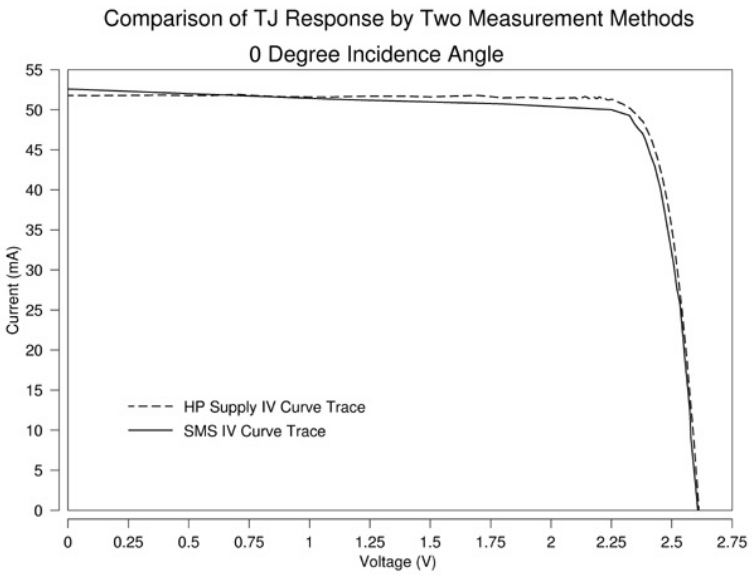

Figure V-9. A comparison of a manual sweep using the CDB (solid line) versus the HP6626A (dotted line).

The remaining tests and their results exhibit similar noise problems, but all the curves have been smoothed. Attempts can be made to eliminate the noise at the DAQ card, but since the SMS digital subsystem will control the analog circuit and be less noisy than the DAQ card, the problem with noise is not expected to be as severe when the two subsystems are integrated.

2. Heating the CDB and its Electronics

Because the temperature varies dramatically in outer space, there is concern for the effect of temperature on the operation of the SMS. The SMS will operate only while the satellite is in a sun-soaked region and will be off when in eclipse. The temperature of the satellite will vary widely from coming out of eclipse to going into eclipse. Thermal analysis show that the upper temperature limit for the SMS, with uncertainties considered, is 15°C and the lower limit is around –15°C [24, 25].

In this test, the CDB is placed under a hot halogen lamp shining onto the board. The temperature on the board is raised to 43 ± 2°C, assuming a far worse case than the predicted upper limit of temperature. Doing so can still show if the electronics are affected by temperature. The heated CDB will take curves of the solar cell kept at 28 ± 1°C. The "heated curves" will be compared to the curve taken by the CDB of the same cell while both were kept at 28 ± 1°C.

Figure V-10 shows the result of the test. It appears that the heat on the electronics does not substantially affect the measurement. The DAQCard noise caused slight differences in the results. The short-circuit currents are close to each other, and both curves follow one another fairly well.

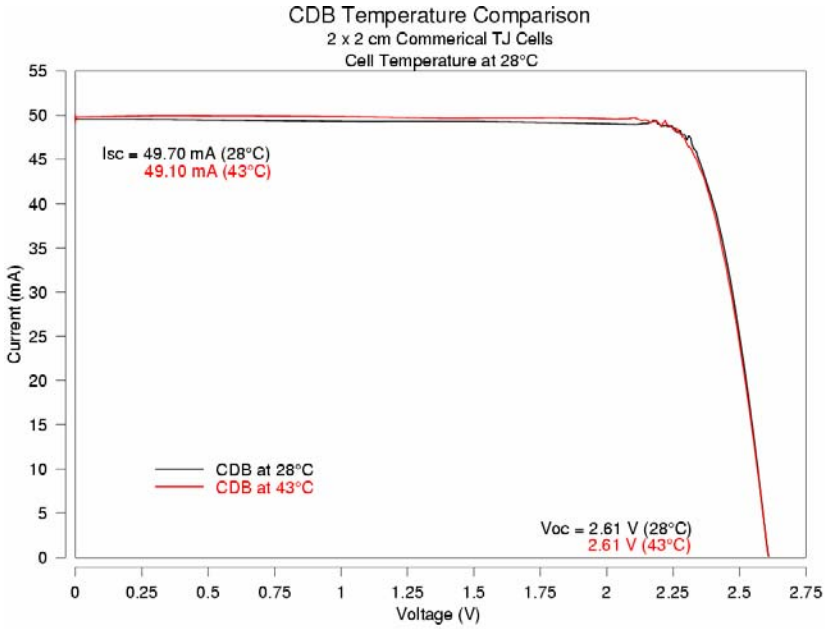

Figure V-10. Smoothed result of a heated CDB versus an unheated CDB, with ITJ cell at room temperature.

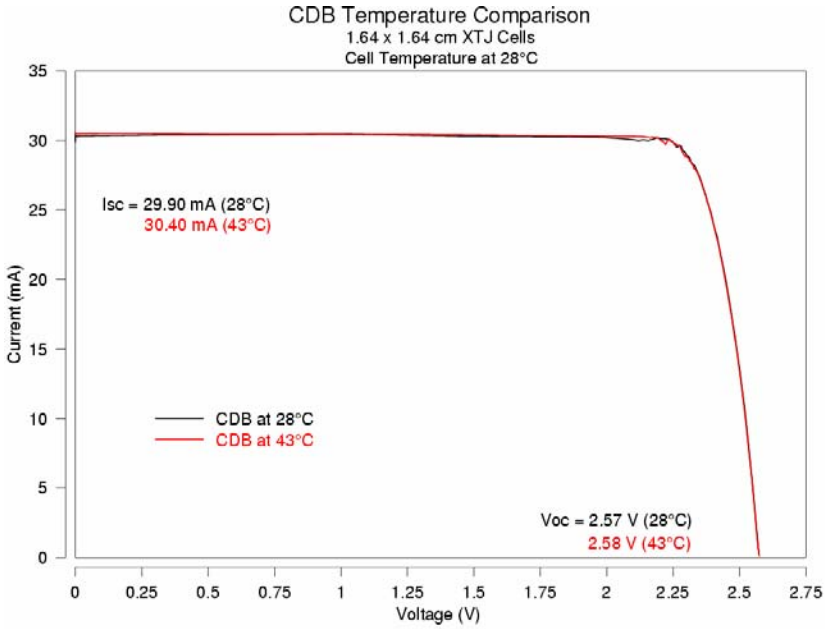

Figure V-11. Smoothed results of a heated CDB versus an unheated CDB, with XTJ cell at room temperature.

For future tests, if the equipment can be set up, the circuit should be subjected to a cold temperature like that expected in orbit and the effects measured. However, from this warm temperature test, it appears that the relatively small temperature differences might not make much difference.

3. Cell Temperature Variation

As with the discussion in the previous subsection regarding the temperature of the satellite and the electronics on orbit, the cells will be subjected to the widest variation in temperatures. The performance of the solar cells will be affected, as discussed in Chapter II. Thermal analysis show that the operating temperature for the cells in orbit will range from –15°C to 35°C. Recall from the discussion on solar cell physics that the open-circuit voltage varies with temperature by an amount dependent on the material of the solar cell. We expect to measure the temperature effects in the *I-V* curves. This test should demonstrate the CDB being able to take accurate data for a range of cell temperatures.

The cells are mounted on the angle plate and the temperature was set by the chilled-water loop to one of three temperatures: 18°C, 28°C, and 38°C. For the triple-junction cells, the expected effects will be mostly on the voltage; V_{oc} will change by about –6 mV/°C. Any change in I_{sc} should be very small and inconsequential for the test temperature range.

Figure V-12 shows the family of curves for the three temperatures for an ITJ cell, taken by the CDB. Looking at the changes in V_{oc}, the theory of –6 mV/°C holds. The data taken by the CDB reflects well with the calculation.

As an example, the 18°C curves by the CDB and HP6626A are used here for a comparison, shown in Figure V-13. Again, for the voltages to the right of the knee, the curves match fairly well. At the knee, the noise on the CDB is apparent. To the left of the knee, the CDB's I_{sc} again falls below the current measured by the HP6626A.

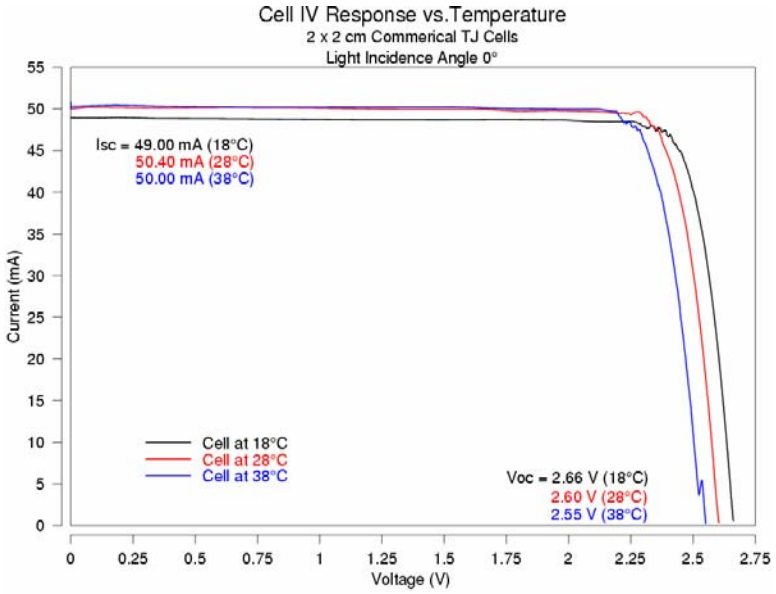

Figure V-12. Effects of temperature on ITJ cell as measured by the CDB. Curves have been smoothed.

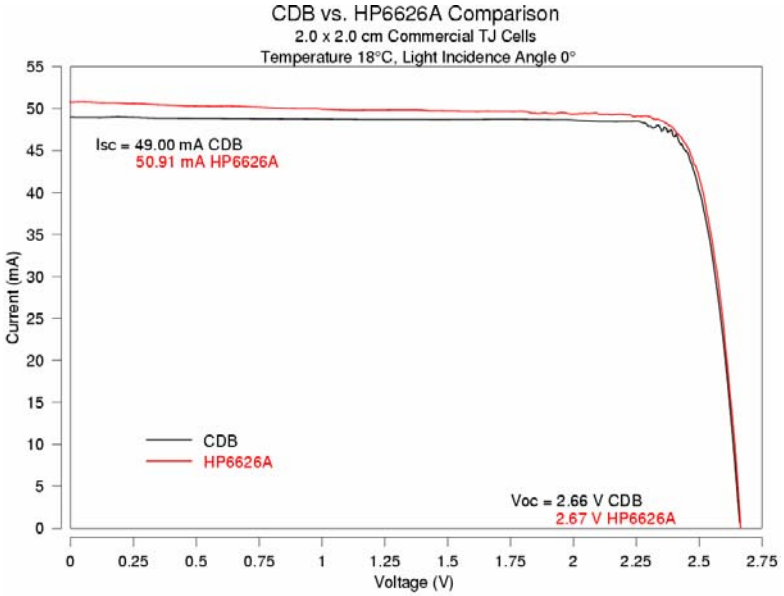

Figure V-13. Comparison of the CDB and HP6626A for variation on cell temperature, ITJ cell at 18°C, curves smoothed.

4. Comparing the Four Channels on the CDB

This test simply activates the four circuits on the CDB, one at a time, to trace *I-V* curves of the same cell, under the same condition. Since the four circuits are identical, identical outputs are expected. Moreover, since the circuits are connected together via a MUX, one circuit should not affect another circuit's operation.

The result of the test is shown in Figure V-14. From the figure, one can see the four channels performed identically, with plots essentially sitting on top of each other. There are slight variations on the I_{sc} likely due to noise and sensitivity, but the differences are very small.

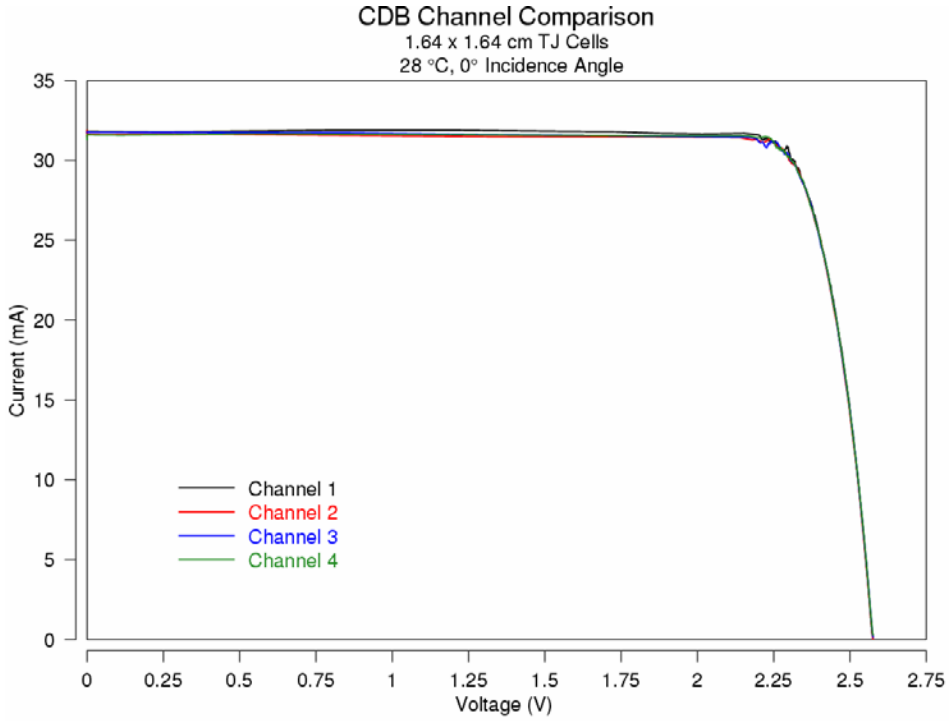

Figure V-14. Comparison of performance by the four channels on the CDB.

The tests described in this chapter were meant to validate the design of the analog circuitry of the Solar-Cell Measurement System onboard NPSAT1. Temperature, sun angle, and performance repeatability were considered during testing. The tests revealed some potential problems with the concept of current-controlled tracing and the circuit's sensitivity to noise. The next and final chapter summarizes the issues that remain and discusses the recommendations to resolve them.

THIS PAGE INTENTIONALLY LEFT BLANK

VI. CONCLUSION

The objective of this thesis project was to thoroughly test the analog current-sink circuit in the SMS onboard NPSAT1 and recommend any necessary changes or note any design flaws on the circuit. The tests are obviously vital prior to the launch of the space-craft to verify the proper operation of the circuit. The tests performed were meant to simulate the conditions expected in space for the solar cells. Temperature and sunlight incidence-angle changes were incorporated.

Originally, the performance criterion for the SMS analog circuit was to be within 2% of the control curve taken by the HP6626A. After running the tests and gathering current-voltage data, it became apparent that noise was plaguing the experiment. The source of the problem appeared to lie with the data acquisition card used to interface the CDB with the computer. As observed on an oscilloscope, the DAQ card's output to the analog circuit had a noise level of about 200 mV peak-to-peak. This noise caused the *I-V* curves to zigzag slightly near the V_{oc} region, and to zigzag wildly near the "knee" of the curve. This was confirmed after probing the line with an oscilloscope and noticing the noise on the display during the sweep. In addition, to ensure the circuit was not at fault, a clean variable power supply was used to set the input voltage for the analog circuit, and a voltmeter used to measure the cell voltage, while recording by hand the current and voltage pairs. The result of this manual sweep was a cleaner curve, although it revealed the high sensitivity at the top of the knee to very minute current variations.

For a more accurate representation in the *I-V* curves, the data sets were smoothed. The smoothing takes into consideration neighboring points in calculating the average. The result was a smoother curve to better represent the cell's performance, although the noise from the DAQ is still causing some errors.

Despite the problem with the noise at the input, it is still appropriate to conclude that the analog circuit is functioning as intended. It was able to match the control curve very well when the voltage is to the right of the knee. At the knee, the noise at the input dominated and one can see the fluctuations in the curve. For most of the tests, the region of the curve from the knee to I_{sc} was not very accurate. This is, however, most likely due to the noise combined with the sensitivity of the cell. Another suspicion for the cause lies

with the fact that the circuit is designed as a current-controlled configuration, and that might not be favorable with *I-V* curves (since *I-V* curves are so flat at the top). A conclusion cannot be stated until a digital subsystem prototype of the SMS is completed and connected to the CDB for testing. The digital subsystem is expected to be substantially less noisy.

If, after testing the analog circuit with the completed digital subsystem, the data still falls short of achieving the 2% error margin goal, a recommendation would be to investigate a new design where the voltage of the cell is set and then measure the current flowing out of the cell. This concept would be similar to how the HP6626A operates. The proposed design would thus be a voltage-controlled concept. This design appears to be more advantageous because it would solve the problem of the sensitivity at the top of the curve. The proposed circuit would sweep from 0 V to V_{oc} by stepping through the voltage. When tracing the curve this way, there will not be a part of the curve that is as sensitive to slight voltage variations as it was with the current-controlled SMS analog circuit (at the top of the knee). However, the actual circuit may not be trivial. The main question that arises is what circuit element and configuration would one use to fix a voltage across the cell?

Future work on the SMS includes the completion and testing of the design of the digital subsystem and the testing of the thermistor and sun-angle sensor circuits. The digital subsystem design was started by Salmon. The completion of the system is important to finding out if the analog circuit can produce accurate data in the absence of noise.

A summary of the work described in this thesis was published in a conference technical paper at the 22nd AIAA International Communications Satellite Systems Conference and Exhibit in May 2004. Interested readers may refer to [26].

APPENDIX A. UNITS AND NUMERICAL QUANTITIES

CONSTANTS

q electronic charge = 1.602×10^{-19} coulomb

m_0 electron rest mass = 9.108×10^{-31} kg

c speed of light in vacuum = 2.998×10^{8} m/s

h Planck's constant $= 6.625\times10^{-34}$ J·s
$= 4.14\times10^{-15}$ eV·s

k Boltzmann's constant $= 1.381\times10^{-23}$ J/K
$= 8.618\times10^{-5}$ eV/K

V_T thermal voltage = kT/q = 25.86 mV (at 300 K)

λ_0 wavelength of 1-eV photon in vacuum = 1.24 μm

PREFIXES

giga (G) = 10^9

mega (M) = 10^6

kilo (k) = 10^3

milli (m) = 10^{-3}

micro (μ) = 10^{-6}

nano (n) = 10^{-9}

pico (p) = 10^{-12}

CONVERSION FACTORS

J $= 1.602\times10^{-19}$ eV

K $= 273 + $ °C

$$°C = \frac{5}{9}(°F - 32)$$

THIS PAGE INTENTIONALLY LEFT BLANK

APPENDIX B. SPECTROMETER CALIBRATION PROCEDURE AND OOIIRRAD SOFTWARE USER MANUAL

This Appendix contains relevant excerpts from the user guide for the OOIIrrad-C application. It contains a step-by-step instruction for calibrating the spectrometer. The user's manual material is reproduced with the consent of Moshe Daniel of Ocean Optics, Inc. The manual is a beta version, and final release has not yet been determined. Readers are advised to visit Ocean Optics' website for the newest information.

The manual mentions a different model of calibration lamp than what is in the SSAG laboratory, and users should simply use the DH-2000-CAL lamp in place of the other model mentioned. Lamp files mentioned are named similarly to the DH-2000-CAL deuterium and halogen lamp files. These files were supplied on a diskette provided by the manufacturer and have also been copied into the installation directory for OOIIrrad.

The installation directory also contains important calibration files (these are with the file extension *.cal). These files contain the calibration settings, and can be chosen to be used as the current setting.

Excerpt from OOIIrrad2 software ver. 2.05.00 PR 10
Reproduced with permission.

What is Irradiance calibration and why do we need it?

Irradiance is the "amount" of light present on a particular area. In our case, this area could be the fiber's cross-section at its tip, cosine corrector's surface or it could be the integrating sphere's surface which, measures the total optical output of a light source inserted into the integrating sphere.

A CCD based spectrometer is an instrument that breaks the light into its components using a grating, like a rainbow on a rainy day, and then measures the intensity at different wavelengths using a CCD.
Different gratings are available for use in different systems. These gratings have different efficiencies. Here are few of the common gratings used.

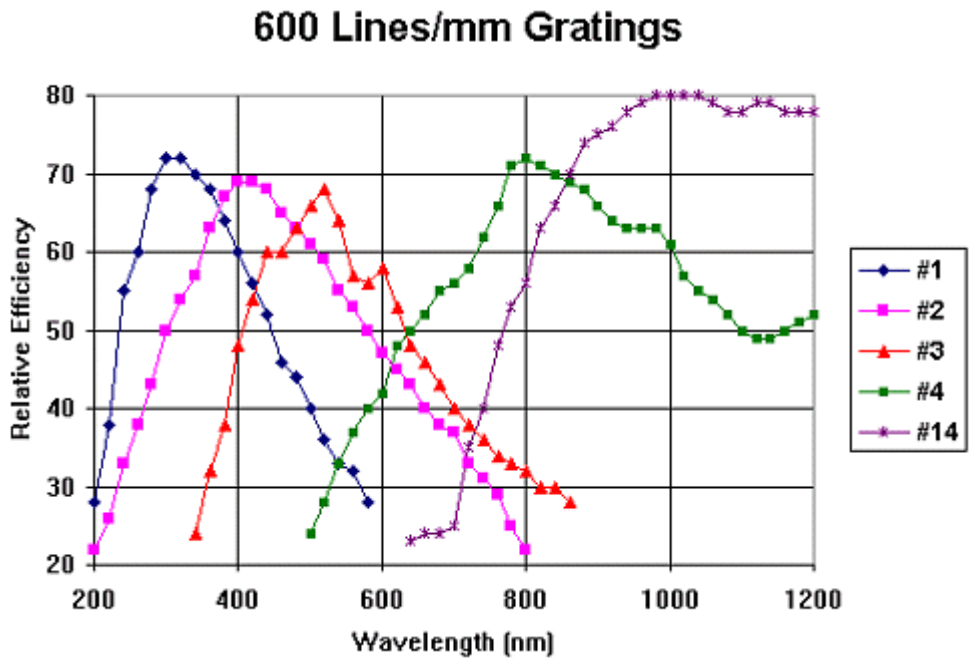

These curves tell us what will the typical scans look like, when an ideal light of even intensities across the spectrum, split into it's wavelength components using these gratings. In addition to grating efficiency curves, there is also an issue with CCD's sensitivity to different wavelengths. Here is a typical CCD sensitivity curve.

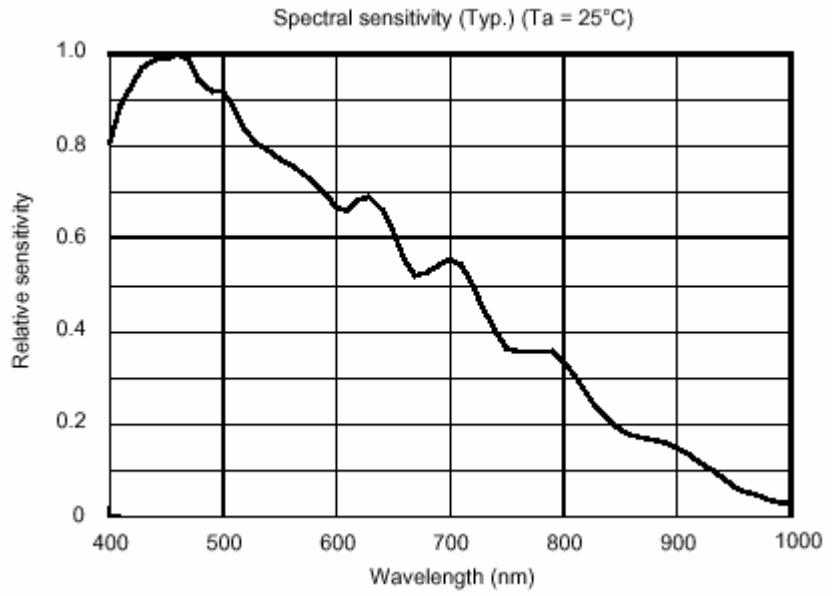

These variations in efficiencies and sensitivities indicate that most systems are different from each other. In most measurements like absorbance, transmittance and reflectance, the absolute response is not crucial because the nature of those measurements is based on relative measurements of the light with and without a sample. A reference measurement without the sample is taken and compared with a measurement with the sample. With irradiance measurements, this is not possible because there is no sample we can remove for a reference measurement. There is

need for a way to create a conversion from raw readings (counts) into real life measurements like Joules and Watts. This conversion factor (Calibration) is created by OOIIrrad application.

Absolute irradiance measurements can be achieved using a light source (calibration lamp) with known spectral output (microwatts per square centimeters per nanometer).
The known spectral output specifies the power at some distance from lamp. After placing the sensing area (fiber tip, CC3 cosine corrector etc.) at this distance from lamp, the application creates a conversion factor, for each pixel, knowing the lamp's output intensity and actual spectrometer reading from light detected (counts). These calibration results are specific to the optical configuration (from spectrometer up to sensing area) used during calibration. This is why Ocean Optics cannot create a calibration for all units shipped. It depends on end-user's system configuration. For example, if a different slit is installed in spectrometer or a different fiber used to collect light, a new calibration is needed.

Relative irradiance measurements can be achieved using a light source that has a known spectrum but in shape only, not in power units. This known shape is defined for many lamps as "Color Temperature". When a reference spectrum is stored for a lamp with a known CT, the application calculates the theoretical spectrum, which corresponds to the CT and creates an internal conversion (calibration) to compensate for the spectrometer's efficiency and sensitivity issues. The result of a relative irradiance measurement is a correct spectrum (in shape) on a scale of "0" to "1".

Quick Start

1. Install the application from Ocean Optics' 'Software and Technical Resource' CD, Ocean Optics' website or directly from installation files received from Ocean Optics. Default installation path and options will work fine for most users.
2. Start the application from the "Start" button. If you chose to keep default installation values, it will be installed in "C:\Program Files\Ocean Optics\OOIIrrad2beta" and accessed via the 'Start | Programs |Ocean Optics | OOIIrrad2beta' menu item.
3. Configure hardware parameters for spectrometer type and A/D options with the 'Configure | Hardware' pull-down menu.
4. Configure spectrometer parameters with the 'Configure | Spectrometer' pull-down menu. There are few tabs:
    a. **Channels** tab allows you to activate and enter wavelength calibration coefficients for each channel. Verify 'Light source inside integrating sphere' is checked only if you do have an integrating sphere and use the LS1-CAL-INT calibrated light source. 'Fiber diameter' defines light collection area: enter '3900' for CC3, '7140' for CC3-DA or bare fiber's diameter in microns. 'Steradians for Candelas' is the optic's solid angle used for calculating Candelas only (when activated). 'Color Temperature' is a reference lamp's known color temperature used for relative irradiance calibration. Click on 'Channel Color' box to choose channel's color.
    b. **Log/Chart** tab lets you choose file name and path for full-spectrum 'Save' action or calculated values' 'Log' action. There is an option to add an index number when automatic saving or logging is enabled. Time chart will display the calculated values on a time based strip chart.
    c. **Timing** tab has check boxes to activate a preset duration for 'experiments' or preset sampling interval.
    d. **General** tab has few options. External trigger allows you to choose between external software or hardware triggers. External triggering feature depends on the particular hardware you have. You will find more information in your spectrometer's documentation. 'Limit display range' allows truncating the graph and displaying graph between two wavelengths. The mini scope window is a scope mode spectrum display that could become visible in non-scope modes to keep you informed about the spectrometer's raw data. You should watch it for saturation and low signal conditions. This application warns you, when mini scope win-

dow is not displayed, of raw spectrum saturation. You can choose to activate a 'Do not warn me about saturation' option. This is especially useful when range of interest is only partial to the spectrometer's full range and you wish to set the integration period so signal is good in the range of interest. Pixel Rotation number will allow you to activate/deactivate scanning more than one spectrometer channel during each of the integration periods. Any value more than "0" means that Pixel Rotation is active with the number specified plus "1" first channels. For example, if you specify "3" it means that Pixel Rotation is ON and every integration period will result in a scan for the first four channels: Master, Slave1, Slave2 and Slave3. To deactivate this mode enter "0". This can be used only with an ADC1000 or ADC2000 A/D cards. Using this tab you can also choose the color assigned to overlaid curves in the graph.

e. **Peaks Measurements** tab lets you choose the values for peak analysis. You can specify how you wish the software to find the peak- using a wavelength range or a cursor on the graph. If you choose the range method, you should specify the start and end of this range. There is a '%' ratio which defines the separation of peaks. Specify the percent of a local minimum that you wish to divide between close peaks. In this tab you can also activate a cursor display. If you have more than one channel, choose the channel that the cursors should lock to.

f. **Irradiance Measurements** tab lets you choose the values you are interested in. Photopic/Scotopic values are calculated over 380 to 780 nm wavelength range. Radiometric values require you to specify the wavelength integration range. Scotopic conditions are defined when the luminance is less than some hundredths of a candela per square meter (cd/m^2). The difference of this scotopic vision (low level) condition compared with photopic (high level) condition affects the calculations for Lumen, Lux and Candela by using the V'(λ) spectral luminous efficiency curve instead of the V(λ) curve. In most cases, photopic condition should be selected (default).

g. **Color Measurements** tab lets you choose the color values you are interested in. Color measurements require you to specify if it is a reflective or emissive measurement and if you want to use the 2° (CIE 1931) or 10° (CIE 1964) observer. If you choose reflective color measurements, you should specify also the 'Illuminant' and 'Reference Tile'. This illuminant is a theoretical CIE defined and has nothing to do with your actual lamp used in the measurement. In most cases when you store the reference spectrum using a 'perfect' reflector, choose the White tile.

5. Set main window parameters
   a. Acquisition parameters are set at the top-right corner. If you have more than one channel active, set parameter for each channel by selecting that channel and then setting values individually. These parameters should be set for a smooth curve with a maximum around 3500 counts. Integration period alone can be changed since the last calibration but a new dark scan should be stored again.
   b. 'Scan' toggle switch is used to activate scanning either in a single-shot or continuous mode.
   c. 'Analysis' toggle switch activates the calculations and their display. This switch will be grayed-out until at least one calculated value is activated in the configuration panel. If only one calculated value is active, it will be displayed under the analysis switch. For more than one, they will be displayed in their own individual windows depending on their category.
   d. Spectral Graph Mode defines the display mode. Color calculations will execute in any of the display modes as long as irradiance calibration has been performed. uW/cm^2/nm mode will cause the color calculation to use the results of the absolute irradiance calibration. All other modes will cause color calculations to execute using the relative irradiance results.

i. Scope mode displays the raw spectrometer data. You should use this mode to verify general operation of the spectrometer and to adjust acquisition parameters before stepping into any of the other modes.
ii. uW/cm^2/nm displays the calibrated irradiance mode data. You should calibrate spectrometer for relative or absolute irradiance first.
iii. Reflectance mode calculates the reflection (transmission) in %. This mode requires a dark scan and a reference lamp scan reflected off a 'perfect' reflector placed at the same location as the sample.
iv. Relative irradiance mode corrects the spectrometer readings by using a lamp with known color temperature as the reference scan. This color temperature has to be entered in the configuration window before storing a reference scan of this lamp. A dark scan has to be stored as well.

e. 'Store Dark' button stores the spectrometer's background spectrum to be subtracted from sample and reference scans in most calculations. If more than one channel are active, this dark scan will be scanned for the active channel in the top-right corner of the application window. Note that this 'background' depends on acquisition parameters so remember to store a new dark scan after any change in these parameters.
f. 'Ref' button stores a reference scan. This reference scan depends on the mode you intend to use. It will affect only the reflectance and relative irradiance modes.
g. File menu items:
i. Open - prompts you to select a previously saved file with the extension '.ird'
ii. Save - prompts you to select a name and path for the graph data. An extension '.ird' will be added automatically.
iii. Export - saves the same data as with the 'Save' option except the header data in the saved file is striped. This is useful when working with applications that do not recognize this header.
iv. Save irradiance as lamp file – saves the power spectrum as a '.lmp' file. This is useful when measuring a lamp's power output and using that as the calibration lamp during a calibration process without using a regression to create a lamp's calibration data from a typical '.lmp' file.
v. Add header to log file – adds a new descriptive header line to the log file depending on the selected calculated values.
vi. Page Setup… - is a standard Windows menu item, which you should be familiar with.
vii. Print – prints the current graph and calculated values, which are visible.
h. Lamp menu items:
i. Current calibration lamp's graph – overlays the most recent calibration lamp's graph onto collected graphs. This is useful as a verification step immediately after an absolute irradiance calibration. Scan the calibration lamp and overlay its given data.
ii. Strobe Enable – turns an output signal ON or OFF. Check your spectrometer documentation for this pin's location. It is useful to activate external devices (lamps etc.).
i. Configure menu items:
i. Hardware – displays a configuration window that sets the hardware selection. Some items in this window depend on other items.
ii. Spectrometer – displays a configuration window that sets all other spectrometer parameters.
j. Calibrate menu items:
i. Absolute irradiance – uses a lamp with know power output to calibrate spectrometer for irradiance readings.

ii. Relative irradiance – uses a lamp with know color temperature to calibrate spectrometer for irradiance readings, which is correct in shape on a scale of 0 to 1.
iii. Color – no actual steps are taken here. This is just to remind you that emissive color measurements rely on either an absolute or relative irradiance calibration.

k. Chart menu items are active only if chart is activated in the configuration window. These menu items let you save, open, print and clear the chart.
l. Windows menu items:
    i. Clear overlaid scans – lets you clear the previously opened spectra
    ii. Show grid – makes the graph's grid visible or invisible.
    iii. Auto scale Y – rescales the graph's vertical scale once to fit the curve in the graph's full area.
    iv. Auto scale X – rescales the horizontal scale to show the spectrometer's full range.
    v. Few windows will be listed depending on the active calculated values. You can select any of these, to bring it to the front, if it is hidden behind another window. If your screen is big enough, place these windows so they are not hidden even if they are inactive.

6. If you received a spectrometer calibration file (with extension '.cal') from Ocean Optics, copy it into this application's folder (C:\Program Files\Ocean Optics\OOIIrrad2beta\). Choose 'Calibrate | Absolute Irradiance' and then choose 'Spectrometer | Active Spectrometer Calibration File'. You will be prompted to select the calibration file you have just copied. If you wish to calibrate the spectrometer for irradiance yourself, follow instructions bellow for either absolute or relative irradiance calibration. When finished, switch spectral graph mode selector to 'Relative Irradiance' or 'uW/cm^2/nm' for absolute irradiance. If you need to change integration period, make sure to store a new dark spectrum with the new integration period. For calculated values, switch the 'Analysis' to the ON position.

Absolute irradiance Calibration

1. Have your calibration lamp handy. Copy its calibration data files into the application's installation folder (C:\Program Files\Ocean Optics\OOIIrrad2beta).
2. Set up your optical path from lamp to spectrometer. This should include any optional components like fibers, integrating sphere, CC3 or CC3-DA. The application needs to know the size of the collection area. In the configuration window there is an entry for fiber diameter in microns. If using a bare fiber, enter the fiber's diameter in microns. If using a cosine corrector (CC3), enter the value '3900' microns. If using a direct attach (CC3-DA), enter the value of '7140' microns.
3. Adjust 'Nom. Integ. Period', in scope mode, for a peak around 3500 counts. For most calibration lamps set the 'Smoothing Size' to around '5'. Keep the 'Scans to average' at '1' only until you decide to start the calibration when you should increase it to a value around 100. This may slow down the response time in the calibration process but will improve the calibration results.
4. Turn off the 'Scan' toggle switch and select 'Calibrate | Absolute Irradiance'. An absolute irradiance calibration window will appear displaying date, spectrometer serial number, lamp serial number, acquisition parameters and three graphs:
    a. Calibration Lamp graph displays the current calibration lamp with its given data points and its fitted mathematical curve
    b. Actual Scan graph displays the spectrometer's actual raw reading of this calibration lamp. It also displays the dark spectrum and the resulting difference between the raw lamp reading and the spectrometer's dark readings. You can see that what the spectrometer reads is nothing like what the lamp's output is. This is why a calibration is needed.

    c. Calibration Curve graph displays the resulting multiplication factor for spectrometer. This factor is uJoules/counts, which allows calculation of energy values for every scan. Power can be calculated by dividing the energy with the corresponding integration period (exposure time).
5. Choose 'Lamp | Select Lamp (file)' to activate the calibration lamp's data. Note that there are two files with the LS-1-CAL. One for bare fibers and one for CC3.
6. Choose 'Spectrometer | Scan Dark' and follow instructions to store the spectrometer's internal background spectrum. This scan will show on the 'Actual Scan' graph.
7. Turn on calibration lamp and let it warm up for at least 20 minutes. Choose 'Spectrometer | Scan Calibration Lamp' and follow instructions to store lamp's reference scan. This scan will show on the 'Actual Scan' graph.
8. Choose 'Spectrometer | Calibrate (no scan)' to create the calibration curve which will be displayed in the 'Calibration Curve'. You will be prompted to name the calibration. This calibration file will be used by the application by default unless a different calibration file is activated.
9. Calibration lamps are usually for either a UV or visible range. Use the 'Windows | AutoScale UV Range' or 'Windows | AutoScale Visible Range' to limit the display and/printout to the relevant range. The saved calibration file always includes the spectrometer's full range and will not be affected by this selection.
10. If you have calibrated one spectrometer for both the UV and visible ranges, you could combine these separate calibrations into one file using the 'Spectrometer | Combine UV/VIS Calibrations':
    a. Open UV calibration file
    b. Open VIS calibration file
    c. Both curves should be close to each other in values at around 400nm. Select the priority of the UV or visible range as the dominant with the 'Spectrometer | UV Range Priority' or 'Spectrometer | VIS Range Priority'. The other curve will be 'stretched' toward the dominant curve to create a smooth transition at the combination wavelength, which is usually 400 nm. This assumes that one of the calibrations is more accurate than the other.
    d. Choose 'File | Save UV/VIS Calibration' to save the combined calibration file. You will be prompted to name this new file.
11. You could activate any calibration file to be the current spectrometer calibration by choosing 'Spectrometer | Active Spectrometer Calibration file'. You will be prompted to select a calibration file with extension '.cal'.
12. You are ready to make absolute irradiance measurements. Close the irradiance calibration window, switch the spectral graph mode to 'uW/cm^2/nm' and flip the 'Scan' toggle switch up to 'ON' position. As a verification to the calibration you should scan the calibration lamp once and then overlay lamp's given data with the 'Lamp | Current Calibration Lamp's Graph' menu option. You can hide it with the same menu item. You can change the integration period and averaging but remember to store a fresh dark spectrum. It is not recommended to change the 'Smoothing Size' compared with this value during the calibration process.

Until a final release is posted on our website, new beta versions will be posted on our FTP site at: ftp://ftp.oceanoptics.com/pub/OOIIrrad2Beta/

Moshe Daniel
MosheD@OceanOptics.com

THIS PAGE INTENTIONALLY LEFT BLANK

APPENDIX C. PROCEDURE TO TRACE I-V CURVES WITH HP6626A

The steps to take an *I-V* curve using the HP6626A are given here. This method is used to obtain a control curve.

To use the HP6626A and the corresponding LabVIEW Virtual Instrument (VI), the HP6626A needs to be manually configured via the front panel of the power supply. Follow these steps to set the bias voltage to 4 V on channel 2:

1. Ensure the connections to the cell are correct. Check the polarities of the cell!
2. Press **LCL** on the front panel to switch to local control (so that it is not expecting commands from the GPIB).
3. Press the right arrow of **OUTPUT SELECT** to select channel 2 (look at the bottom left side of the LCD to see the arrow pointing to the appropriate output channel).
4. Once channel 2 is selected, press **VSET**.
5. Enter **4**, then press **ENTER**.
6. Press **ISET**, and enter a current that is a little above the expected short-circuit current for the solar cell being tested. A safe value to use is 250 mA. This step is to ensure the power supply is outputting a 4 V bias that is not disturbed by the current. To enter 250 mA, press **. 2 5 0 ENTER**.
7. The HP6626A is ready to trace a curve via GPIB command. The VI will automatically take control when it is run. You may select to view channel 1 to observe the voltages and currents as the VI steps through the cell voltages.

To use the HP6626A VI to trace an *I-V* curve:

1. Open the appropriate VI. There is one VI to trace a cell with an open-circuit voltage less than 1.1 V, and one VI to trace a cell with an open-circuit voltage around 2.6 V (triple-junction cells). Both VIs will decrease the voltage increment to 0.01 V once the trace is near the knee, so that it can get more data points at the knee. The difference is that the first VI will do this at 0.4 V of the cell (or at 4.4 V including the bias), while the second VI (for TJ cells) will do this at 2.4 V (or 6.4 V with the bias).
2. For *Starting Voltage*, ensure 4.0 is entered (should already be there by default)
3. For *Voltage Increment*, enter what you would like. A usual value is 0.1 V.
4. For *Ending Voltage*, enter the expected V_{oc} + 4. The 4 V is necessary to account for the cell bias. The data obtained by the VI will have this 4 V. When processing data, simply subtract 4 V from the voltage.
5. Click the run button (the arrow at the left side of the toolbar) to run the VI. It will ask the user to save the file when the trace is complete.

THIS PAGE INTENTIONALLY LEFT BLANK

APPENDIX D. COUPON DRIVER BOARD CIRCUIT SCHEMATIC AND BOARD LAYOUT

The circuit schematic and the board layout of the Coupon Driver Board (CDB), second version, are presented here. The circuit schematic contains components for sun-angle sensors and thermistors that were not used in this thesis, but will be used on NPSAT1. The CDB is only a test platform and is not the actual board to be used on NPSAT1. The sun-angle sensor and thermistor circuits are also prototypes and will require testing in the future. Salmon [21] and Draper [22] provide descriptions for those circuits.

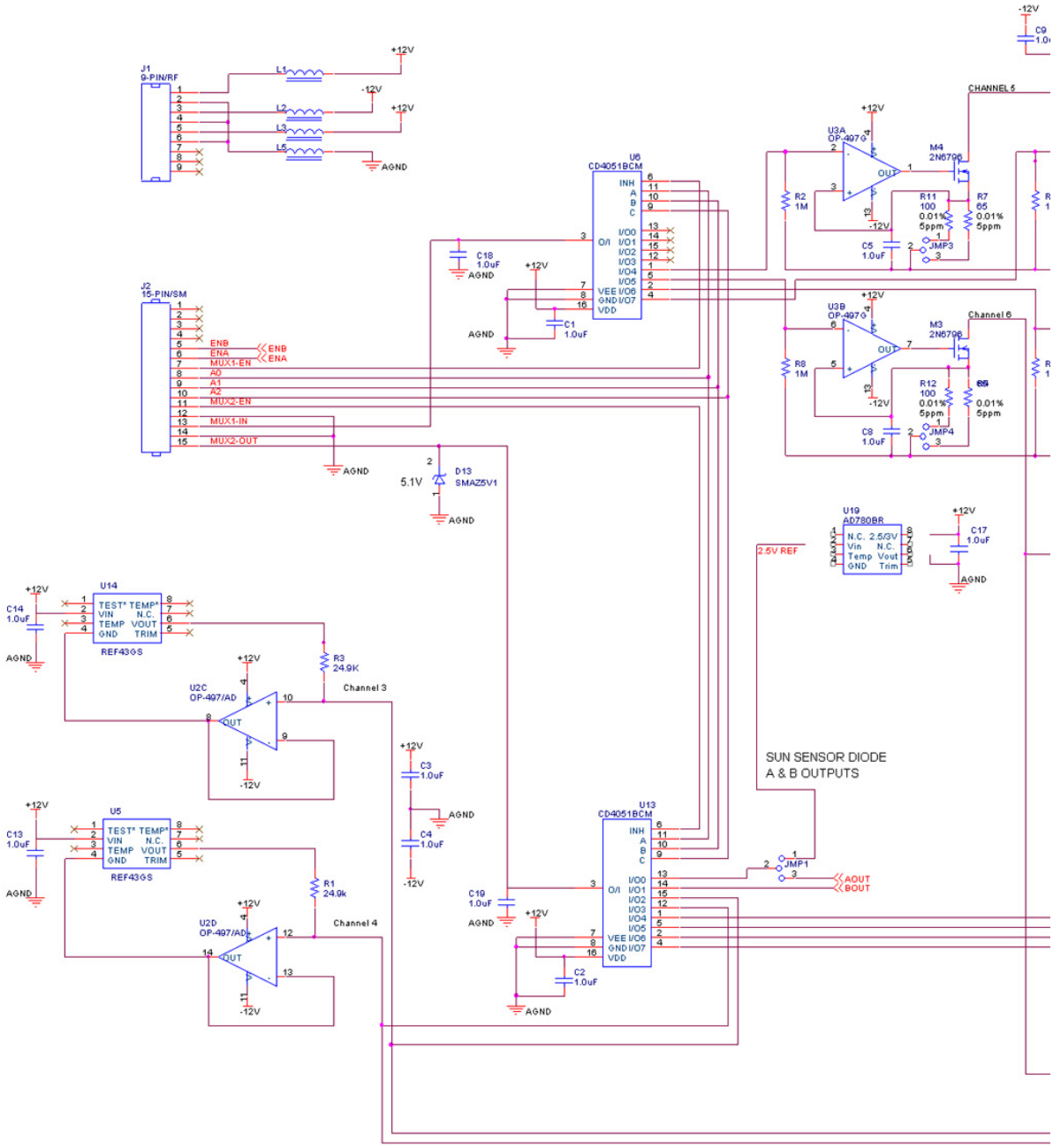

Figure D-1. Circuit schematic for the Coupon Driver Board, part 1 of 2. For the right side of the schematic, see the next figure.

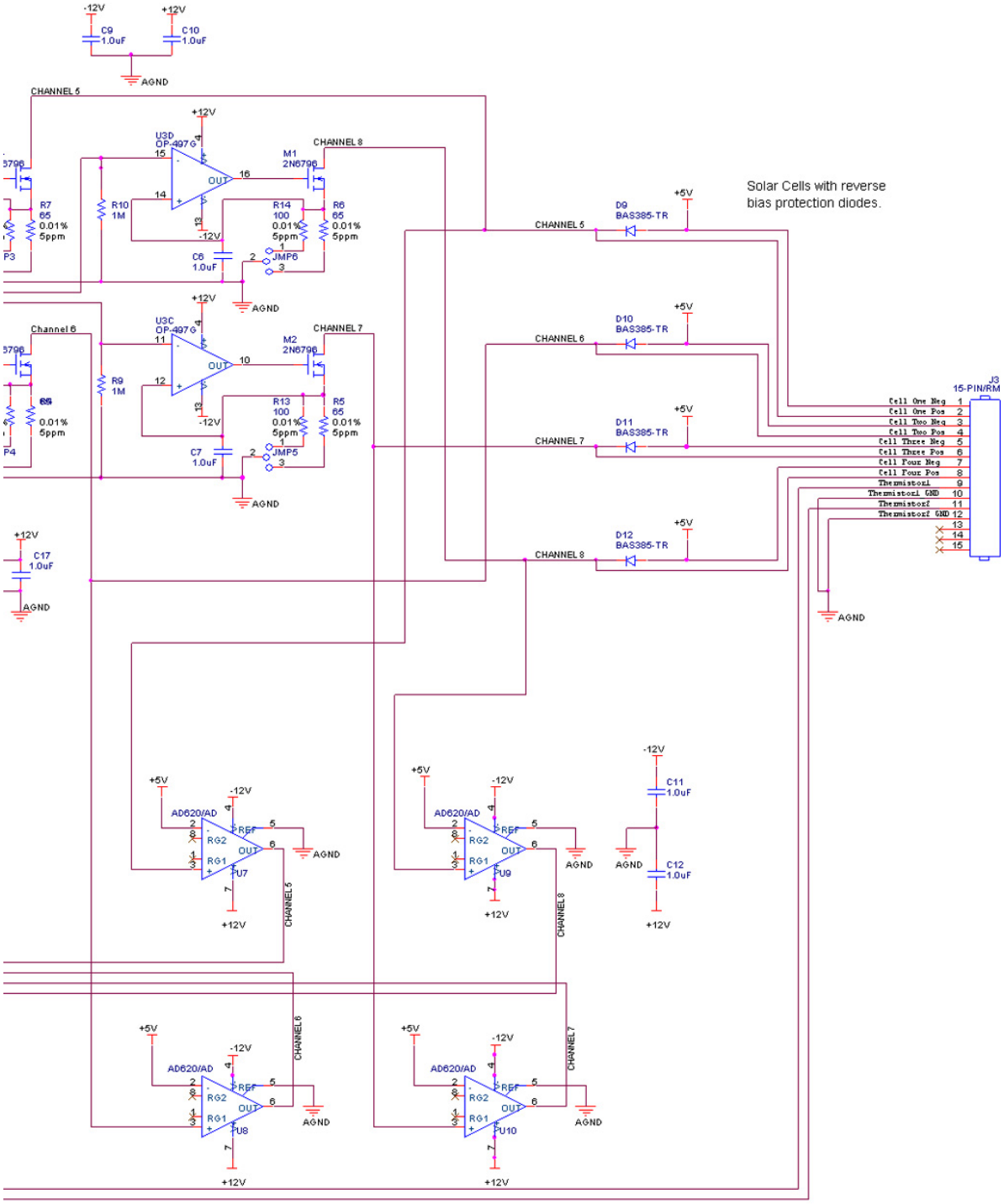

Figure D-3. Circuit schematic for the Coupon Driver Board, part 2 of 2.

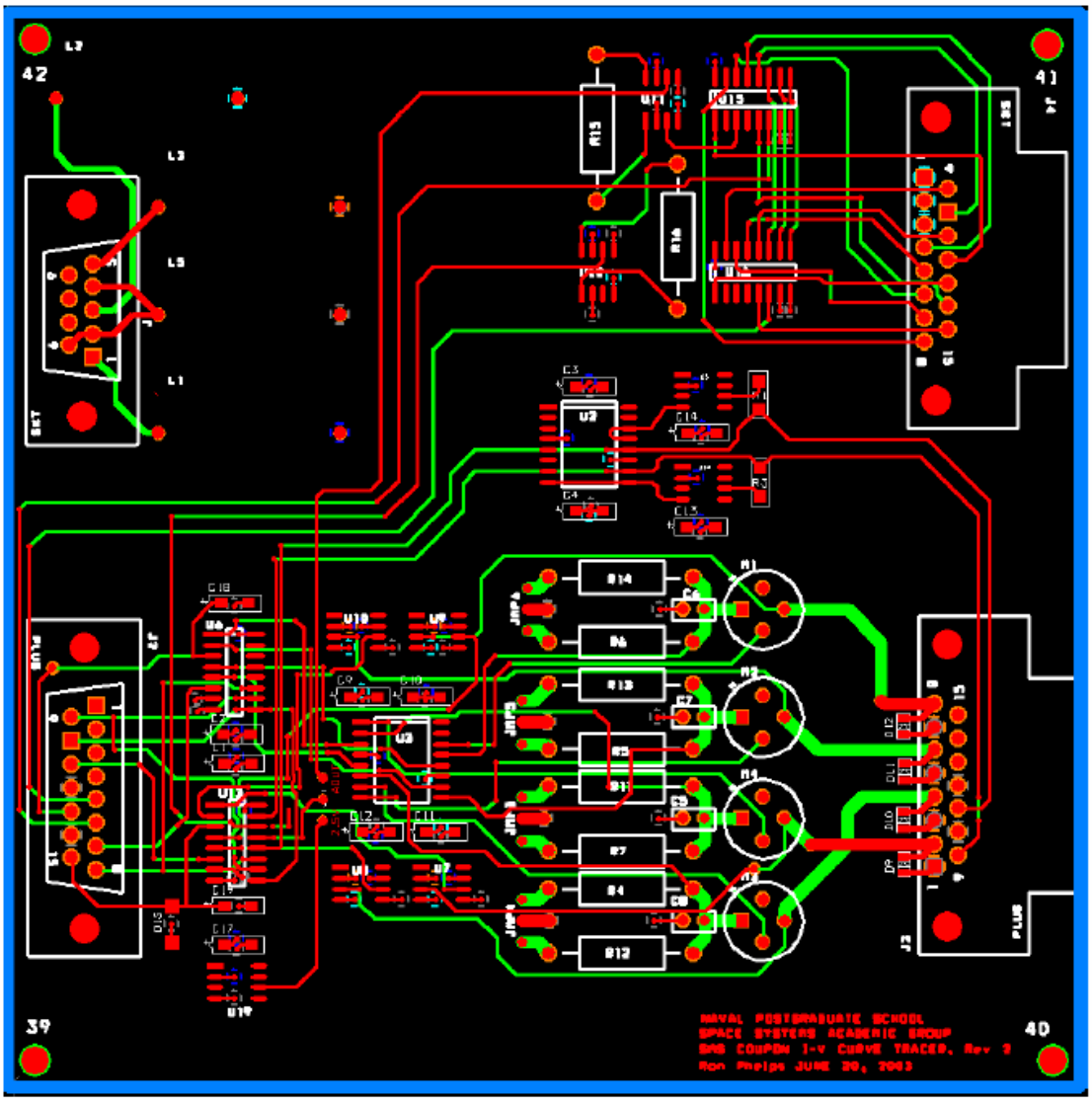

Figure D-3. Printed circuit board layout for the second version of Coupon Driver Board.

APPENDIX E. CDB VIRTUAL INSTRUMENT SOURCE CODE

A portion of the Virtual Instrument code for the Coupon Driver Board is presented in this appendix. The original program by Tara Holz had code for channel 4 and the calibration channel only, both described in Draper [22]. The code was modified include the other three channels. The code for channel 1 (labeled Test Cell 1 in the code) is included here. The code for the remaining channels is similar except for the MUX addressing. The MUX addresses for the other channels are listed in Table V-2. The functions of each frame are briefly described in Table V-1 and described in detail by Draper. There are nine frames for each test cell channel.

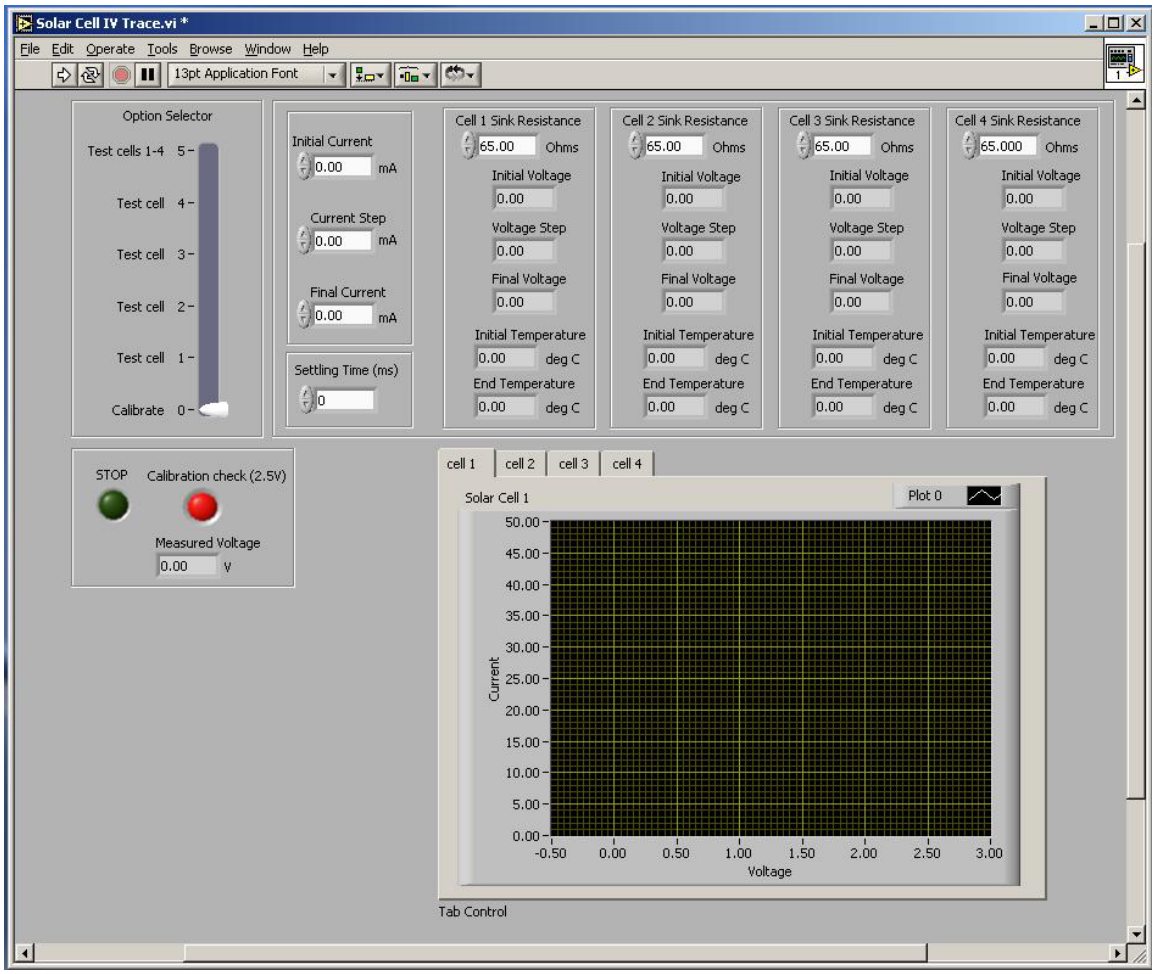

Figure E-1. User interface of the Coupon Driver Board VI.

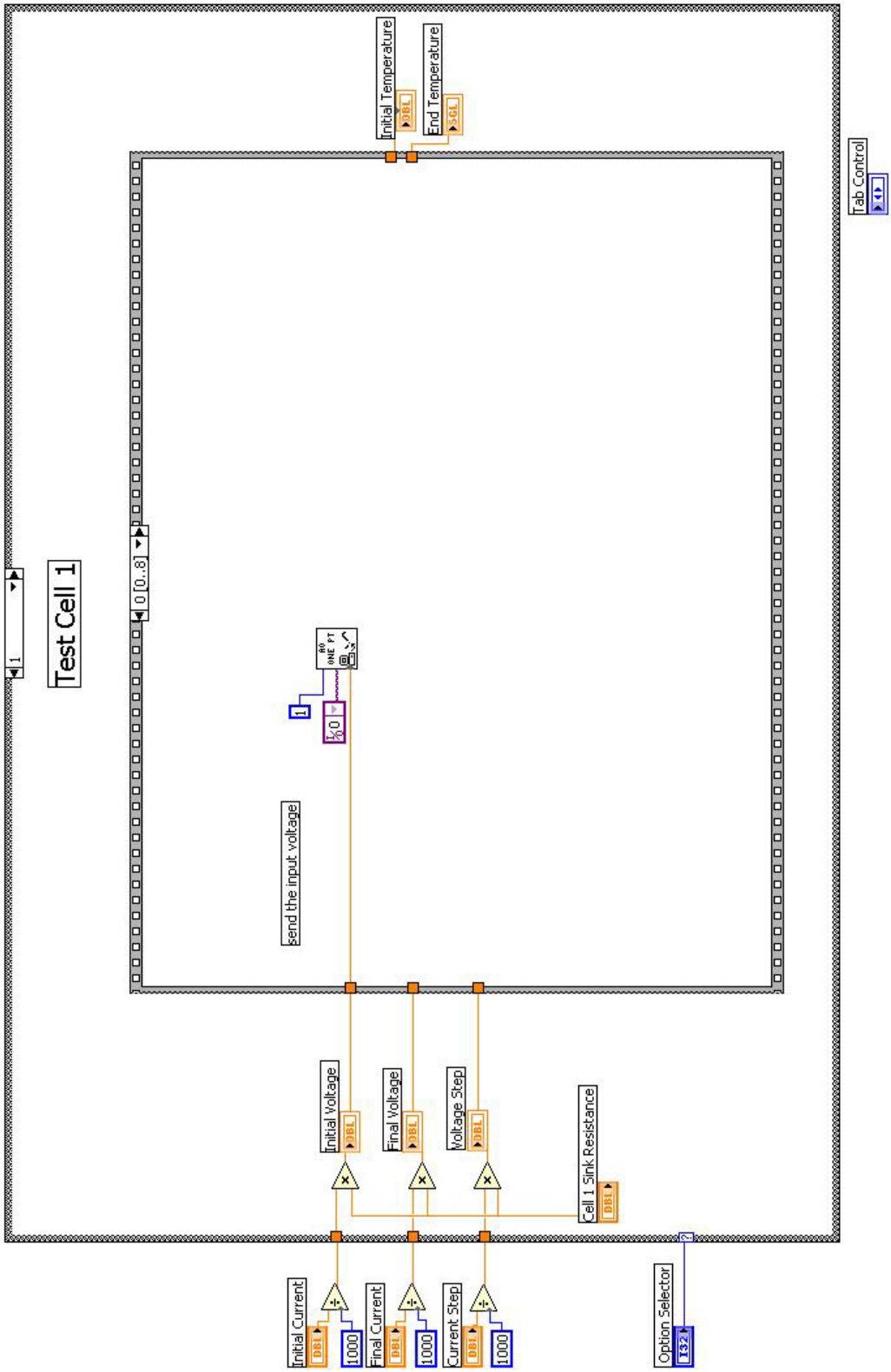

Figure E-2. Frame 0 for channel 1. Other channels have the same code.

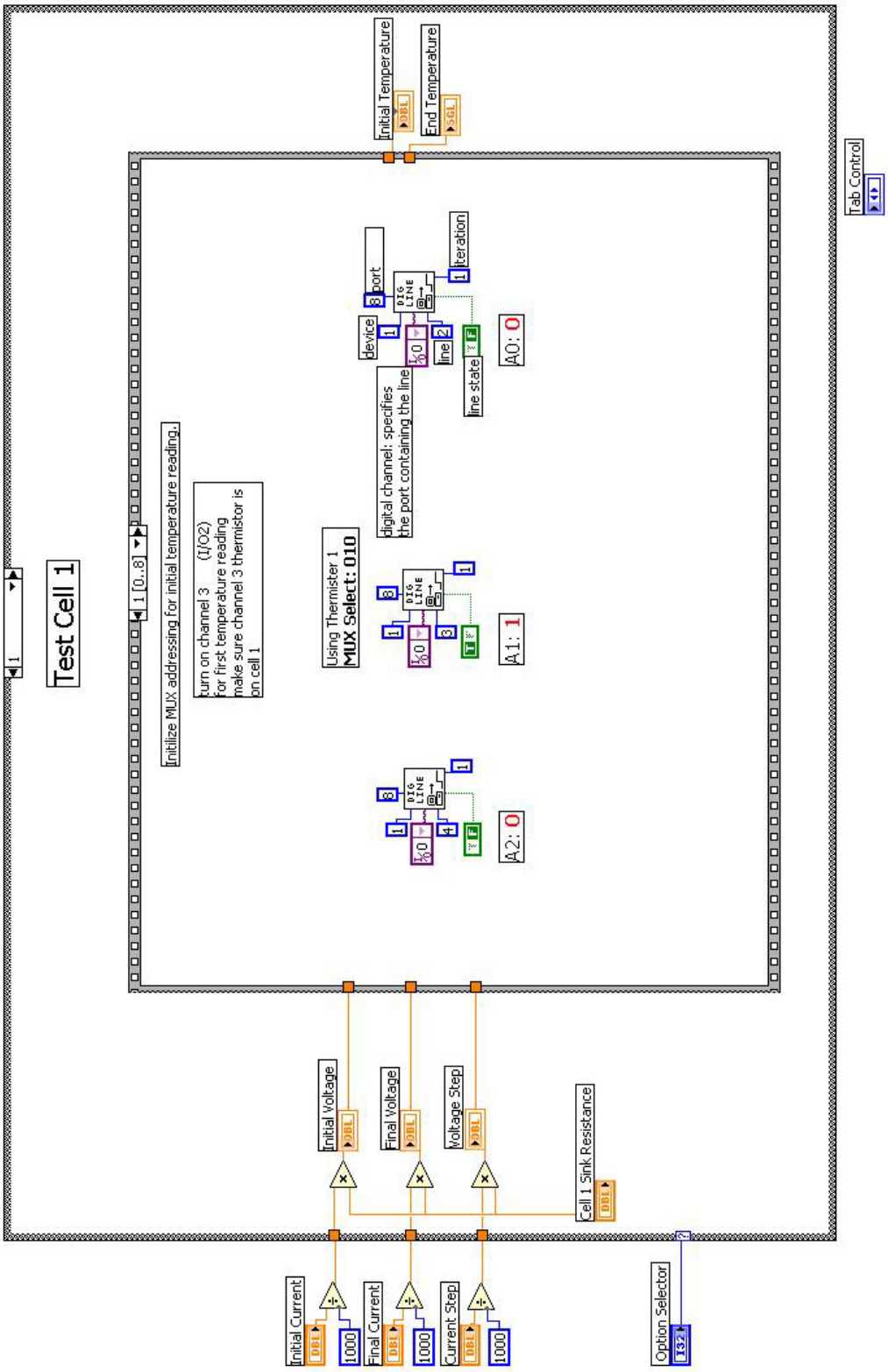

Figure E-3. Frame 1 for channel 1. The other channels will have different MUX addresses, shown in red numbers in the code here. See Table V-2 for the addresses for the other channels.

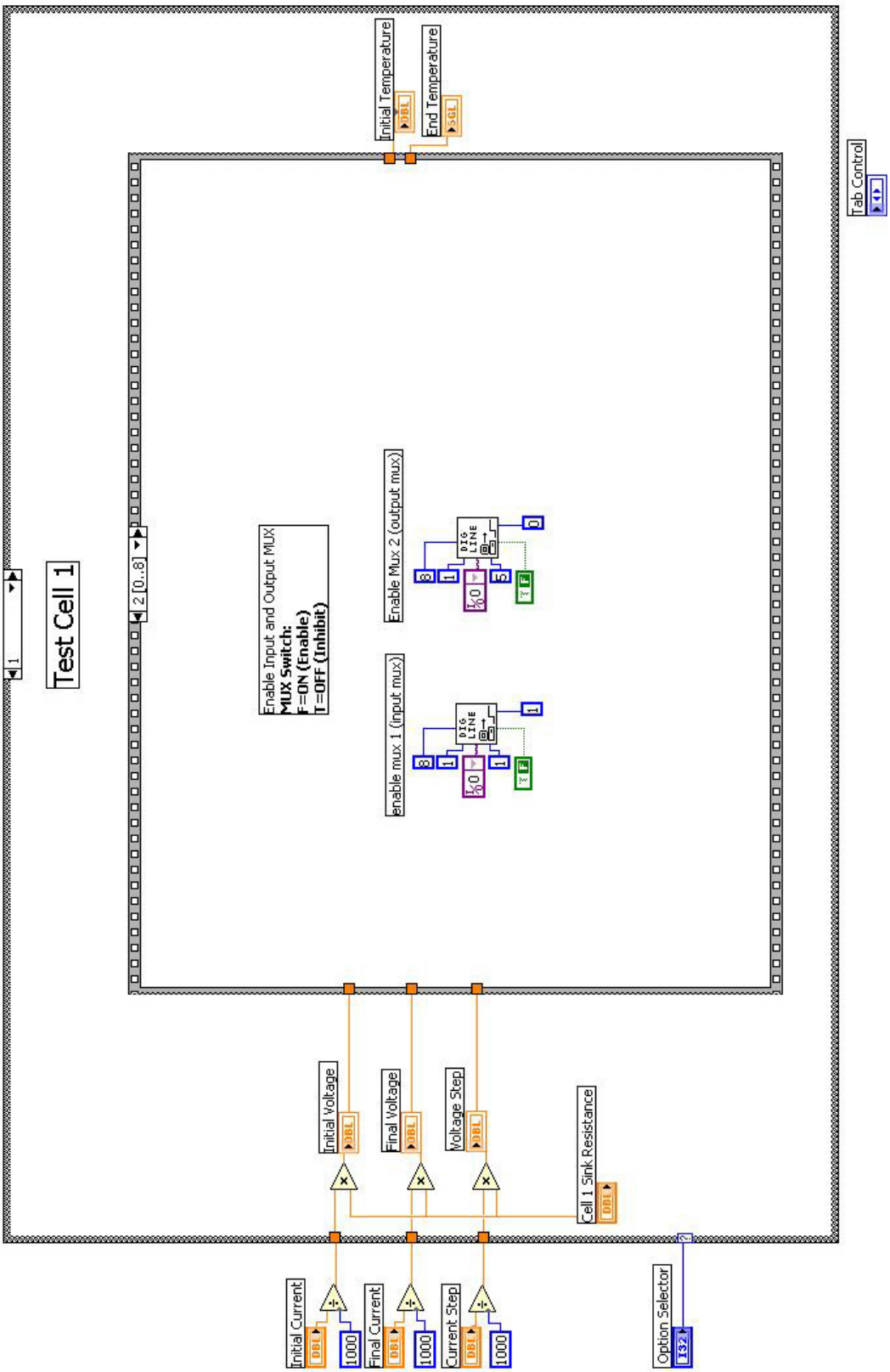

Figure E-4. Frame 2 for channel 1.

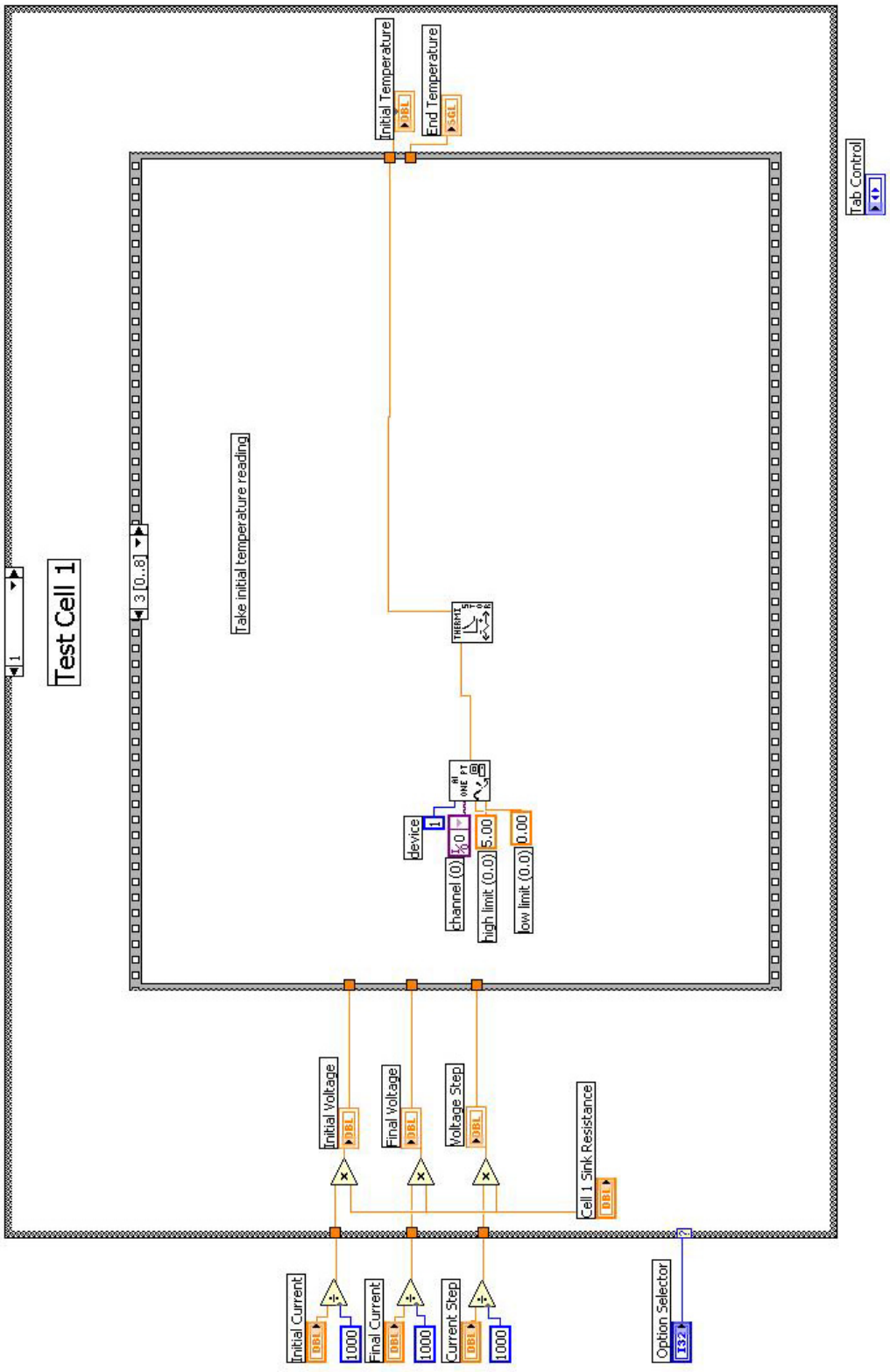

Figure E-5. Frame 3 for channel 1.

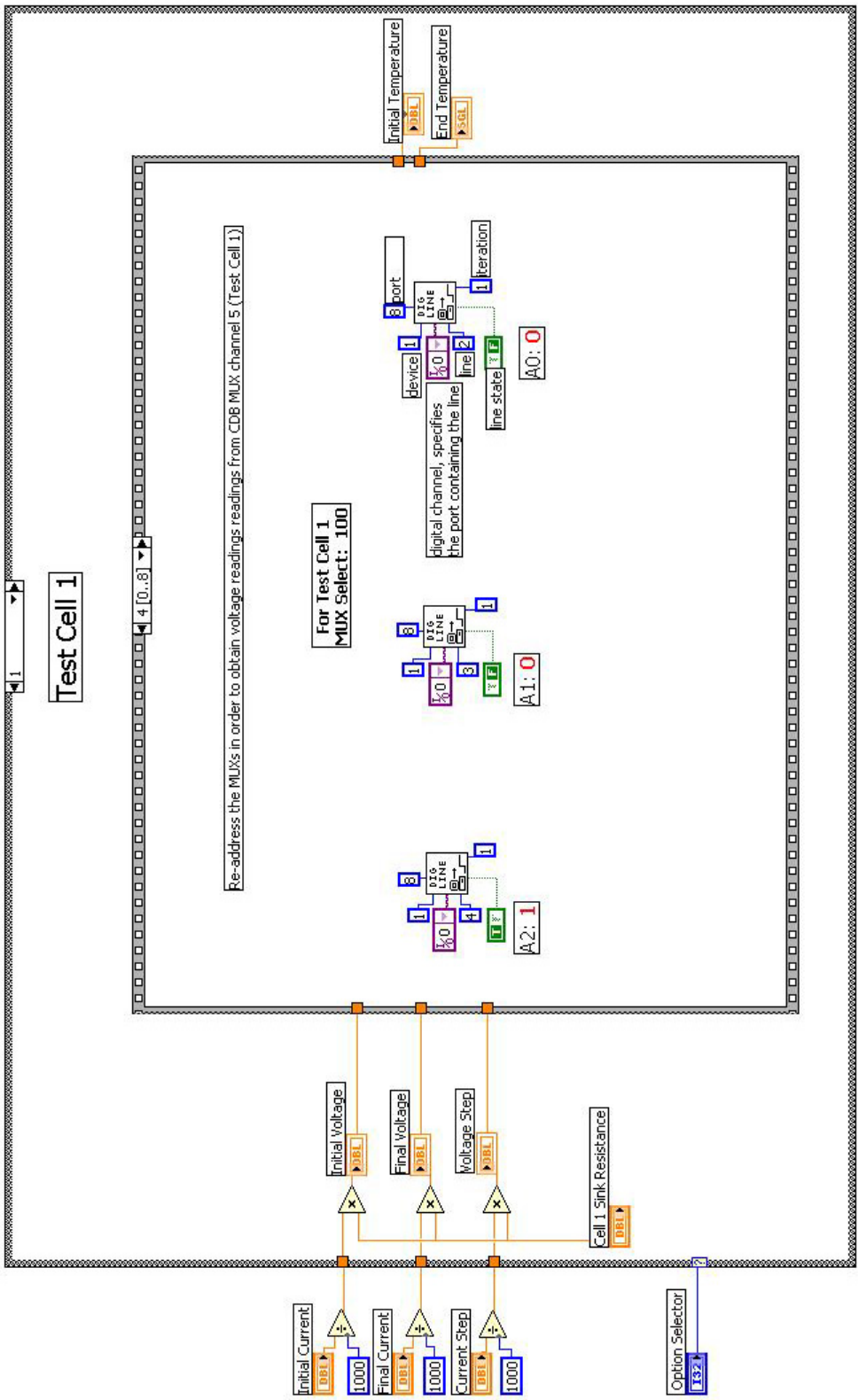

Figure E-6. Frame 4 for channel 1. The MUX addresses in red will be different for other channels. See Table V-2 for the addresses for the other channels.

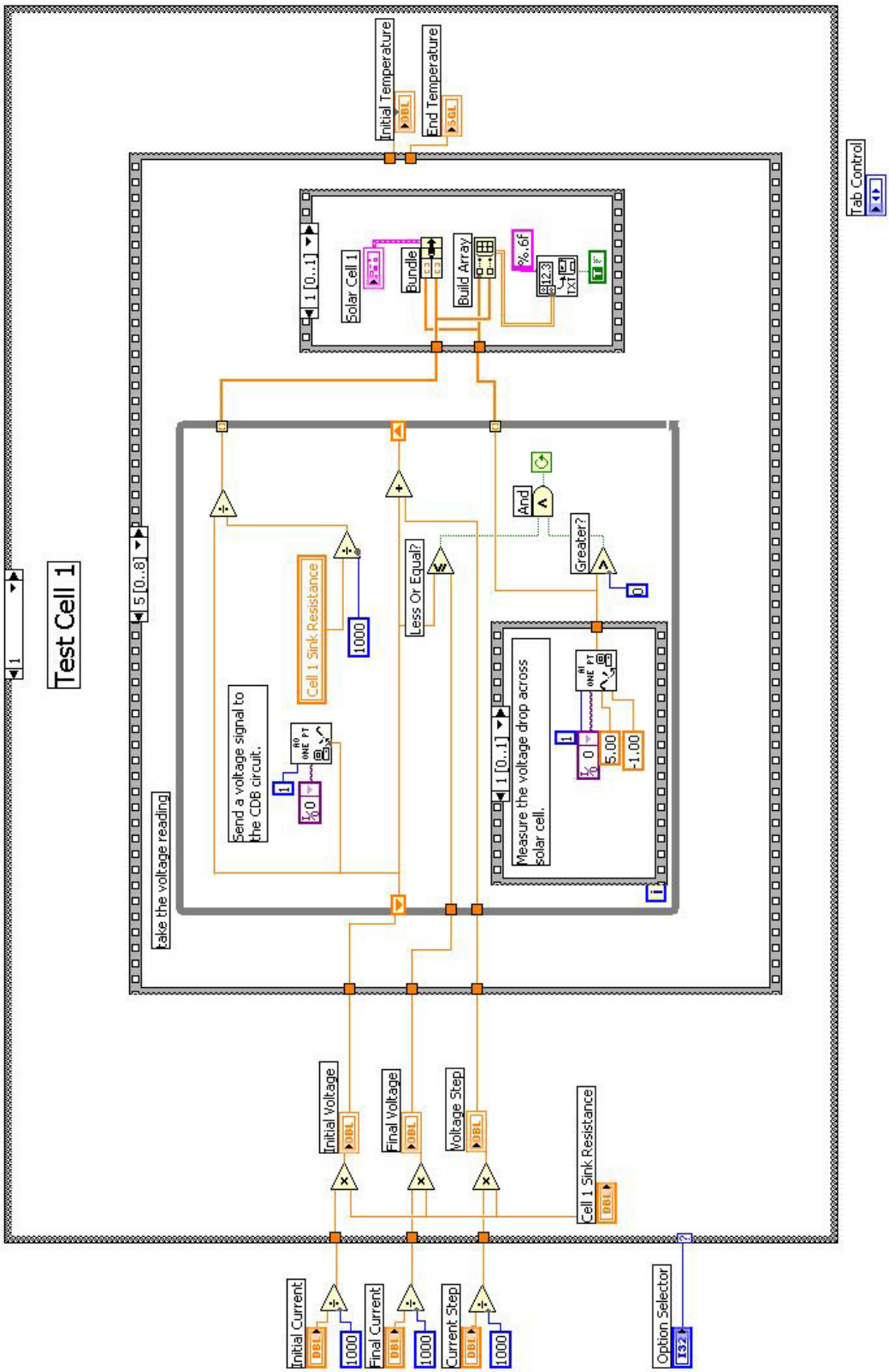

Figure E-7. Frame 5 for channel 1.

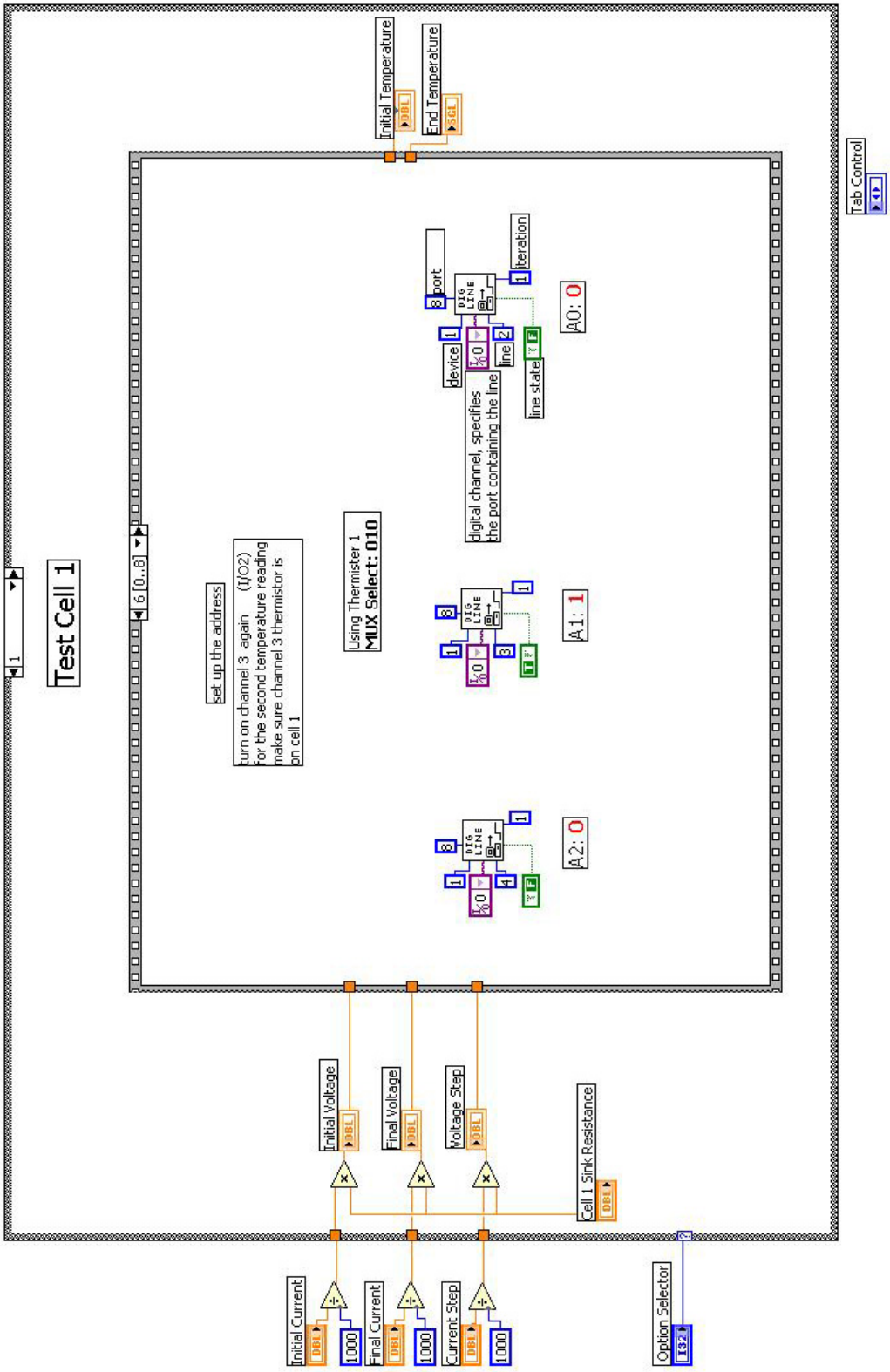

Figure E-8. Frame 6 for channel 1. The MUX addresses in red will be different for other channels. See Table V-2 for the addresses for the other channels.

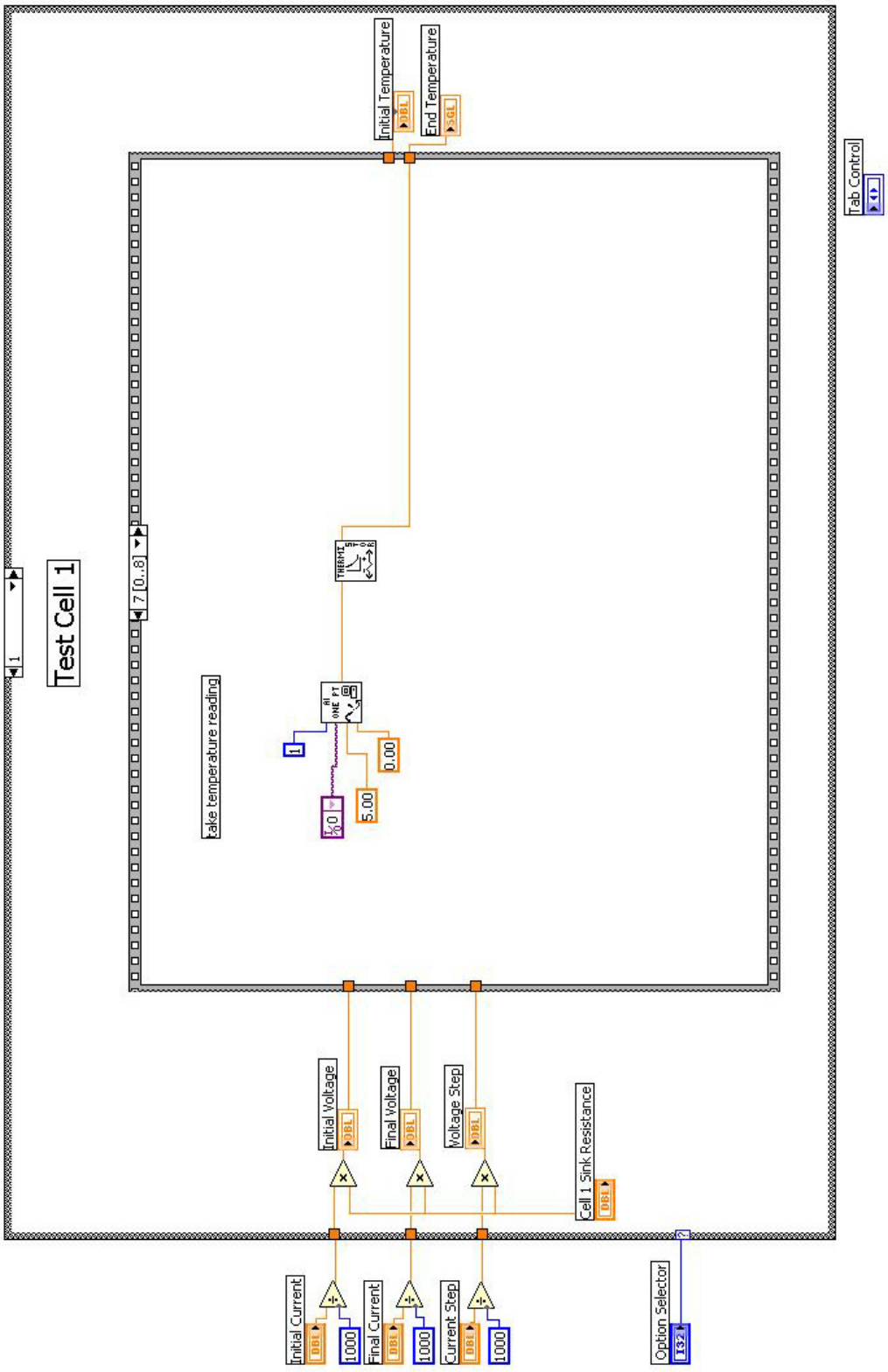

Figure E-9. Frame 7 for channel 1.

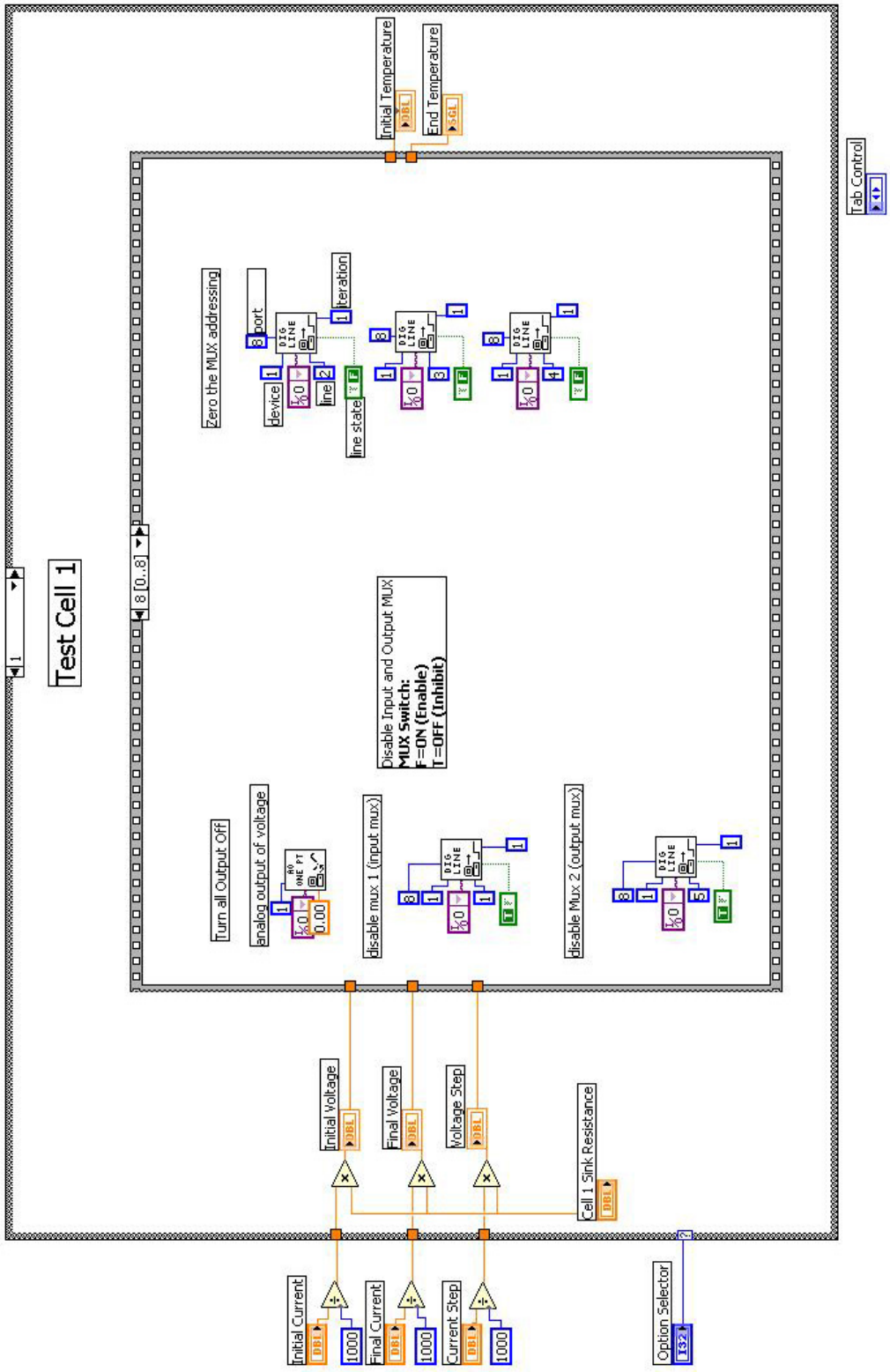

Figure E-10. Frame 8 for channel 1.

APPENDIX F. COMPLETE TEST RESULTS

All of the plots from the tests performed on the SMS analog circuit using the Coupon Driver Board (CDB) are included here, a total of 21 plots. Plots presented in Chapter V are also repeated here. For the incidence angle and temperature tests, a "family of curves" is shown, followed by a graph of comparison of the CDB and HP6626A for each of the angles and temperatures. The cells were illuminated by the solar simulator with spectrum shown in Figure IV-6.

In all of the plots by the CDB, there is tremendous noise near the knee of the curve. This was partially caused by the DAQ card and, at times, was caused by surrounding noise from other lab equipment, especially the vacuum pump in the lab used to suck the cell down on the mounting plate. But for most of the curves, only the part to the right of the knee matches the HP6626A control curve very well. Some curves actually match the HP6626A curve in all regions. In the plots here, smoothing was done on the curves.

A. VARIATION OF THE LIGHT INCIDENCE ANGLE

1. Commercial Improved Triple Junction Cell

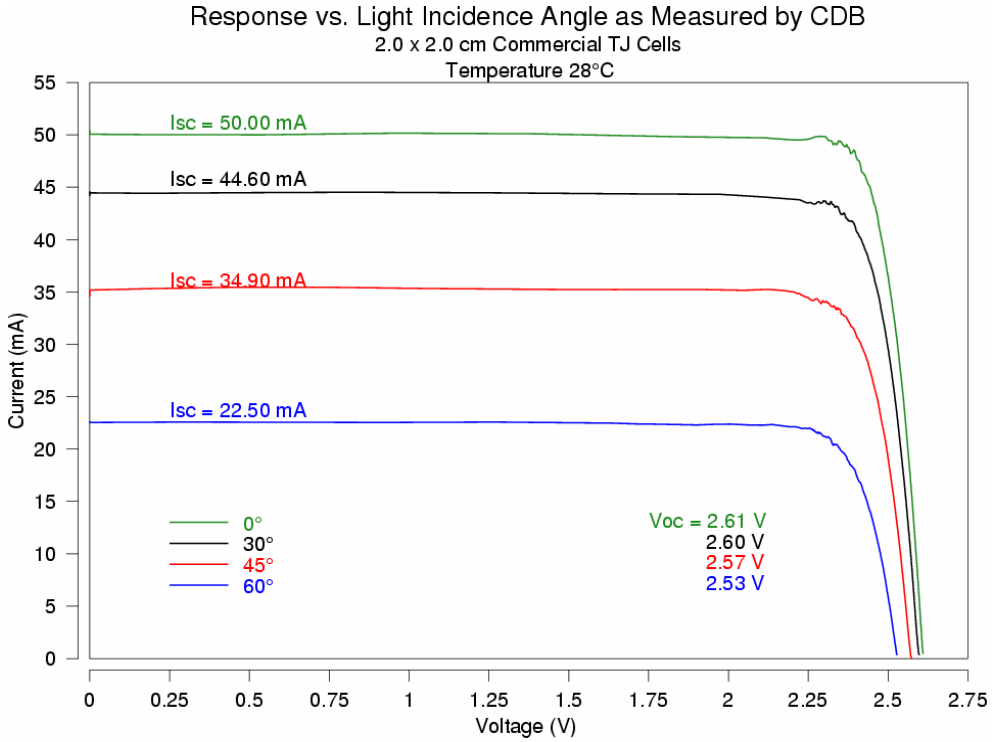

Figure F-1. Light incidence angle effect on Spectrolab ITJ cell.

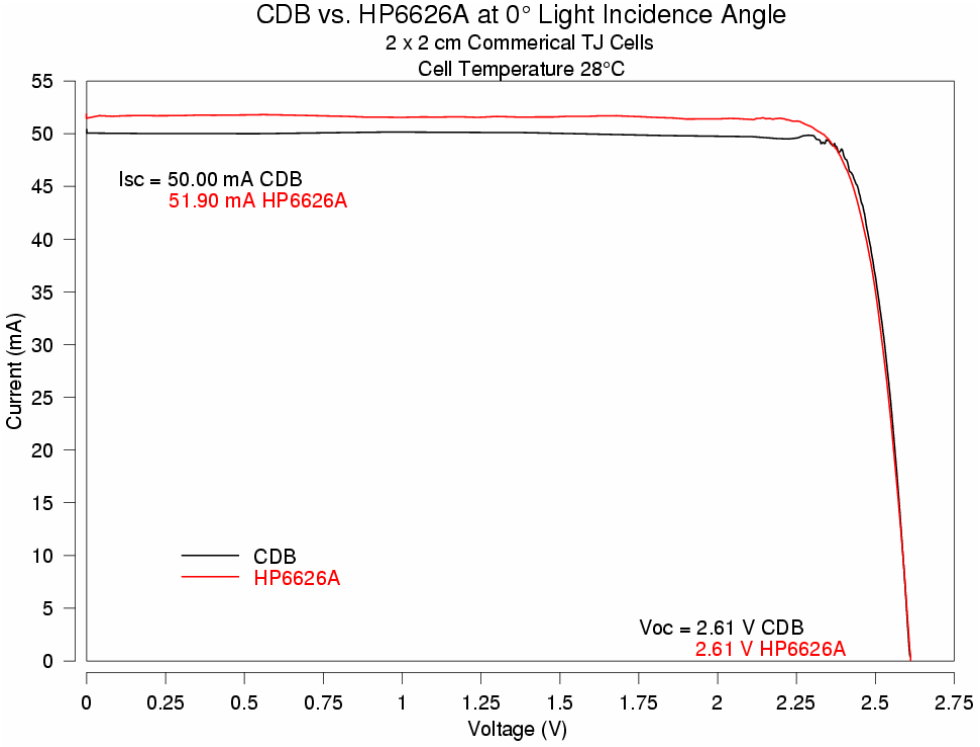

Figure F-2. Comparison of CDB to HP6626A for ITJ cell at perpendicular incidence angle.

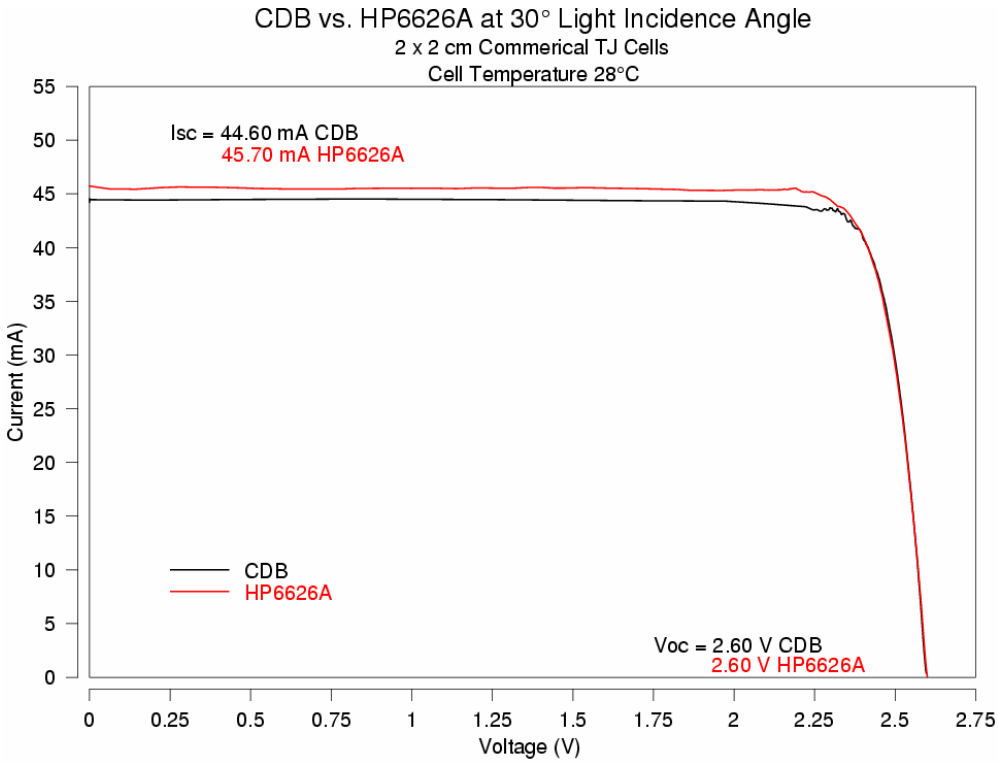

Figure F-3. Comparison of CDB to HP6626A for ITJ cell at 30° from the normal.

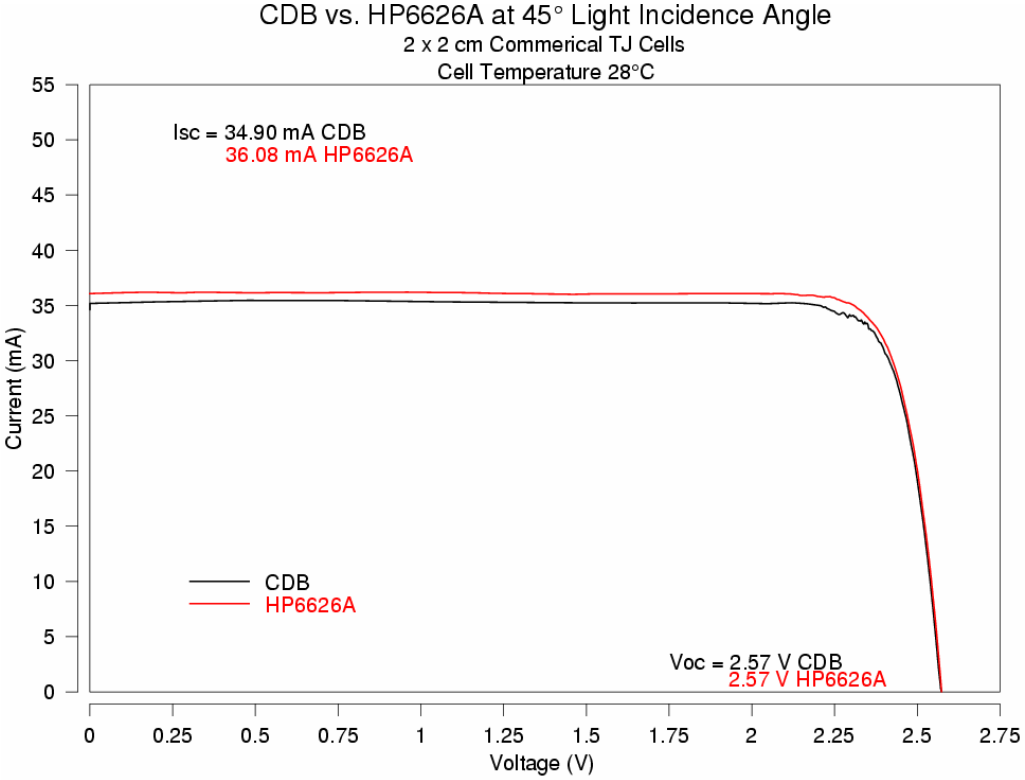

Figure F-4. Comparison of CDB to HP6626A for ITJ cell at 45° from the normal.

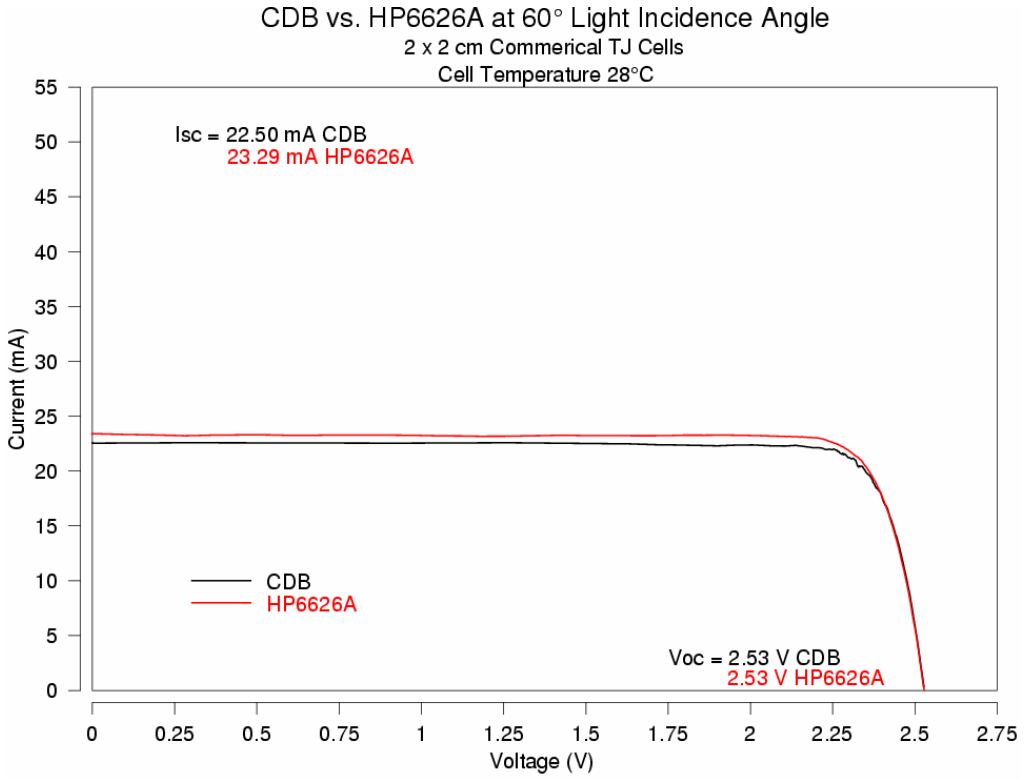

Figure F-5. Comparison of CDB to HP6626A for ITJ cell at 60° from the normal.

2. Experimental Triple Junction Cell

For some reason the results obtained here in this section for the XTJ cells are the best of all the results. The CDB curves matched the HP6626A very well in all regions. There is no clear explanation why this is so.

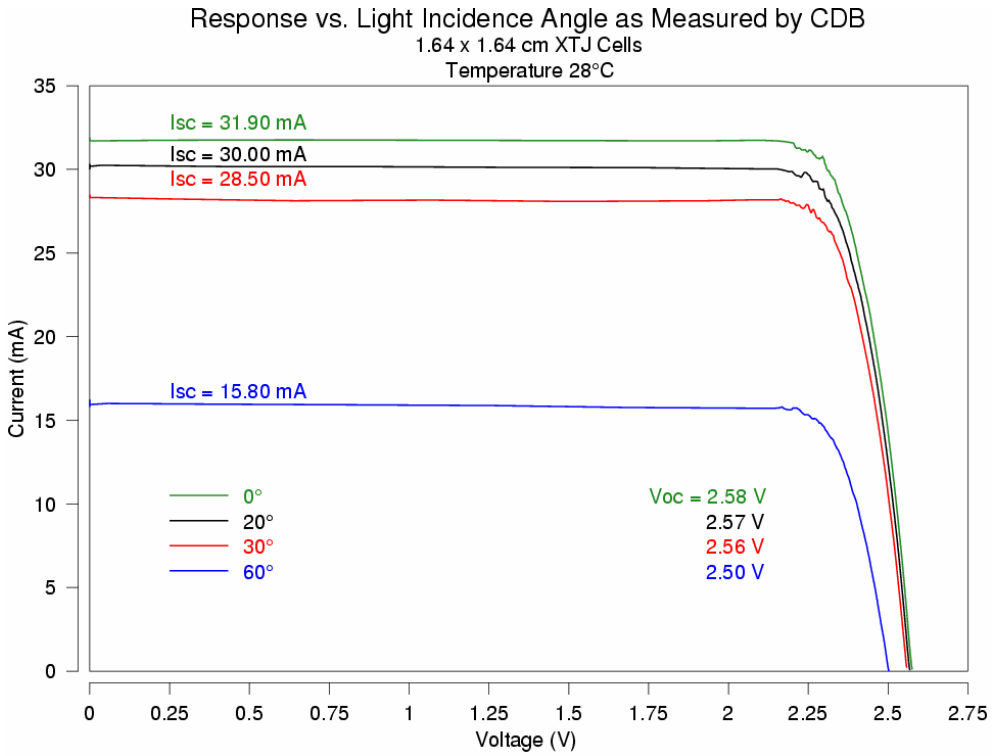

Figure F-6. Light incidence angle effect on Spectrolab XTJ cell.

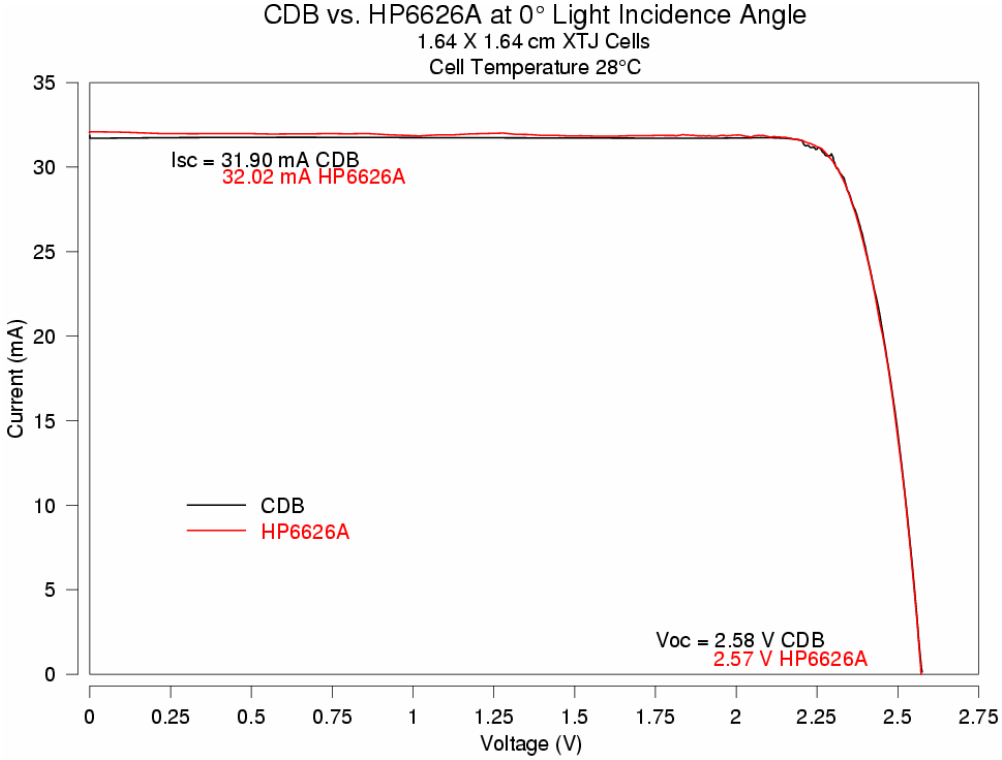

Figure F-7. Comparison of CDB to HP6626A for XTJ cell at 0° from the normal.

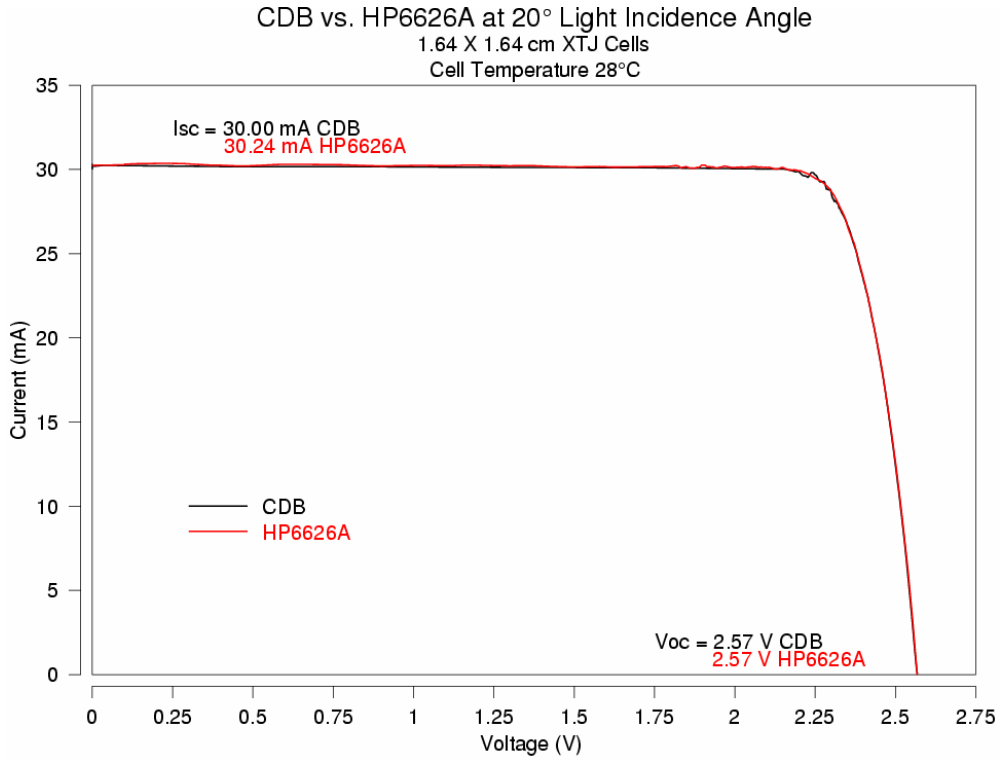

Figure F-8. Comparison of CDB to HP6626A for XTJ cell at 20° from the normal.

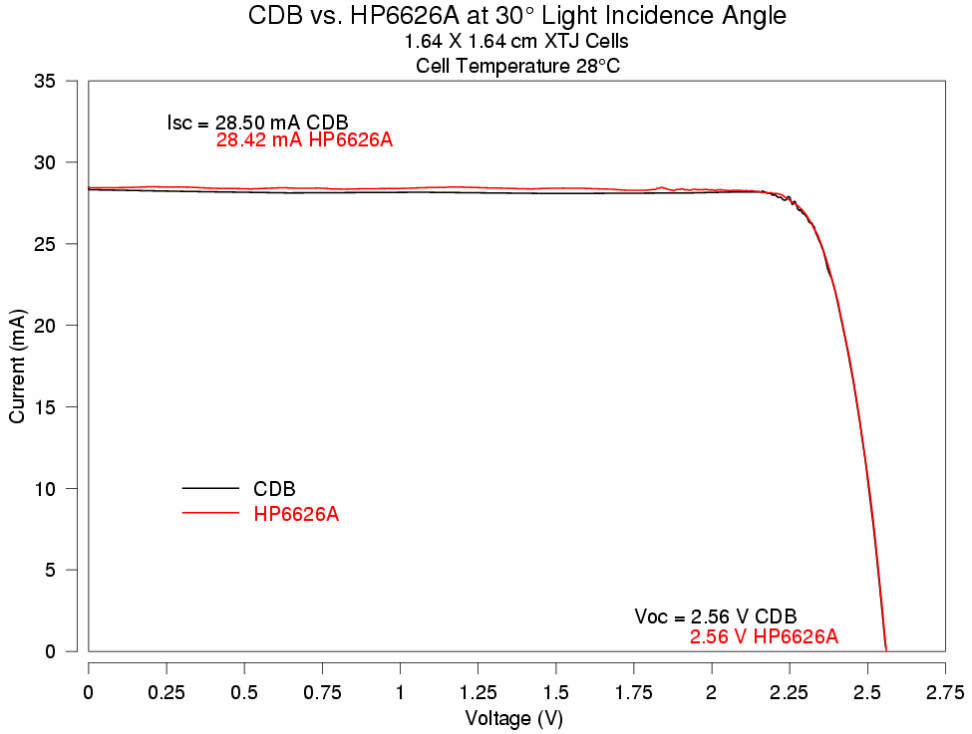

Figure F-9. Comparison of CDB to HP6626A for XTJ cell at 30° from the normal.

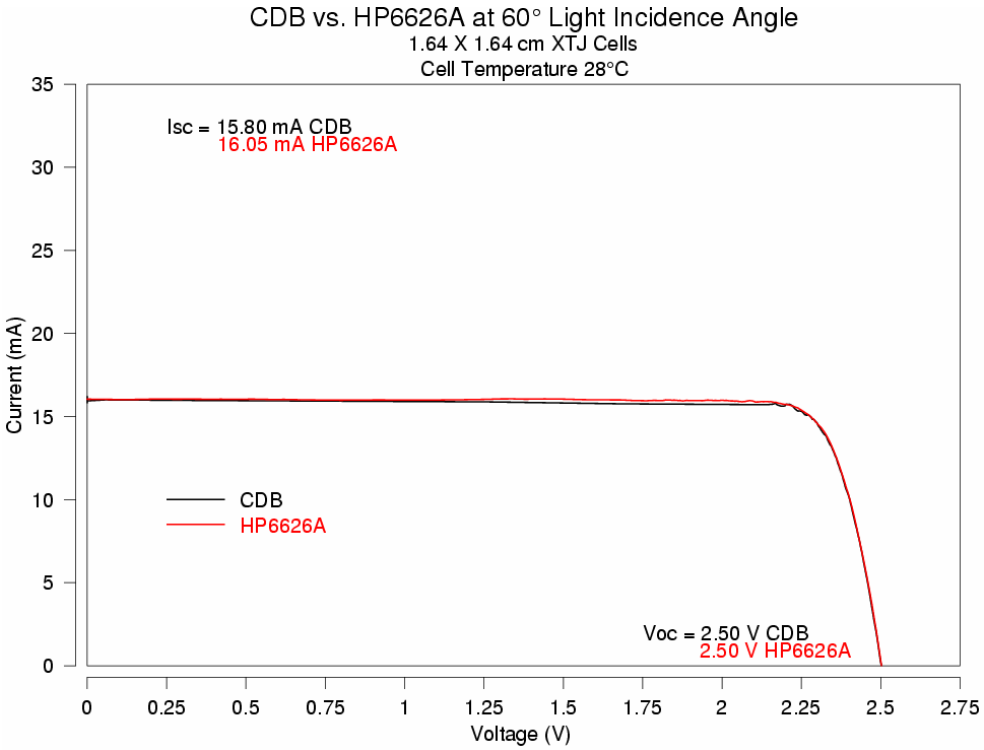

Figure F-10. Comparison of CDB to HP6626A for XTJ cell at 60° from the normal.

B. VARYING THE TEMPERATURE ON THE CDB ELECTRONICS

Two plots are presented here, one for the experimental cells, and one for the commercially-available ITJ cell, both are by Spectrolab.

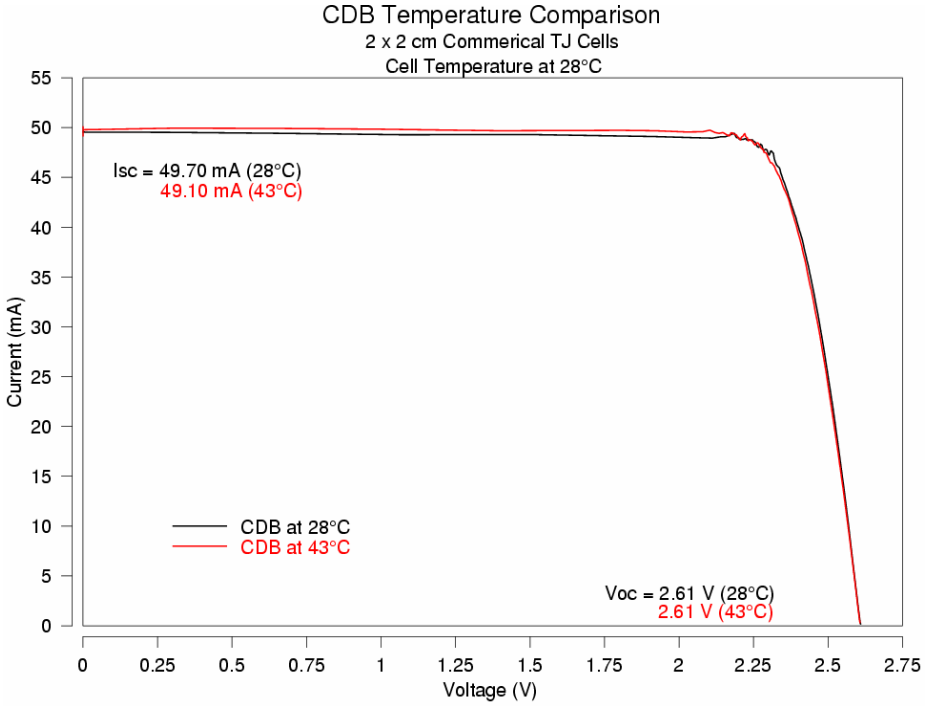

Figure F-11. CDB temperature comparison with an ITJ cell.

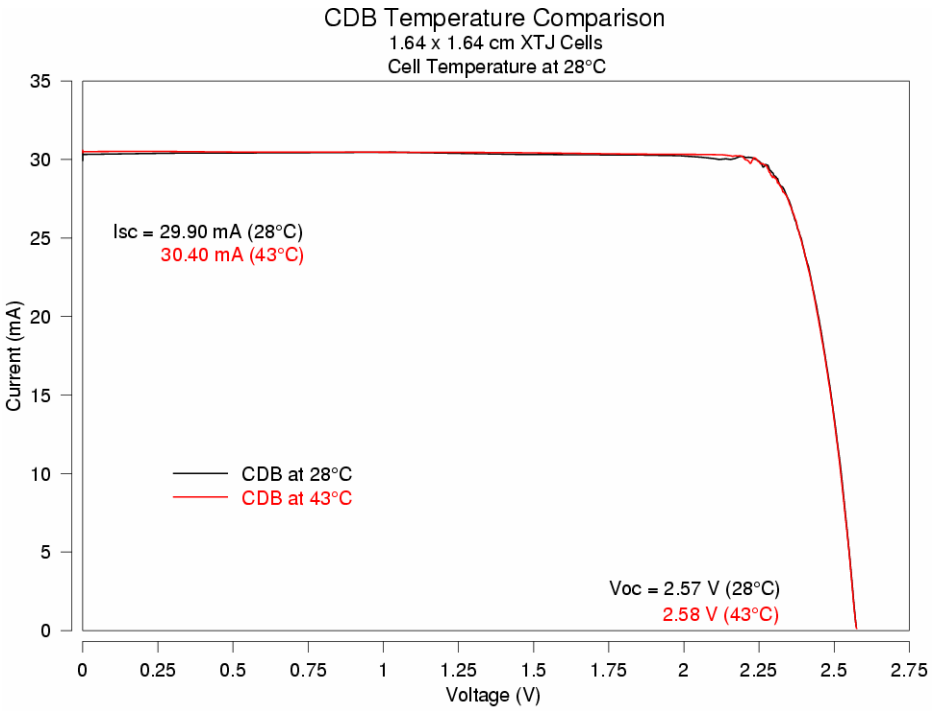

Figure F-12. CDB temperature comparison with an XTJ cell.

C. VARIATION OF THE CELL TEMPERATURE

1. Commercial Improved Triple Junction Solar Cell

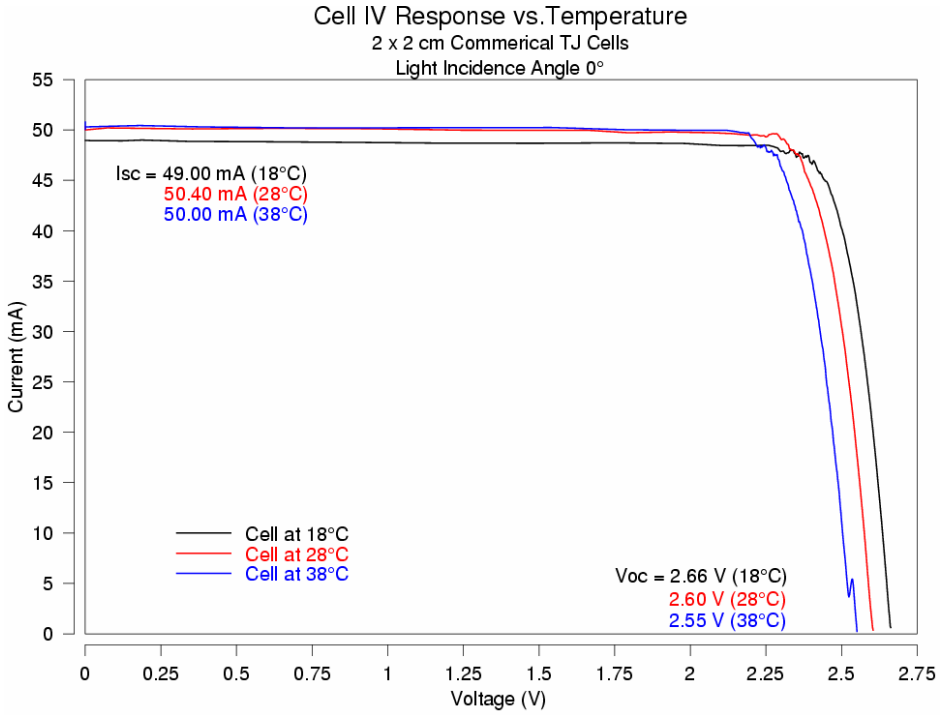

Figure F-13. Cell temperature effect on commercially-available Spectrolab ITJ solar cells.

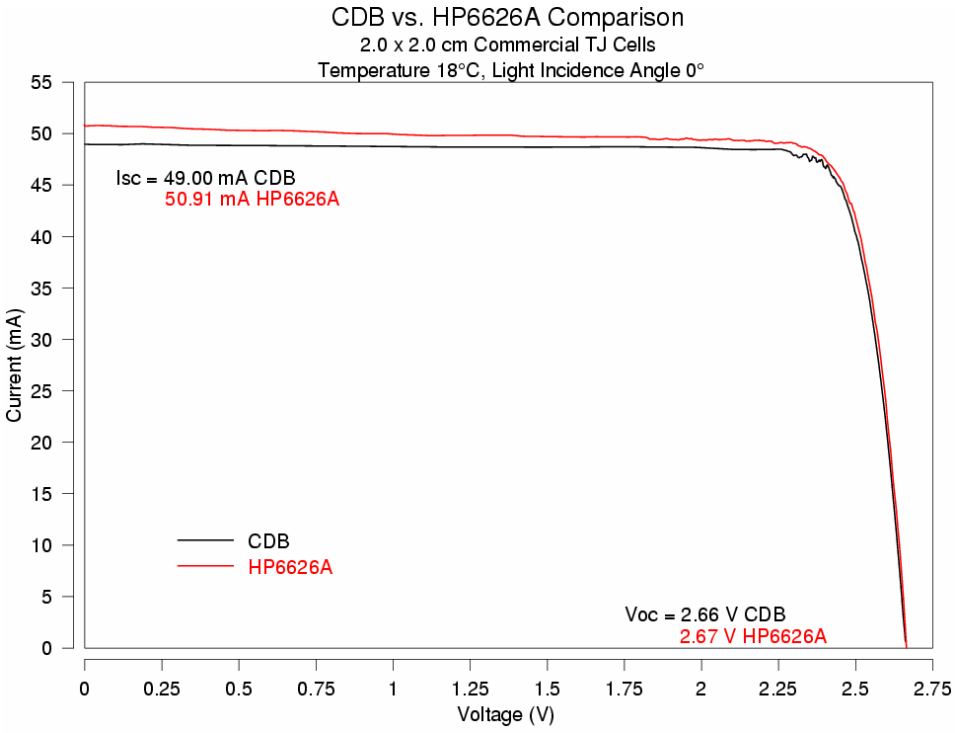

Figure F-14. Comparison of CDB to HP6626A for ITJ cell at 18°C.

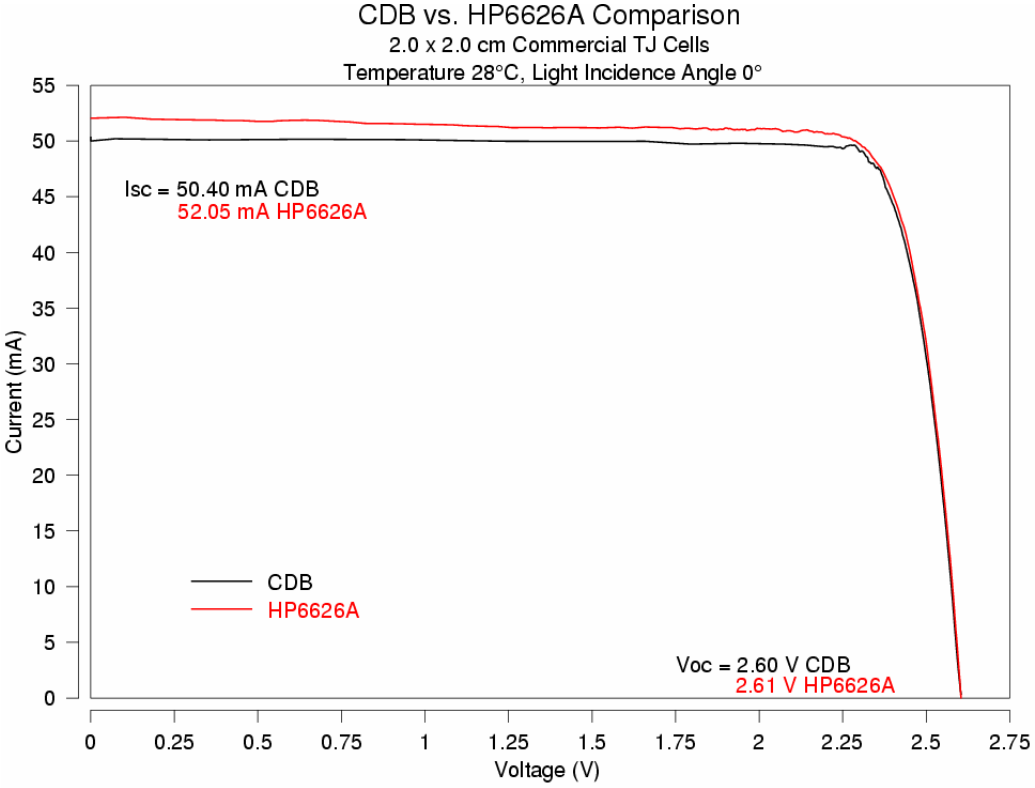

Figure F-15. Comparison of CDB to HP6626A for ITJ cell at 28°C.

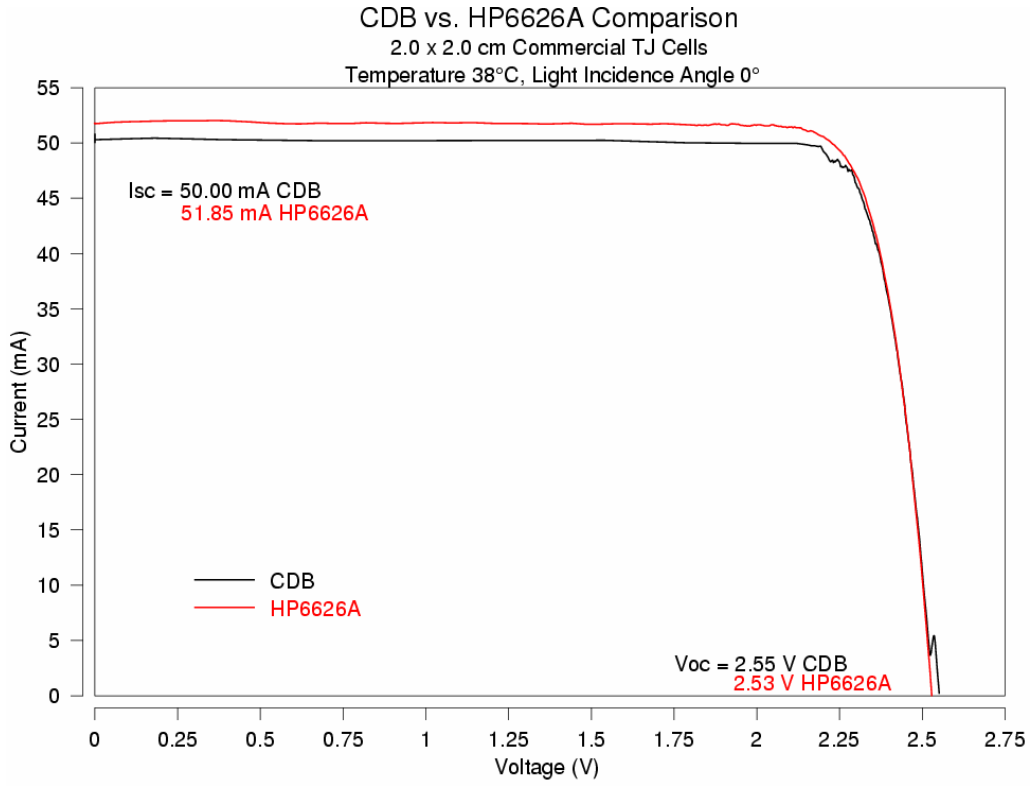

Figure F-16. Comparison of CDB to HP6626A for ITJ cell at 38°C.

2. Experimental Triple Junction Cell

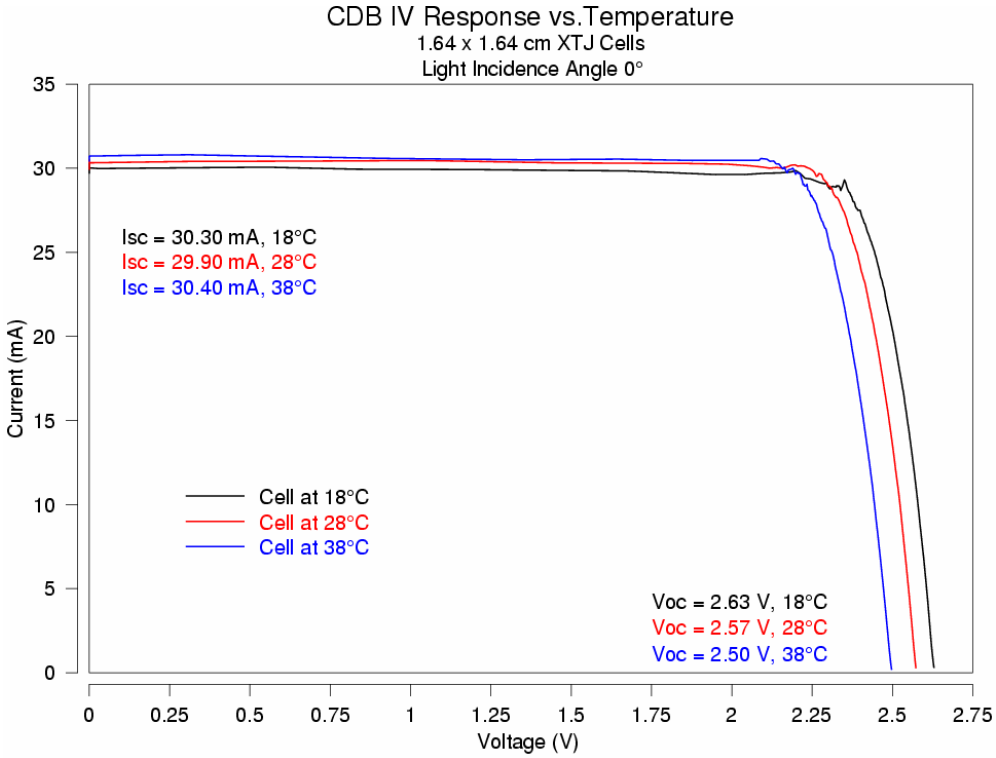

Figure F-17. Cell temperature effect on Spectrolab experimental solar cells (XTJ).

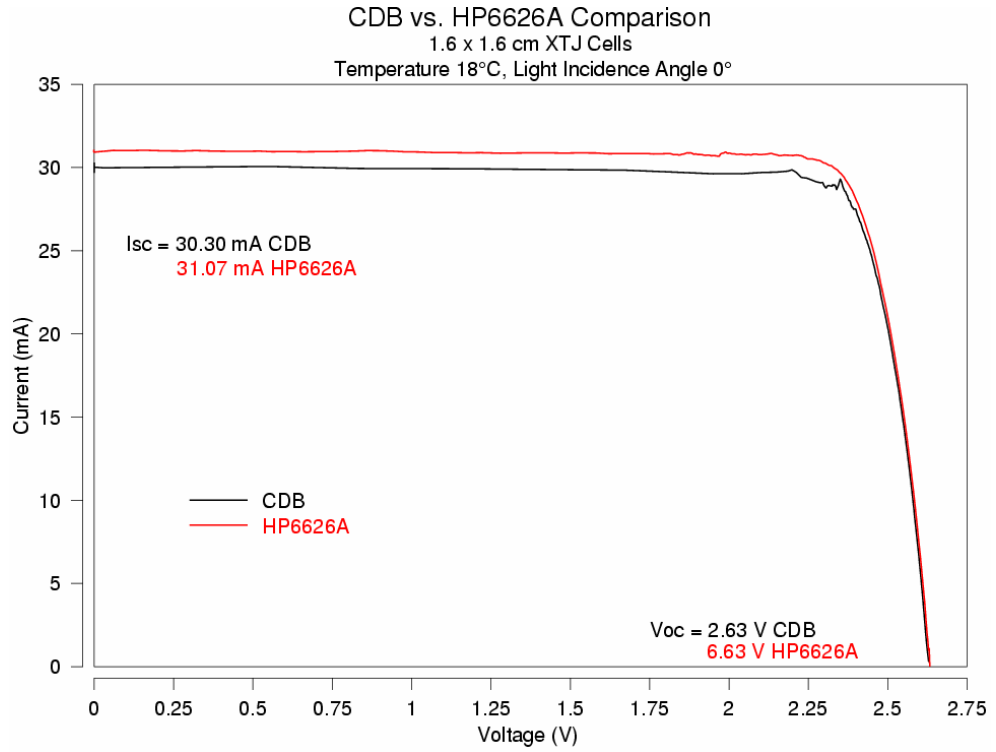

Figure F-18. Comparison of CDB to HP6626A for XTJ cell at 18°C.

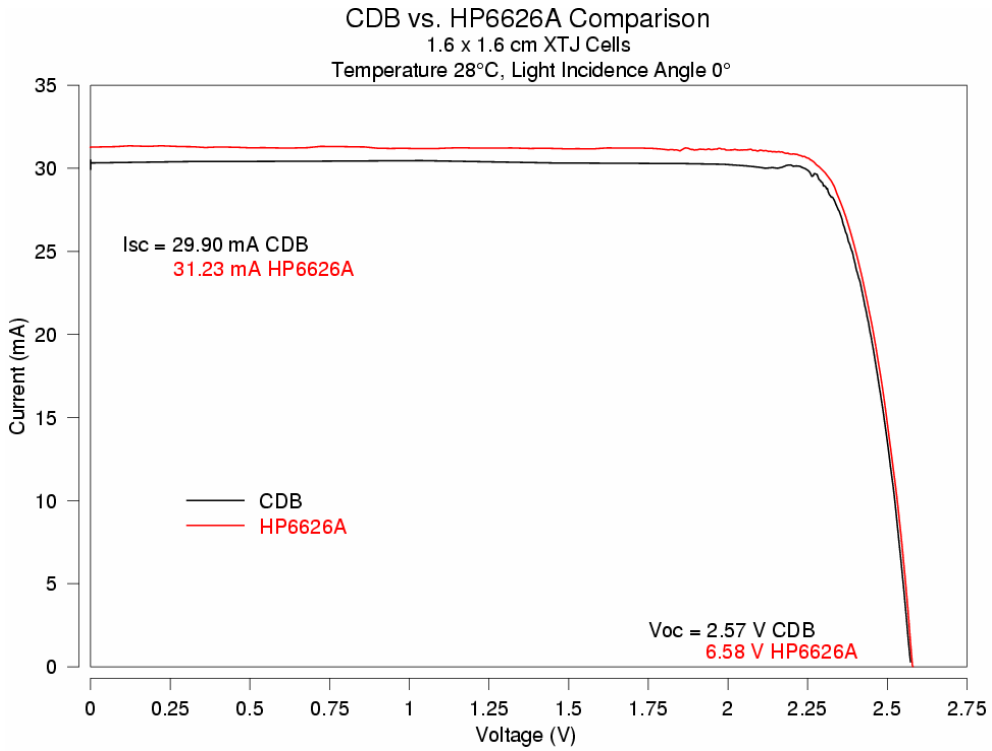

Figure F-19. Comparison of CDB to HP6626A for XTJ cell at 28°C.

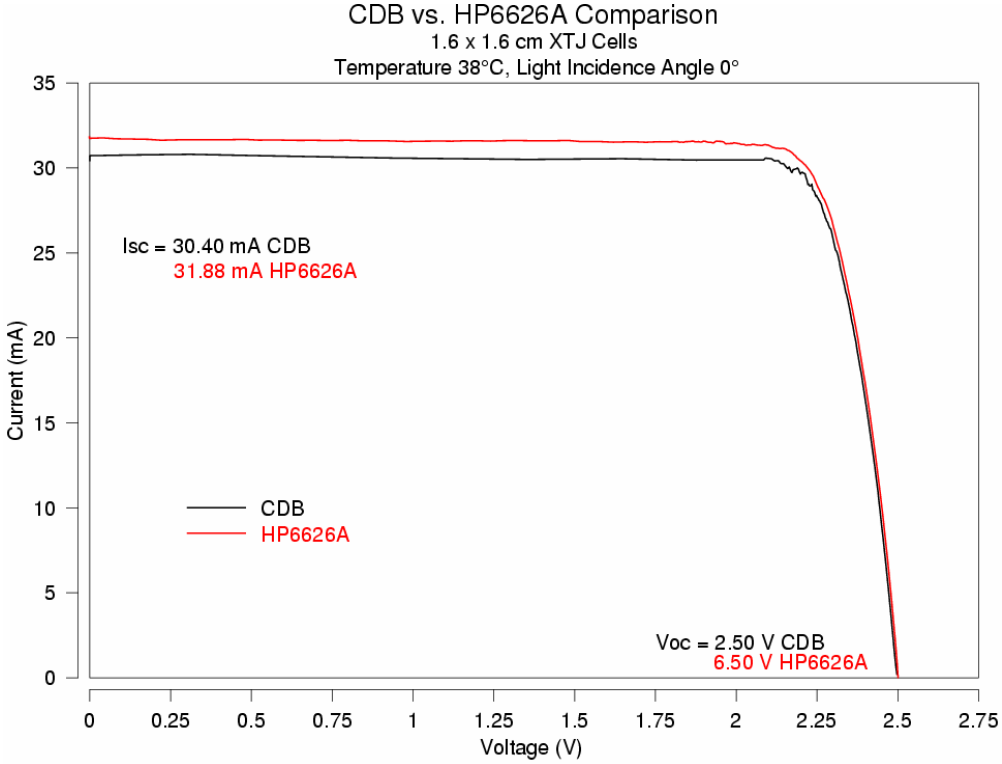

Figure F-20. Comparison of CDB to HP6626A for XTJ cell at 38°C.

D. COMPARISON OF THE CHANNELS ON THE CDB

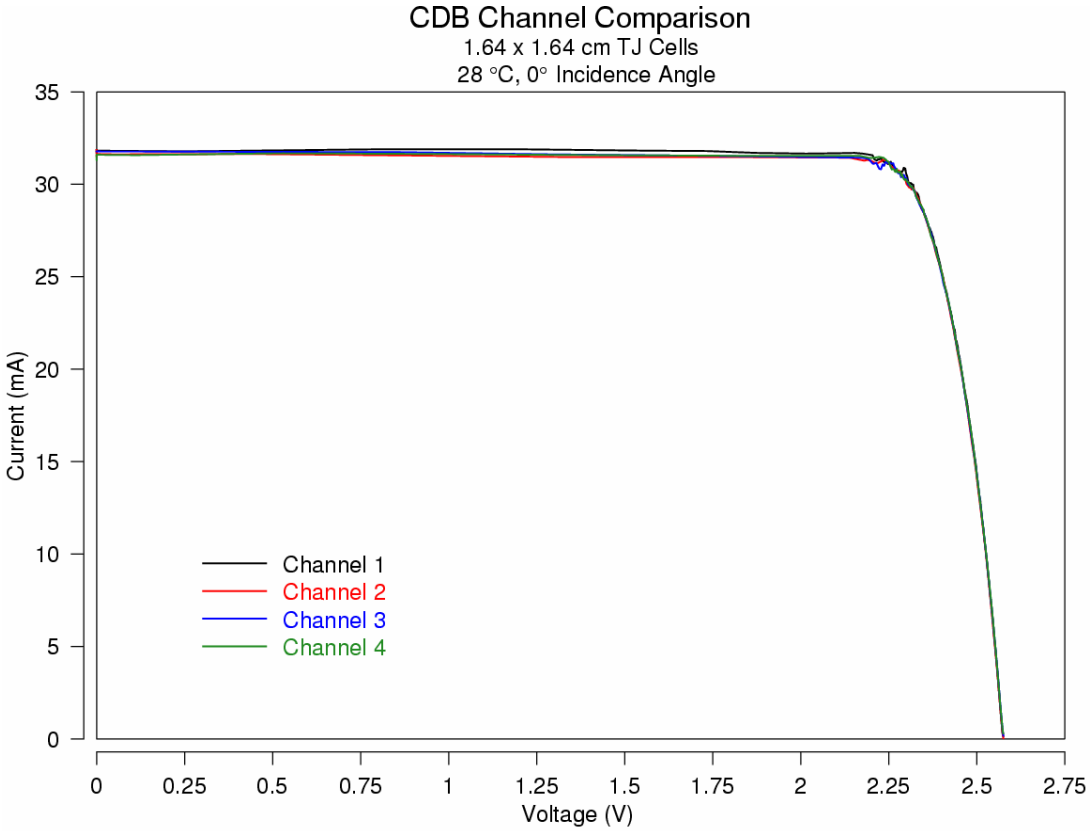

Figure F-21. ***I-V*** **curves taken by the four channels on CDB under the same conditions.**

LIST OF REFERENCES

1. Callaway, R.K., *An Autonomous Circuit for the Measurement of Photovoltaic Devices Parameters*, Master's Thesis, Naval Postgraduate School, Monterey, California, September 1986.

2. Fahrenburch, A.L, and Bube, R.H., *Fundamentals of Solar Cells – Photovoltaic Solar Energy Conversion*. Academic Press, Inc., New York, 1983.

3. Jet Propulsion Laboratory, "Solar Cell Array Design Handbook – Volume 1." National Aeronautics and Space Administration, 1976.

4. Green, M.A., *Solar Cells: Operating Principles, Technology, and System Applications*. Prentice-Hall, New Jersey, 1982.

5. Oriel Instruments, *Introduction to Solar Simulators*, [www.lot-oriel.com/pdf_it/all/light_solar_intro.pdf]. Last accessed March 2004.

6. Hu, C., and White, R.M., *Solar Cells – From Basic to Advanced Systems*. McGraw-Hill, New York, 1983.

7. Viswanathan, C.R., *An Introductory Text on Basic Semiconductor Devices*, Course Notes at the University of California, Los Angeles, 1995.

8. Mazer, J.A., *Solar Cells: An Introduction to Crystalline Photovoltaic Technology*. Kluwer Academic Publishers, Boston, Massachusetts, 1997.

9. Michalopoulos, P., *A Novel Approach for the Development and Optimization of State-of-the-Art Photovoltaic Devices Using Silvaco*, Master's Thesis, Naval Postgraduate School, Monterey, California, March 2002.

10. Sedra, A.S., and Smith, K.C., *Microelectronic Circuits*, 4th ed., Oxford University Press, New York, 1998.

11. Boeing Spectrolab, "Photovoltaic Products Data Sheets," [http://www.spectrolab.com/prd/space/cell-main.asp]. Last accessed June 2004.

12. Michael, S., Course Notes for EC3230 (unpublished), Naval Postgraduate School, Monterey, California, January 2004.

13. Horning, J.A., and Sakoda, D., "Overview of the NPS Spacecraft Architecture and Technology Demonstration Satellite, NPSAT1," *Proceedings of the 16th Annual AIAA/USU Conference on Small Satellites*, paper SSC02-I-4, Logan, Utah, August 2002.

14. Naval Postgraduate School, "Space Systems Academic Group." [www.sp.nps.navy.mil]. Last accessed March 2004.

15. Salmon, J.B., Phelps, R., Loomis, H.H., and Michael, S., "Solar Cell Measurement System for NPS Spacecraft Architecture and Technology Demonstration Satellite, NPSAT1," *Proceedings of the 17th Annual AIAA/USU Conference on Small Satellites*, paper SSC03-X-4, Logan, Utah, August 2003.

16. CAD models and system diagrams by Dan Sakoda, NPS Space Systems Academic Group

17. Leonard, B.S., "NPSAT1 Magnetic Attitude Control System," *Proceedings of the 16th Annual AIAA/USU Conference on Small Satellites*, paper SSC02-V-7, Logan, Utah, August 2002.

18. Ebert, D.A., Hulme, C.A., Loomis, H.H., and Ross, A.A., "Configurable Fault-Tolerant Processor (CFTP) for Space Based Applications," *Proceedings of the 17th Annual AIAA/USU Conference on Small Satellites*, paper SSC03-XI-5, Logan, Utah, August 2003.

19. Hulme, C.A., *Testing and Evaluation of the Configurable Fault Tolerant Processor (CFTP) for Space Based Application*, Master's Thesis, Naval Postgraduate School, Monterey, California, December 2003.

20. Boeing Spectrolab, NPSAT-1 Mid-Panel Solar Array Layout, March 2003.

21. Salmon, J.B., *Naval Postgraduate School Satellite 1 Solar Cell Measurement System*, Master's Thesis, Naval Postgraduate School, Monterey, California, September 2003.

22. Draper, M.B., and Stockton, H.E., *Measuring the Degradation of Solar Cells Due to Exposure to Ion Engine Plasma Exhaust*, Master's Thesis, Naval Postgraduate School, Monterey, California, September 2003.

23. Ocean Optics, Inc, product description. [www.oceanoptics.com]. Last accessed March 2004.

24. Prater, G., Sakoda, D., and Grant, A., "Overview of the Naval Postgraduate School Small Satellite, NPSAT1," *22nd AIAA International Communications Satellite Systems Conference & Exhibit 2004*, paper AIAA 2004-3273, Monterey, California, May 2004.

25. Naval Postgraduate School Technical Report NPS-SP-03-001, *Computer Aided Thermal Analysis of a Technology Demonstration Satellite (NPSAT1)*, by M. Gruhlke, May 2003.

26. Lo, B.W., Phelps, R., and Michael, S., "Evaluation and Testing of the Solar Cell Measurement System Onboard the Naval Postgraduate School Satellite NPSAT1," *22nd AIAA International Communications Satellite Systems Conference & Exhibit 2004*, paper AIAA 2004-3267, Monterey, California, May 2004.

THIS PAGE INTENTIONALLY LEFT BLANK

INITIAL DISTRIBUTION LIST

1. Defense Technical Information Center
   Fort Belvoir, Virginia

2. Dudley Knox Library
   Naval Postgraduate School
   Monterey, California

3. Chairman, Code EC
   Department of Electrical and Computer Engineering
   Naval Postgraduate School
   Monterey, California

4. Chairman, Code SP
   Space Systems Academic Group
   Naval Postgraduate School
   Monterey, California

5. Professor Sherif Michael, Code EC/Mi
   Department of Electrical and Computer Engineering
   Naval Postgraduate School
   Monterey, California

6. Professor Hersch Loomis, Code EC/Lm
   Department of Electrical and Computer Engineering
   Naval Postgraduate School
   Monterey, California

7. Ron Phelps, Code SP
   Space Systems Academic Group
   Naval Postgraduate School
   Monterey, California

8. ENS Benson W. Lo, USNR
   Department of Electrical and Computer Engineering
   Naval Postgraduate School
   Monterey, California